Dissertation

FLEXIBILITY IN ORGAN RESEARCH – A 3D CELL CULTURE MODEL OF THE HUMAN PLACENTA

Basic requirements and methods

submitted by

Julia FUCHS,

M.Sc. M.Sc. B.Sc.

for the Academic Degree of

Doctor of Medical Science

(Dr. scient. med.)

at the

Medical University of Graz

Gottfried Schatz Research Center for Cell Signaling, Metabolism and Aging

Division of Cell Biology, Histology and Embryology

under the Supervision of

Priv.-Doz. Dr.nat.techn. Dagmar BRISLINGER, M.Sc.

2020

Statutory Declaration

I hereby declare that this thesis is my own original work and that I have fully acknowledged by name all of those individuals and organizations that have contributed to the research for this thesis. Due acknowledgment has been made in the text to all other material used. Throughout this thesis and in all related publications I followed the guidelines of “Good Scientific Practice and Ombuds Committee at the Medical University of Graz”.

Graz, February 2020

Julia Fuchs

Disclosures

Please note that parts of this doctoral thesis are already published in:

Fuchs, Julia; Mueller, Marc; Daxböck, Christine; Stückler, Manuela; Lang, Ingrid; Leitinger, Gerd; Bock, Elisabeth; El-Heliebi, Amin; Moser, Gerit; Glasmacher, Birgit; Brislinger, Dagmar *(2018): Histological processing of un-/cellularized thermosensitive electrospun scaffolds. Histochemistry and cell biology. DOI: 10.1007/s00418-018-1757-7*

All co-authors here presented gave their written consent to re-use the data from the publication within this thesis. The following co-authors contributed to the data shown in the thesis:

- Marc Müller[2] and Birgit Glasmacher[2] conducted the fabrication and characterization of PCL/PLA scaffolds. SEM images of the PCL/PLA fibers were taken and arranged by them.
- Christine Daxböck[1] and Manuela Stückler[1] contributed with immunofluorescence staining shown in Figure 11, Figure 12, and Figure 21.
- Ingrid Lang[1] helped with her knowledge in IHC and cell isolation of primary endothelial cells, and provided endothelial cells from the human vena iliaca for the project.
- Elisabeth Bock[1] and Gerd Leitinger[1] supported with their expertise in electron microscopy and helped to apply acrylic resin embedding of the samples shown in Figure 9 and Figure 10.
- Gerit Moser[1] contributed with her extensive expertise in the field of embryology and trophoblast invasion.
- Amin El Heliebi[1] supported the design of primers and padlock probes for mRNA targeting by *in situ* padlock probe approach shown in Table 5 and Figure 15.
- Dagmar Brislinger[1] supervised the experimental design and provided critical discussions along the whole project. She supported the research work and revised the manuscript and thesis.

[1] Department of Cell Biology, Histology and Embryology; Gottfried Schatz Research Center; Medical University of Graz, Austria

[2] Institute for Multiphase Processes; Leibniz University, Hannover, Germany

Copyright permission to use illustrations and/or tables has been obtained from the respective copyright holders and is stated with the corresponding license number below relevant images.

Acknowledgements

This thesis was performed at the Medical University of Graz, Doctoral Program for Translational Molecular and Cellular Biosciences at the Division of Cell Biology, Histology and Embryology, Gottfried Schatz Research Center.

This work was supported by the Austrian Science Fund (FWF Project: Flexibility in Organ Research", Proj. Number: PIR 7, recipient: Dagmar Brislinger), Christian Doppler Research Association ((CDG) Proj. Number: PIR7-B28) and the Deutsche Forschungsgemeinschaft (DFG, German Research Foundation) for the Cluster of Excellence REBIRTH (EXC 62/1).

I would like to thank the members of the Doctoral School for Translational Molecular and Cellular Biosciences for the funding of bench costs.

At this point, some personal words…

I would like to express my deepest gratitude to my supervisor Dr. Dagmar Brislinger for giving me the opportunity to conduct the Doc. scient. med. Program under her supervision and for her tireless support and guidance in working and private spheres during this process.

I would further express my thanks to Dr. Stadlbauer-Köllner and Prof. Günter Koraimann for the productive discussions and their support as members of my dissertation committee.

My sincere thanks go to all my colleagues and friends from the Division of Cell Biology, Histology and Embryology for their constant care and assistance, their countless encouraging words and the numerous amusing conversations during the daily work.

Finally, I would like to thank my family and all the wonderful people who supported me in every thinkable way during the period of this doctoral thesis.

I will always associate this time with cheerful memories.

Thank you!

Table of Contents

Abbreviations and Definitions

2D:	Two-dimensional
3D:	Three-dimensional
°C:	Degree Celsius
ANOVA:	Analysis of variance
CK7:	Cytokeratin 7
CO_2:	Carbon dioxide
CT:	Cytotrophoblast
d:	days
ECM:	Extra cellular matrix
EGM-MV:	Endothelial Cell Growth Medium - microvascular
EVT	Extravillous Trophoblast
FBS:	Fetal bovine serum
g:	Grams
h:	hour
HBSS:	Hanks' Balanced Salt Solution,
hCG:	Human chorionic gonadotropin
HE:	Hematoxylin/Eosin
HIVEC:	human iliac vein endothelial cells
IF:	Immunofluorescence
Ig:	Immunoglobulin
IHC:	Immunohistochemistry
IUGR:	Intrauterine growth restriction
L:	Liter
µg:	Micrograms
µl:	Microliter
µm:	Micrometer
µM:	Micromolar
mg:	Miligram
mM:	Milimolar
ml:	Milliliter
mm:	millimeter
min	minute
M:	Molar
ng:	Nanogram
nm:	Nanometer
nM:	Nanomolar
O_2 :	Oxygen
PBS:	Phosphate-buffered saline
PCL:	Polycaprolactone
PE:	Preeclampsia
PFA:	Paraformaldehyde
PLA:	Polylactic acid
PS:	Penicillin/Streptomycin
kGy:	Kilo Gray
pH:	Potential of hydrogen
RNA:	Ribonucleic acid
RT:	Room temperature
SEM:	Scanning electron microscopy
SMA:	Smooth muscle actin
SCT	Syncytiotrophoblast
NaCl:	Sodium chloride
SD:	Standard deviation
TBS:	Tris-buffered saline
U:	Units
vWF:	Von Willebrand factor

Zusammenfassung

Die Invasion von Trophoblasten in das mütterliche endovaskuläre System ist ein entscheidender Schritt im Implantationsprozess der menschlichen Blastozyste in den Uterus. Fehlschläge in diesem Prozess sind oft mit Schwangerschaftspathologien verbunden, die schwere Komplikationen für die Mutter und den Fötus zur Folge haben. Daher ist es notwendig, innovative Forschungsmethoden zu entwickeln, um unser Wissen in diesen Prozess zu erweitern und neue Behandlungsmöglichkeiten zu finden. 3D-Zellkultursysteme spielen bei der Untersuchung des Invasionsprozesses von Trophoblasten eine wichtige Rolle, da sie die Möglichkeit bieten Situationen möglichst *in vivo*-nahe nachzustellen.

Um die Interaktion zwischen Trophoblasten und den mütterlichen Endothelzellen in der frühen Schwangerschaft weiter zu untersuchen, wurde in dieser Arbeit ein neuartiges matrixbasiertes 3D-Zellkultursystem angewandt. Dabei wurden biologisch abbaubare PCL/PLA Hohlfasern verwendet. Geeignete histologische Verarbeitungsmethoden und die Validierung von Antikörpern zur Charakterisierung plazenta-spezifischer Zelltypen sind Grundvoraussetzungen, um die Proben dieses 3D-Plazenta-Modells analysieren zu können. Da PCL/PLA Hohlfasern thermosensitive Eigenschaften besitzen, mussten diese mit einem speziell entwickelten Einbettungsverfahren unter der Verwendung von Paraffin mit niedrigem Schmelzpunkt histologisch verarbeitet werden. Die Kombination dieses Verfahrens mit einer hitzereduzierten enzymatischen Antigendemaskierung machte es möglich, Zellen zu identifizieren und analysieren, welche in die PCL/PLA Membran eingewandert sind. Mit Hilfe einer computergestützten Auswertung, wurden die Proben quantitativ und qualitativ analysiert.

Die quantitative Evaluierung der Immunfluoreszenzfärbung zeigte das Intensitätsmuster von 17 plazenta-spezifischen Antikörpern. Die zughörige qualitative Analyse ergab, dass bestimmte Antigendesmaskierungsmethoden zur Färbung mehrerer Zelltypen innerhalb eines Gewebes führen. Um eine umfassende Interpretation der Daten histologischer Präparate gewährleisten zu können, ist es notwendig, quantitative Analysen immer in Kombination zugehöriger qualitativer Analysen zu betrachten.

Die erfolgreiche Etablierung der Paraffineinbettung mit niedrigem Schmelzpunkt in Kombination mit der enzymatischen Antigendemaskierung mit Pepsin zur histologischen Charakterisierung zeigte, dass Trophoblastenzellen im angewandten 3D-Zellkultursystem unter normoxischen (21% O_2) Bedingungen zu proliferieren beginnen. Unter hypoxischen (2.5% O_2) Bedingungen zeigten die Trophoblasten eine Einwanderung in das PCL/PLA-Fasernetzwerk. Unter Verwendung der Zelllinie ACH-3P wurde diese Migration in Richtung primärer Endothelzellen auch als Co-Kultur dargestellt.

Abstract

Trophoblast invasion into the maternal endovascular system is a crucial step in the implantation process of the human blastocyst. Failures in this process are often associated with pregnancy pathologies that cause severe complications for the mother and the fetus. Therefore, it is necessary to establish innovative research methods to improve our knowledge about placental implantation and enable new kinds of treatments. 3D cell culture systems play a major role in the investigation of these processes, as they offer the possibility to reflect *in vivo*-like situations.

A novel matrix-based 3D placenta cell culture system to investigate the interaction of trophoblasts and maternal endothelial cells in early human pregnancy is currently established in our lab. This system uses biodegradable and thermosensitive PCL/PLA hollow fibers. An appropriate histological processing method and validation of antibodies for the characterization of placenta specific cell types are basic requirements to fulfil the needs of this 3D placenta model. The thermosensitive PCL/PLA samples were histological processed with our established low-melting-point paraffin embedding method focusing on the histological examination of the trophoblast migration towards endothelial cells under normoxic (21% O_2) and hypoxic (2.5% O_2) conditions.
By the combination of a low-melting-point paraffin embedding and a heat-reduced enzymatic antigen retrieval method it was possible to identify and analyse migrated cells within the membrane. Computational assisted evaluation was done to analyse the samples in a quantitative and qualitative way. Quantitative analyses of the immunofluorescent staining showed the intensity pattern of 17 placenta specific antibodies. Qualitative analysis revealed that certain antigen retrieval methods lead to the staining of several cell types within the tissue.

The successful establishment of low-melting-point paraffin embedding combined with enzymatic antigen retrieval with pepsin for the histological characterization, revealed proliferation of trophoblast cells under normoxic conditions whereas cells started to migrate into PCL/PLA fiber network of the membrane under hypoxic conditions in our novel 3D placental cell culture system.

Using the cell line ACH-3P, trophoblast migration towards primary endothelial cells also was shown under co-culture conditions. In addition, it is important to mention that for histological preparations a quantitative analysis must be accompanied by a qualitative analysis and vice versa in order to provide a comprehensive interpretation of the data.

1 Introduction

1.1 The human placenta

The human placenta is a highly specialized transitional organ specifically developed for the needs of the fetus during pregnancy. To fulfil these requirements, the placenta and its surrounding tissue are functionally modified as the pregnancy progresses. These modifications include vasculogenesis and angiogenesis, arterial dilation to increase the blood flow within the placenta and changes of the arterial walls. Furthermore, the protein and receptor expression patterns, as well as the metabolic and hormonal profile changes (1–3).

The placenta fulfils a variety of functions that are crucial for a successful pregnancy. It provides the fetus with the necessary supply of oxygen and nutrients (2, 3), while eliminating waste products such as carbon dioxide and urea (4, 5). In addition, the placenta produces and secrets various growth factors, hormones and cytokines necessary for the optimal development of the fetus (2, 3, 6). Apart from its metabolic and transport functions, this organ also constitutes a protective barrier against various kinds of pathogens (1, 3, 7).

In a genetic view, the placenta combines two completely different sides. On the one hand, there is the maternal side, also known as decidua that directly develops from the endometrium of the uterus. On the other hand, there is the fetal side originating from the chorion that is derived from the trophoblast and the extraembryonic mesoderm. The chorionic villi, finger-like protrusions, contain a numerous amount of vascularized structures that determine the exchange of nutrients, gases and waste products between the mother and the fetus (1, 8).

1.2 Extravillous Trophoblast Invasion

Trophoblast invasion into the uterus is a crucial step in the implantation process of the human blastocyst. Implantation takes place interstitially by enveloping the blastocyst through the endometrium (9, 10).

When implantation and placentation have been initiated, placental villi develop, containing a mesenchymal nucleus surrounded by cytotrophoblast (CT) stem cells, which fuse to form the overlying multinucleated syncytiotrophoblast (SCT) and the anchoring villi. During the first two weeks of gestation, CT cells migrate through the SCT layer and build columns that differentiate into extravillous trophoblast cells (EVTs) as shown in Figure 1 and Figure 2 (3, 11, 12). Subsequently, these extravillous trophoblasts begin to proliferate extensively and migrate from the tips of the anchoring villi into placental structures as decidualized endometrium and myometrium. These EVTs are then classified as interstitial trophoblasts (Figure 2, route 1) (3, 12, 13). The process of trophoblast differentiation into an invasive phenotype is strictly regulated regarding spatial as well as temporal aspects, which making it essential for the success of the pregnancy. This phenotypic change is indispensable for cell migration (3)

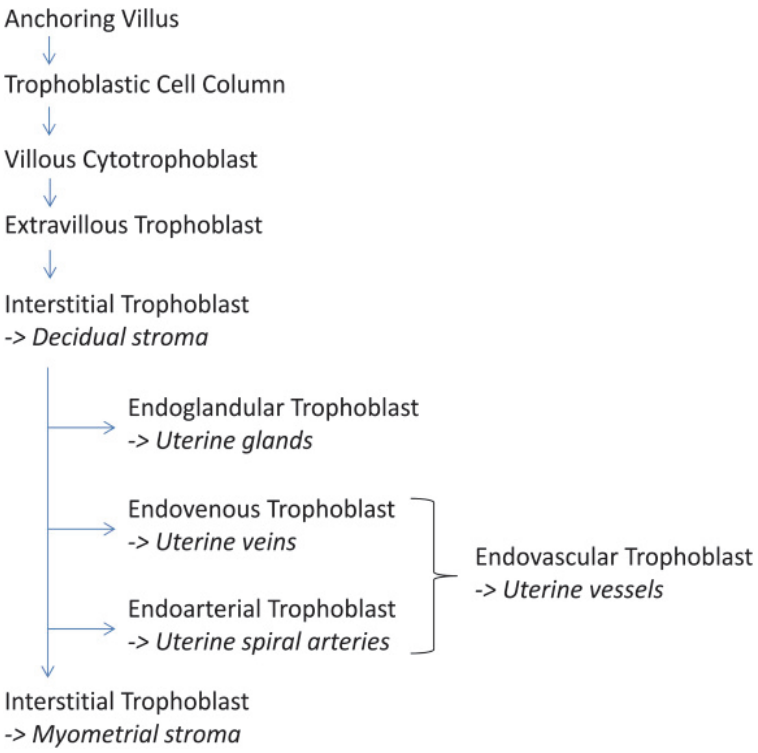

Figure 1: Nomenclature of various subtypes of trophoblast cells depending on their location. Reproduction from Moser *et al.* 2017 (18) with permission of publisher "W.B./SAUNDERS CO. LTD." by license number 1015353-1.

There are significant phenotypic differences between invasive extravillous trophoblasts and villous CTs which are reflected in the expression of cell surface molecules and in the secretion of cytokines, growth factors and proteases (13). As they move in the decidua, interstitial trophoblast cells become multinucleate and round and form placenta bed giant cells (14). These non-proliferating placenta bed giant cells are regarded as the endpoint of differentiation of the extravillous route (11, 15). Trophoblast cells also migrate in a retrograde direction and invade through the uterine interstitium along the spiral arteries (3, 9). This results in a comprehensive remodelling of the arterial walls and an extension of the arterial lumen to ensure a sufficient blood circulation for the fetus (9).

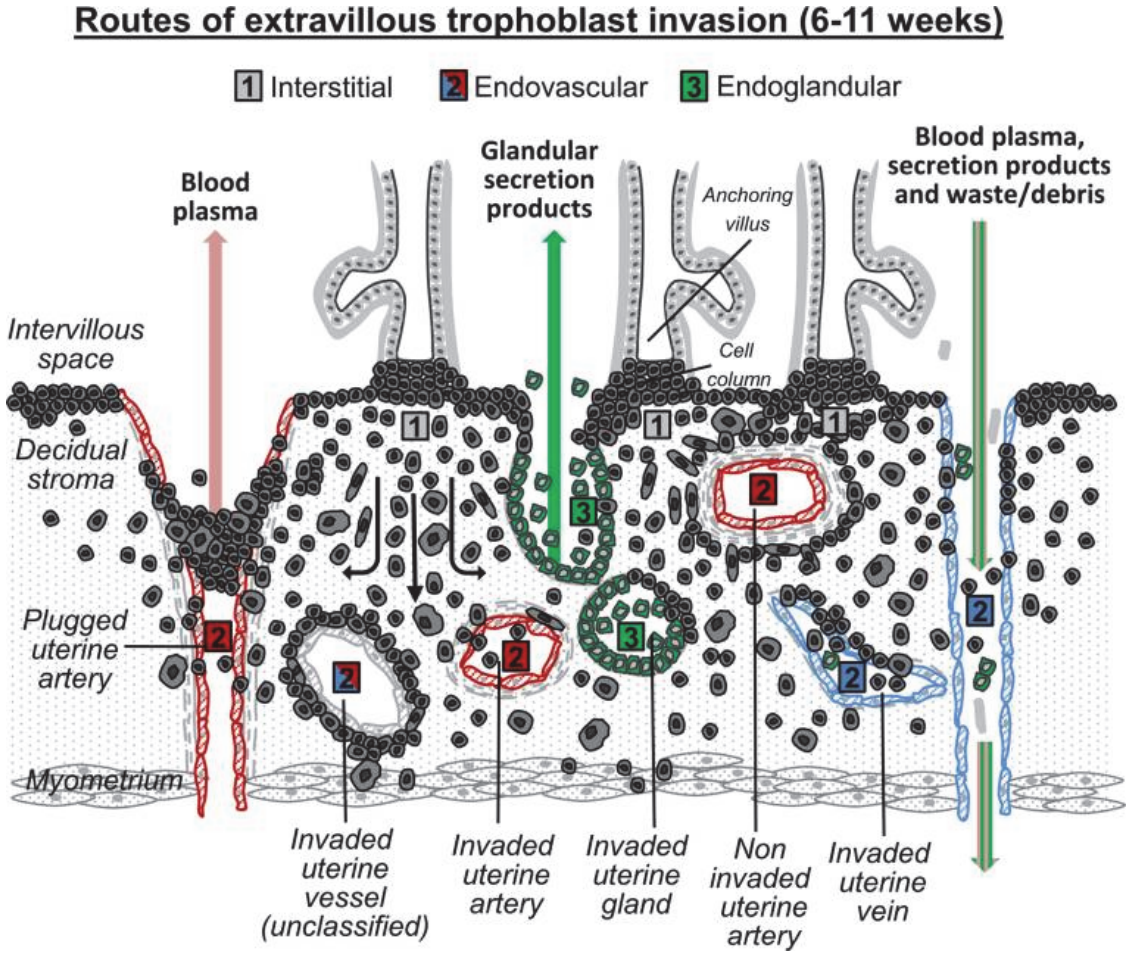

Figure 2: Extravillous trophoblast invasion. EVT originate from cell columns of anchoring villi. The interstitial trophoblast (**1**) invades through the decidua into the maternal myometrium and attaches the placenta to the uterus. Endovascular trophoblasts (**2**) invade into spiral arteries, line and remodel them to establish the maternal blood flow towards the placenta. Endoglandular trophoblasts (**3**) invade into uterine glands and thereby support histiotrophic nutrition of the embryo.

Reproduction from Moser *et al.* 2017 (12) with permission of publisher “SPRINGER-VERLAG” by license number 4680761409556.

In the early 2000s the scientific community assumed that EVTs only invade into arteries and not into other placental tissue structures (3). Recent publications from Moser *et al.*, however, refuted this statements and showed that EVTs also migrate into veins, lymphatic vessels or glandular structures (12, 16, 17). Therefore a new definition of the terminology of extravillous trophoblast had to be introduced (Figure 1) (12).

According to the latest classification by Moser *et al*., EVTs invading into arteries or veins are summarised under the term endovascular trophoblasts (10, 12). Cells that are only invading and transforming the uterine spiral arteries are referred to as endoarterial trophoblasts. These cells plug, line and remodel spiral arteries, decreasing the flow of maternal blood. As a consequence, the fetus is supplied with an appropriate amount of nutrients and protected against oxidative damage. Trophoblasts invading into uterine veins are termed endovenous trophoblasts (Figure 1) (12, 16, 18). The invasion routes of endovascular trophoblasts are shown in Figure 2, route 2.

Another side branch of EVTs invade into the uterine glands. These cells are called endoglandular trophoblasts (Figure 1) (19). The invasion routes of endoglandular trophoblasts are shown in Figure 2, route 3. The trophoblast replacement of uterine gland epithelial cells and opening of the uterine glands to the intervillous space provide the embryo with histiotrophic nutrition before the onset of maternal blood flow (19). Apart from the histiotrophic nutrition of the embryo during the implantation process, it is still unclear what exact role uterine glands play in pregnancy.

However, recent findings indicate that even after implantation, these glands continue to supply nutrient components such as proteins, carbohydrates and lipids as well as immunosuppressive factors to the intervillous space of the placenta. It is speculated that failure in the invasion process of the uterine glands can cause pregnancy pathologies and may be responsible for spontaneous miscarriages due to the lack nutrition for the embryo. Thus, the impact of the uterine glands during pregnancy is currently under research (19, 20).

1.2.1 Role of Oxygen in Trophoblast Invasion

Oxygen plays a central role in the process of differentiation and invasion of extravillous trophoblasts. In the first trimester of pregnancy extravillous trophoblast invasion of the spiral arteries leads to a blockage of these vessels until the end of the first trimester (Figure 2, route 2) (9). These extravillous trophoblast-plugs only leave space for plasma to seep through and generate a physiological hypoxic environment. This physiological and thus normoxic oxygen concentration for the embryo is about 2.5% (21, 22). Measurements showed that the oxygen concentration in the endometrium in the first trimester of pregnancy is significantly higher (13). Thus, the early pregnancy time span is characterized by a steep oxygen gradient from the decidua towards the embryo (10).

At the lowest oxygen concentration of the gradient, the proximal parts of the cell columns of anchor villi are located (Figure 3). The trophoblast cells are stimulated to increase their proliferation activity by that gradient that is an essential factor for placental growth. Additionally, trophoblasts have a low invasive capacity due to the low oxygen concentration (10, 23, 24). Hence, less reactive oxygen species are produced, which minimizes the risk of genetic disorders of the embryo.

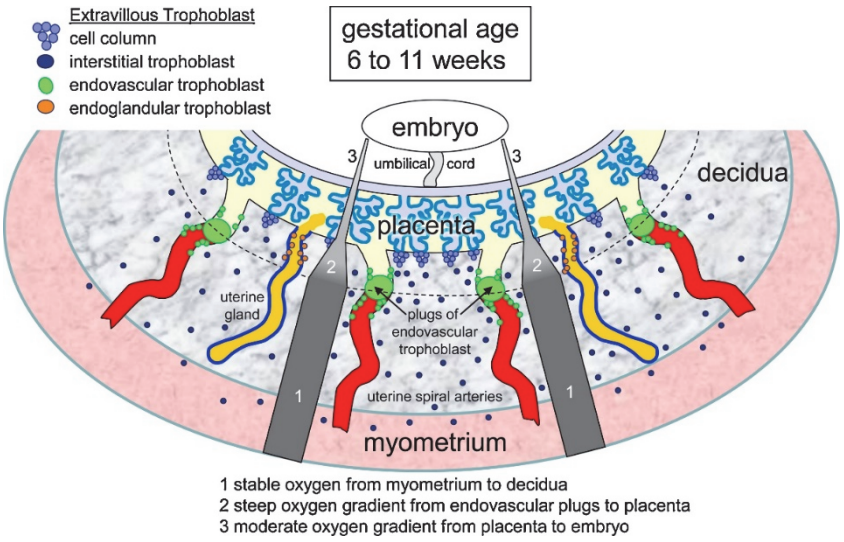

Figure 3: Oxygen gradient during the first trimester of human pregnancy. The grey bars with numbers 1–3 indicate oxygen changes from the myometrium to the embryo. **3** displays the area of the lowest oxygen concentration of about 2.5%. This value rises towards decidua to 21% oxygen (**1**), creating a gradient with increasing oxygen levels (**2**).
Reproduction from Huppertz et al. 2014 (10) with permission of publisher “Elsevier” by license number 4757051197714.

The pressure generated by the proliferating trophoblasts forces their daughter cells towards the maternal tissue, which increases the oxygen concentration at the end of the distal parts. This switches the EVTs from their proliferative to an invasive potential. Thus, endovascular trophoblasts invade the spiral arteries and form plugs that are dissolved at the beginning of the second trimester, allowing maternal blood cells to enter the intervillous space. Consequently, the oxygen concentration rises and the oxygen gradient disappears. (10)

Regarding these factors, it is not surprising that increased oxygen levels in early pregnancy can lead to complications and spontaneous abortion (23–25).

1.3 Prenatal complications

Failures of trophoblast invasion and spiral artery transformation are often associated with pregnancy pathologies like pre-eclampsia (PE) and intrauterine growth restriction (IUGR). These disorders receive a lot of attention as they cause severe complications for the mother and the fetus (26, 27).

With a prevalence of 2-8% among pregnancies, pre-eclampsia accounts for more than 50,000 maternal deaths worldwide each year (28, 29). Typically, the clinical signs of a severe progression begin in the second trimester of pregnancy as a result of abnormal implantation and are characterized by symptoms such as hypertension and proteinuria (30). The pathophysiology of PE is not yet fully understood due to its complexity and broad clinical presentation (27, 31). However, it is assumed that the incorrect transformation of the spiral arteries is caused by changes in the expression of cell adhesion molecules and matrix metalloproteinases (32). Consequently, placental ischemia and oxidative stress lead to endothelial dysfunction that is responsible for the clinical symptoms (29, 32). Since no causal therapy exists to date, the only effective treatment option is premature delivery (27).

IUGR affects between 7-9% of pregnancies globally, with a strong association of unexplained stillbirths (33). Here, the fetus cannot develop its full growth potential due to anatomical and functional complications. The main symptom leading to IUGR is placental insufficiency that results in an impaired fetoplacental blood flow further causing hypoxia and acidosis.

IUGR can be classified into an early and a late stage of occurrence. The late onset of IUGR is usually accompanied by mild complications for the newborn (31). Early onset IUGR very often occurs in combination with PE and usually causes rapid deterioration of the fetal conditions such as severe neurological, metabolic, cardiovascular and respiratory disorders

that result in a high mortality and morbidity rate (26, 34). New systematic approaches are constantly being explored to reduce the complications that occur following an IUGR diagnosis (31). So far, the mechanism behind this pregnancy complication has not been fully understood, resulting in a lack of effective therapies (32).

It is necessary to establish innovative methods in research in order to improve our knowledge of pregnancy-associated diseases like PE and IUGR and provide further treatment. 3D cell culture systems play a major role in the investigation of pregnancy-associated diseases as they can be used to reflect *in vivo*-like situations, and may contribute to a better understanding of pregnancy-related pathologies.

1.4 ACH-3P – A first trimester trophoblast cell line

A wide range of trophoblast-derived cell lines have been extensively studied to model the multiple and diverse functions of the human trophoblast (35–37). Research is also conducted on invasion processes with primary trophoblasts. However, due to the availability of first trimester placental tissue and the lifespan of primary first trimester trophoblasts in cell culture, these investigations are limited due to terminal differentiation and entering phases of apoptosis (38). *In vitro* 3D cell culture experiments with first trimester trophoblasts have not been used for long-term cell culture in this study.

Combining first trimester trophoblast properties with the proliferation potential of the choriocarcinoma cell line AC1-1 makes ACH-3P a useful candidate for studying trophoblast invasion *in vitro* (38).

As the choriocarcinoma cell line ACH-3P was created by fusion of first trimester trophoblasts and the choriocarcinoma cell line AC1-1, the cell line contains subpopulations of villous and extravillous trophoblasts, with their associated expression patterns (38, 39).

The expression of specific EVT markers as cytokeratin 7, HLA-G (HLAG- positive and negative trophoblasts (39)), integrin α5β1, MMP-2 and MMP-9 is a characteristic of the expression pattern of the ACH-3P cell line. In addition, markers for proliferating CTs and villous SCTs, such as integrin α6β4 and β-hCG are present in the expression pattern. Besides the expression of trophoblast-specific cell surface markers, ACH-3P cells also provide the potential to invade extracellular matrices and form a transcriptome similar to the parental first trimester trophoblast (38).

Combining the properties of first trimester trophoblasts and the proliferation potential of the choriocarcinoma cell line turns ACH-3P into a very suitable cell line to investigate trophoblast invasion *in vitro*. ACH-3P has been successfully used in research, confirming its potential as a cell line that offers substitution for first trimester trophoblasts in certain aspects (39–41).

1.5 3D Cell culture systems

The importance of the conventional cell culture is non-controversial. Biochemical pathways and effects of treatments in single cell types can be identified in standardized processes. Nevertheless, the gap between a two-dimensional cell culture experiment and a complete organism is difficult to bridge, thus results can hardly be related. Experiments in the two-dimensional cell culture lack the proper environmental context and structural architecture that often leads to changes in the cellular functions (42). In addition, traditional animal experiments are costly and ethically questionable since they cannot reliable predict clinical outcomes. The physiology, pathophysiology, function and formation of an organ are in their complexity worth to investigate. Although tissue and organ cultures pose a challenge to the experimental design, investigations based on these systems will represent the *in vivo* situation closer than conventional two-dimensional cell culture (42–44). Therefore, research on the establishment of three-dimensional cell cultures should be intensified and promoted.

3D-cell culture offers the possibility to simultaneously grow different cell populations in a controlled manner so that *in vivo*-like structures and functions can be observed and reproduced. These systems offer the possibility for increased cell-cell contact, communication and even activation of signalling pathways (43). Depending on the cell material and the cultivation method, several three-dimensional culture models exist. Usually, cell lines are used in the first step to establish a novel 3D-cell culture system. In a second step, experiments can be conducted with primary cells isolated directly from donor material (45). Also the cultivation of whole tissue explants on scaffolds is a common application in 3D-cell culture (45, 46).

In general, two types of 3D-cell culture systems can be distinguished, which are referred to as either scaffold-based or scaffold-free techniques.

1.5.1 Scaffold-free 3D cell culture systems

In contrast to 2D-cell cultures that show monolayer structures, 3D-cell cultures produce multi-layered cell aggregates with complex tissue organisation comparable to the *in vivo* situation (42, 47).

The most common scaffold-free type of 3D-cultures are cell aggregates, so-called spheroids, which serve as physiological models. Generally, spheroids are smaller and less resistant than cell aggregates obtained by matrix-based 3D-cell cultures (48). The most important methods to generate these systems include the forced floating method, the hanging drop method (49, 50) and the agitation method (50).

The forced floating method uses well plates coated with low adhesion-polymers. After a centrifugation step, these well plates are filled with cell suspension enabling the formation of spheroids (42, 50).

The hanging drop method involves placing an aliquot of cell suspension in a MicroWell MiniTray (51). By inverting the plates, the aliquots are transformed into droplets which form compact and homogeneous spheroids at their tips (50, 51).

Agitation-based approaches that use bioreactors also offer an alternative way to obtain spheroids. By inserting a suspension of cells into a rotating bioreactor, isolated cells gradually coalesce into aggregates as they are prevented from adhering to the reactor wall by continuous stirring. This results in a broad variety of spheroids (43, 50).

1.5.2 Scaffold-based 3D cell culture systems

The need for a matrix becomes obvious with the increasing size and complexity of the respective 3D model. In addition to spatial control, cellular aggregates also require a careful exchange of nutrients and gases. Aggregate thicknesses of 1-2 mm lead to increased cell death, as these thicknesses causes insufficient mass transfer, mainly due to a limited exchange of nutrients and waste materials (49, 52, 53). Thus, spheroids are composed of cells in several stages, including proliferating, resting, apoptotic, hypoxic and necrotic cells and are restricted regarding their growth size (43).

As already mentioned, scaffolds provide a practical support for 3D cell culture. Their porosity facilitates the transport of oxygen, nutrients and waste. Thus, it is also possible to supply cells that migrate within the scaffold network. Upon cell proliferation, the maturing cells interact with each other and subsequently develop structures that behave similarly to their originating tissue. In addition, 3D cell culture systems using scaffolds offer a larger surface area to the cells compared to systems without matrix support (50, 52).

It is important that the structure of the scaffold, imitates the properties of the tissue to be developed in scale and function. As the size and complexity of scaffolds increase, however, it becomes more difficult processing them for analytical purposes. To prevent potential difficulties such as those caused by the immune system, the material of the scaffold also needs to provide biocompatible properties to create optimized conditions for cell growth (52). Thus, scaffolds for 3D cell culture systems can be fabricated to different textures using a broad range of materials. These textures include hydrogels or solid scaffolds. Materials that are used for scaffolds vary from synthetic or natural polymers to materials such as metals, glass and ceramics (42).

1.5.2.1 Hydrogel scaffolds

Hydrogels are one of the most commonly used type of scaffolds in 3D cell culture as this material exhibits mechanical properties of a tissue-like structure. The gel-like material actually mimics and serves as an artificial extracellular matrix (ECM), which contains nutrients and soluble factors enabling cells moving within the gel. In addition, cells can interact through direct and indirect communication within hydrogels by excreting chemotactic factors (52, 54). As a replacement for native ECM, hydrogels actually contain a high amount of water and natural biomolecules such as fibrin, gelatine, hyaluronic acid, alginate, agarose, laminin or collagen in various compositions. The solidification process of a gel is often difficult, turning the production and manipulation of gels into a challenging task (54, 55).

1.5.2.2 Solid scaffolds

According to the experimental setup, various types of polymers can be used for scaffold construction. For this purpose, different types of polyester, polyethylene glycol, polyamide, polyglycolic acid or polylactic acid can be found, ranging from inert to biodegradable. Since polymers are easier to modify, they offer a wider range of possibilities for an optimal scaffold construction (54, 56). The most common natural non-gel polymers used for tissue engineering are fibrin, alginate, silk, hyaluronic acid and chitosan. Polylactic acid (PLA), polyglycolic acid and polycaprolactone (PCL) are preferred as synthetic polymers as they can be removed easily by natural physiological degradation processes during *in vitro* tissue formation or after implantation into the body (57, 58).

In addition to the polymers mentioned above, materials such as bioglass or bioceramics are also used as scaffolds as these materials improve the ability of tissue regeneration. Since metals exhibit high compressive strength and excellent fatigue resistance, porous metallic scaffolds, usually made of titanium and tantalum, can also serve as a matrix (50, 57). Often material combinations are applied for scaffold construction. They usually consist of two or more distinctly different materials, such as ceramics in combination with polymers. These combinations offer improved mechanical and physiological properties compared to using only one type of material (48, 57, 58).

1.6 Models to mimic the feto-maternal interface

So far, the following systems have been described in the literature and are already being used in research.

1.6.1 Animal Models

One of the most frequent and widespread methods to study the placental function is animal testing, especially for medical purposes. The use of pregnant animals is a preferred *in vivo* model for investigating the functionalities and pharmaceutical effects of drugs in the placenta. However, the physiology of the human placenta differs enormously from the placenta in animal models making data comparisons difficult. In addition, the time-consuming aspect as well as the financial and ethical constraints imposed by animal experiments are crucial for the decision of researchers to abandon these types of placental experiments (59, 60).

1.6.2 Human placental-explant culture systems

A suitable *in vitro* model that is close to the *in vivo* pattern of trophoblast differentiation is provided by using placental explants from fresh human placenta. Explants from first trimester placental tissue are cultivated on a matrigel bed or in co-culture with maternal decidua. This allows the villi to adhere to and invade into the material, mimicking the establishment of the placenta and its development in the maternal uterus (61). The placental explant model offers several advantages. In contrast to isolated cells, the topology of intact villi is preserved, including all major fetal cell types. In this way all mechanisms of paracrine regulations remain unaffected. Thus, this model mimics trophoblast functions in a more realistic way including the production and release of secretory components, proliferation, growth and differentiation. Placental explant cultures can be performed using tissues from the first trimester placentas as well as from term placentas. Therefore it is possible to compare results during early and late pregnancy (61, 62).

1.6.3 Placenta-on-a-chip / Microfluidic devices

The micro-engineered placenta-on-a-chip represents a new generation of technology that is becoming more demanding in the examination of the placenta. Microfluidic placenta systems are designed for the analysis of drugs rather than the investigation of invasion processes and are thus an adequate model to study the placental barrier.

The placental barrier is a semi-permeable membrane that acts as an interface between maternal and fetal blood circulation during pregnancy. *In vivo*, it consists of trophoblasts and endothelial cells separated by a basement membrane matrix. To establish the multi-layered structure of the placental barrier, two types of placental cells, including trophoblasts

(BeWo) and endothelial cells (HUVEC), are cultured on opposite sides of the cell matrix (63, 64). Therefore, the placenta-on-a-chip *in vitro* model represents the endothelium and the trophoblastic epithelium to enable the interfaces of the fetal and the maternal side of the placenta. A certain arrangement of the cells can be obtained due to the generated flow conditions of the microfluidic devices. Microfluidic systems for placenta experiments allow to collect data in a comparatively short period, reduce sample utilization and mimic the flow of fluids in parallel layers. However, the main problem of the placenta-on-a-chip system is that so far, only few efficient tests for pharmaceutical evaluation can be performed (59, 65).

1.6.4 3D bio-printed Placenta Model

Using bio-printing technology, a placenta model with spatial control of maternal and fetal cells, growth factors and extracellular matrix can be produced. A bio-printing platform makes it possible to reproduce the spiral geometry of the maternal vessels *in vitro* to produce biophysical properties that are very close to those of the placenta. The ability to combine different cell types and biomaterials makes bio-printing particularly attractive for the engineering of the highly complex placental tissue. The 3D placenta bio-printed model was developed to investigate and quantify cell migration. With this model, conclusions about epidermal growth factors can be made on the migration behaviour of trophoblasts and human mesenchymal stem cells. Even though the bio-printed placenta model is a simplified model, it will help to develop more complex and physiological models in the future (66).

1.6.5 Spheroid and Organoid Models

Three-dimensional spheroid and organoid cultures carry the potential to restore *in vivo*-like phenotypes in many *in vitro* organ systems.

Spheroids are 3D cultures consisting of cell aggregates generated from a single cell type or from a multicellular mixture of cells. They are established from immortalized cell lines, primary cells, or fragments of human tissue (59, 61).

The most commonly used spheroid system regarding placenta experiments is the use of the HTR8/SVneo cell line cultivated to spheroids (67). There are also placental spheroid systems consisting of several cell types e.g. mesenchymal fibroblasts that are used to build core structures on which trophoblasts are co-cultivated in a second step (68).

3D spheroids partially express the placental transcriptome and exhibit dynamic invasive behaviour when embedded in an ECM environment. Therefore, placental spheroids provide a useful model for studying trophoblast invasion. In addition, producing spheroids is convenient and inexpensive. Using established cell lines, spheroids are an accessible and versatile tool for researchers (61).

Organoids are typically derived from a single adult stem cell or embryonic stem cell. Building the organoid system, the researchers first isolate proliferating trophoblast cells from first trimester human placentas, seed them into matrigel drops and culture them in a specifically developed trophoblast organoid medium (69).

Organoid cultures are based on self-organisation of progenitor cells, formed by embedding them in a gel-like medium that mimics the extracellular matrix. The self-organization of primary cells leads to tissue-specific organization, as well as to a dynamic balance of stem and differentiated cells. The cultures organize themselves into villi-like structures and secrete placenta-specific peptides and hormones including human chorionic gonadotropin. The organoids also differentiate into extravillous trophoblast cells that invade three-dimensional cultures. Certain organoid cultures still grow even after culturing them for one year, thus exceeding the period of a human pregnancy (69). Due to all these properties organoids provide a suitable model to investigate human placental development and trophoblast invasion.

1.6.6 Establishment of a matrix-based 3D placenta cell culture system

The wide range of possibilities offered by 3D cell culture systems allow different approaches to be applied in artificial placenta models. An appropriate model must be selected individually, according to the scientific question. For studies concerning trophoblast invasion, different models are required than for investigations of the placental barrier. Several *in vitro* placenta model systems exist, but fail to reproduce all important features of the human placenta *in vivo*.

In this thesis the basic requirements and methods for the establishment of a novel *in vitro* matrix based 3D placental cell culture model were performed.

The 3D cell culture model of the placenta consists of an electrospun hollow fiber of polycaprolactone modified with polylactide acid (PCL/PLA) that is fixed in a metal housing to create two discriminative compartments. The inner surface, facing the lumen, representing the inner compartment and an outer compartment (Figure 4). Both sides of the hollow PCL/PLA fiber can be cultivated with cells.
The PCL/PLA mesh allows a cross-talk of cells by the exchange of paracrine factors or offers a direct cell-to-cell contact. The cells in the inner and outer compartments are cultured under conditions appropriate to their requirements. These include nutrient supply fluctuations in oxygen concentration or flow rate (Figure 4).

In the 3D cell culture model of the placenta the inner compartment represents the maternal spiral artery. For this purpose, the PCL/PLA hollow fiber is cellularized with primary endothelial cells from the human vena iliaca (HIVEC) on the inner surface of the membrane.

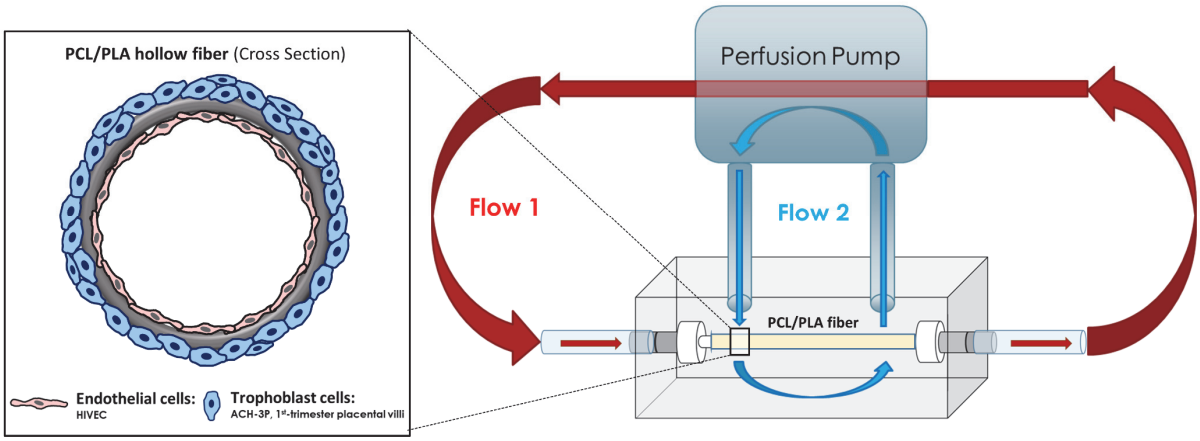

Figure 4*:* Endothelial cells are seeded on the inner surface while trophoblast cells are cultured on the outer surface of the PCL/PLA scaffold. Subsequently, the PCL/PLA hollow fiber is integrated in the bioreactor. An inner and/or an outer flow can be imitated using a perfusion pump system. Cells in the inner and outer compartment are applied to conditions appropriate to their requirements, regarding oxygen concentration, nutrition supplies, or flow rates.

Trophoblast cells like ACH-3P cells or villi from first-trimester placentas are cultured on the outer surface of the PCL/PLA hollow fiber mimicking the *in vivo* situation of trophoblast invasion in the first trimester of placental development.

Initially, investigations are performed using static conditions. Oxygen rates are set to either hypoxic (2.5% O_2) or normoxic (21% O_2) conditions.

At a later stage of the project, the system will be connected to a perfusion circuit to mimic the physiological blood flow by applying a defined shear stress to the cells. The internal and external circulation could thus be treated using different flow rates. In a further step, the trophoblast cells in the outer compartment could be cultivated under hypoxic conditions using 2.5% oxygen, while the endothelial cells in the inner compartment are cultured under normoxic oxygen conditions of 21%. This treatment would produce an oxygen gradient equivalent to the *in vivo* conditions occurring during trophoblast invasion.

2 Aims

The present study aimed to establish basic requirements and methods for a novel matrix-based 3D placenta cell culture system to investigate the interaction of adult endothelial cells and trophoblast cells in early human pregnancy. Focusing on the endovascular trophoblast invasion route, human iliac venous endothelial cells, the trophoblast cell line ACH-3P as well as first trimester placenta villi were used for this project.

We aimed to establish a heat-sensitive histological processing and enzymatic antigen retrieval method for the histological characterization of cells within thermosensitive samples used for the 3D cell culture model of the human placenta. The work focused on the automated quantitative and qualitative characterization of the expression pattern of migrated cells within the matrix using placenta-specific antibodies.

The main objectives were summarised as follows:

Establishment of basic requirements and methods for a novel matrix-based 3D placenta cell culture system focusing on the endovascular trophoblast invasion route, such as

- Histological processing by establishing histological processing and enzymatic antigen retrieval method for thermo-sensitive materials
- Automated quantitative and qualitative histological Characterization of migrated cells within PCL/PLA material using placenta specific relevant antibodies
- Histological characterization of trophoblast invasion under normoxic (21% O_2) and hypoxic (2.5% O_2) conditions

3 Material and Methods

Please note that parts of the "Material and Methods" section are based on the publication of Fuchs *et al.* 2018 (58).

3.1 Fabrication of multilayer grafts

Vascular scaffolds were developed and manufactured by our cooperation partner Dr.-Ing. Marc Müller at the Institute of Multiphase Processes at Leibniz University Hannover. In short, the scaffolds were fabricated using PCL (Mn = 70,000 – 90,000, Sigma Aldrich, Taufenkirchen, Germany) and PLA (poly-L-lactic acid, Mw = 150,000, Natureplast, Ifs, France) polymers.

For conventional single cell culture ACH-3P cells, a two-layered PCL/PLA tube was produced. The inner layer was spun from a blend of PCL (100 mg/ml) and PLA (50 mg/ml), while the outer layer was spun from pure PCL (200 mg/ml).
In contrast, mono-layer tubes with a blend of PCL (200 mg/ml) and PLA (100 mg/ml) were used for tissue cultivation of first trimester placental villi and co-cultivation of ACH3P cells and HIVEC enabling the cells to migrate through the tube.

Polymers were dissolved in 2,2,2-trifluoroethanol (Sigma Aldrich, Taufenkirchen, Germany) with a stirrer for at least 24 h.

The electrospinning process was performed with a custom-made setup that consisted of a high-voltage power supply, a polymer reservoir with a 0.8 mm hollow needle as a nozzle and a grounded collector. A mandrel of stainless steel with a diameter of 4 mm, rotating at 1.000 rpm, was used as a collector. The applied voltage was set to 20 kV, and the distance between the nozzle and collector was 28.5 cm. Each layer was spun for 5 minutes at a flow rate of 3 ml/h (58).

3.2 Material characterization

Measuring of the inner and outer layer grafts fiber diameters was done by using scanning electron microscopy (VP-SEM S3400, Hitachi Europe, Krefeld, Germany). Samples were obtained from eight different scaffolds and coated with gold-palladium using a sputter coater (Sputter Coater SC7620, Fa. Emetich) for 45 seconds at a distance of 5 cm. Five images per sample were acquired, resulting in a total number of 40 images for each layer of the scaffold. Images were acquired at an accelerating voltage of 15 kV, a distance of 7 mm (eucentric) and a magnification of 4000-fold. A line was drawn from the top left to the bottom right of the SEM image. Fiber diameters were measured where the line crossed the fiber using AxioVision 4.7 (Carl Zeiss, Jena, Germany) with three measurements left and right

from the diagonal line, respectively (Fig. 1). At least 10 fibers were measured per image (58).

3.3 Tissue collection

Human first trimester placentas were obtained from the Department of Obstetrics and Gynaecology (Medical University of Graz, Austria) from elective surgical terminations of pregnancy (gestational age between 9 and 10 weeks) after approval by the ethics committee of the Medical University of Graz (No. 31-019 ex 18/19). Informed consents of the women were obtained. For the preparation of formalin-fixed paraffin-embedded (FFPE) sections, the tissue was fixed in 3.7% neutrally buffered paraformaldehyde (PFA; Diapath S.P.A., Martinengo BG, Italy) for 24 h and embedded in standard paraffin as described in Fuchs *et al.* 2018 (58).

3.4 Cell / Tissue Culture

Human first trimester trophoblast cell line ACH-3P (38) kindly provided by Gernot Desoye (Department of Obstetrics and Gynecology, Medical University Graz, Austria) was cultured in low-glucose Dulbecco's modified Eagle medium: Nutrient Mixture F-12 (Sigma-Aldrich, St. Louis, MO, USA) supplemented with 10% fetal bovine serum (FBS; Thermo Fisher Scientific, Waltham, Massachusetts, USA), 1% L-glutamine (200 mM; Thermo Fisher Scientific) and 1% penicillin-streptomycin (PS; Thermo Fisher Scientific).

Primary human vena iliaca endothelial cells (HIVEC) were used as a model for adult human endothelial cells and for the cultivation of the inner compartment of the PCL/PLA hollow fibers. HIVECs were kindly provided by Ingrid Lang-Olip (Division of Cell Biology, Histology and Embryology, Medical University of Graz, Austria). Collecting, storing, and cultivating of these cells was approved by the Ethics Committee of the Medical University of Graz, Austria (No. 19-293 ex 07/08). HIVECs were cultured in T75 cell culture flaks coated with 1% gelatine in Endothelial Cell Basal Media – MV (PC-C-22120, Promocell GmBh, Heidelberg, Germany) supplemented with Endothelial Cell Growth Medium MV SupplementMix and 1 % PS (Thermo Fisher Scientific).

Medium for ACH-3P cells and HIVECs was changed every 2–3 days. All cells were cultivated under standard culture conditions in a 95% humidified atmosphere at 37 °C, 5% CO_2 and 21% O_2. Cells were counted using the automated CASY® Cell Counter + Analyzer (Innovatis AG, Bielefeld, Germany). For respective experiments ACH-3P and HIVECs were also cultivated at reduced oxygen conditions (2.5% O_2).

3.5 Preparation of cellularized and tissue cultured scaffolds of PCL/PLA scaffolds

The PCL/PLA scaffolds were sterilized by gamma irradiation with doses of 25 kGy in accordance with the EN 13485 and ISO11137 criteria (MEDISCAN, Kremsmünster, Austria). Sterile tubular PCL/PLA scaffolds with a length of 50 mm and an inner diameter of 4 mm were used and defined as uncellularized.

The tubular PCL/PLA scaffolds can be cellularized on the internal side as well as on the external side. Scaffolds were coated with 20 µg/ml fibronectin (Sigma-Aldrich, St. Louis, MO, USA) from human foreskin fibroblasts, which was diluted in PBS to a final volume of 10 ml and were air-dried for 1 h at 37 °C before the cells were seeded. On each end of the tubular PCL/PLA scaffold a Luer-Lock was fixed, in order to insert the tube into a metal housing (58).

3.5.1 External Colonization of tubular PCL/PLA scaffolds

For the external colonization of the tubular PCL/PLA scaffolds with ACH-3P cells, sterile medium is injected into the graft with a syringe. The scaffolds were fixed in a small metal housing with Luer-Lock connections. The outer scaffold surface was seeded with ACH-3P cells by filling the metal housing with a 15 ml cell suspension (5×10^5 cells/ml). Non-attached cells were removed after cells being allowed to attach for 5 h at 37 °C in the incubator. To achieve a homogenous cell colonization on the outer scaffold surface, a second seeding step was performed. For this, the graft was rotated 180°, and the ACH-3P cell suspension (5×10^5 cells/ml) was filled into the metal housing. Non-attached cells were removed after 5 h at 37 °C. The attached ACH-3P cells were cultured in growth medium for 14 d without a medium change. A schematic representation of a cellularization of PCL/PLA scaffolds on the external side of the tubular PCL/PLA scaffold is shown in Figure 5.

3.5.2 Internal colonization of tubular PCL/PLA scaffolds

For the internal colonization of the tubular PCL/PLA scaffolds with HIVECs, the sterilized scaffolds were fixed in a metal bioreactor with Luer-Lock connections. 3-way stopcocks were fixed at each end of the outer tubes of the bioreactor. Per tube 1.5 x T75 flaks HIVEC (confluent, 115100/p7) were seeded into the internal compartment. 1 ml HIVEC suspension was aspirated with a syringe and injected into the graft until the suspension could be seen in the supplying silicone tube. At this point the 3-way stopcock was closed and the remaining cell suspension was injected into the PCL/PLA hollow fiber until the medium appears on the scaffold surface. Then the supplying 3-way stopcock was closed to maintain the pressure

in the tube and the syringe was removed. Subsequently, the bioreactor was filled with the required medium to completely cover the PCL/PLA hollow fiber with liquid.

The housing, containing the PCL/PLA hollow fiber, was covered with a sterile lid and incubated under standard culture conditions in a 95% humidified atmosphere at 37 °C, 5% CO_2 and 21% O_2. Non-attached cells were removed after 24 h by changing the medium in the inner compartment by rinsing the tube with fresh medium. A schematic representation of a cellularization of PCL/PLA scaffolds on the internal side is shown in Figure 5.

3.5.3 External tissue culturing of tubular PCL/PLA scaffolds

First-trimester placentas were collected after planned terminations and from recurrent spontaneous abortion (RSA) (gestational age between 9 and 10 weeks) after receiving informed consent. Approval was granted by the ethical committee of the Medical University of Graz (No. 31-019 ex 18/19 and No. 31-333 ex 18/19). The tissue was rinsed in 1 × HBSS, supplemented with 1% PS, placed in culture media (low-glucose Dulbecco's modified Eagle medium: Nutrient Mixture F-12), supplemented with 10% FBS, 1% L-Glutamin and 1% PS. Chorionic villi were dissected under a stereo microscope, applied to the PCL/PLA scaffold and cultivated under standard culture conditions in a 95% humidified atmosphere at 37 °C, 5% CO_2 and 21% O_2 for 7 days. A schematic representation of a tissue cultured PCL/PLA scaffold on the external side is shown in Figure 5.

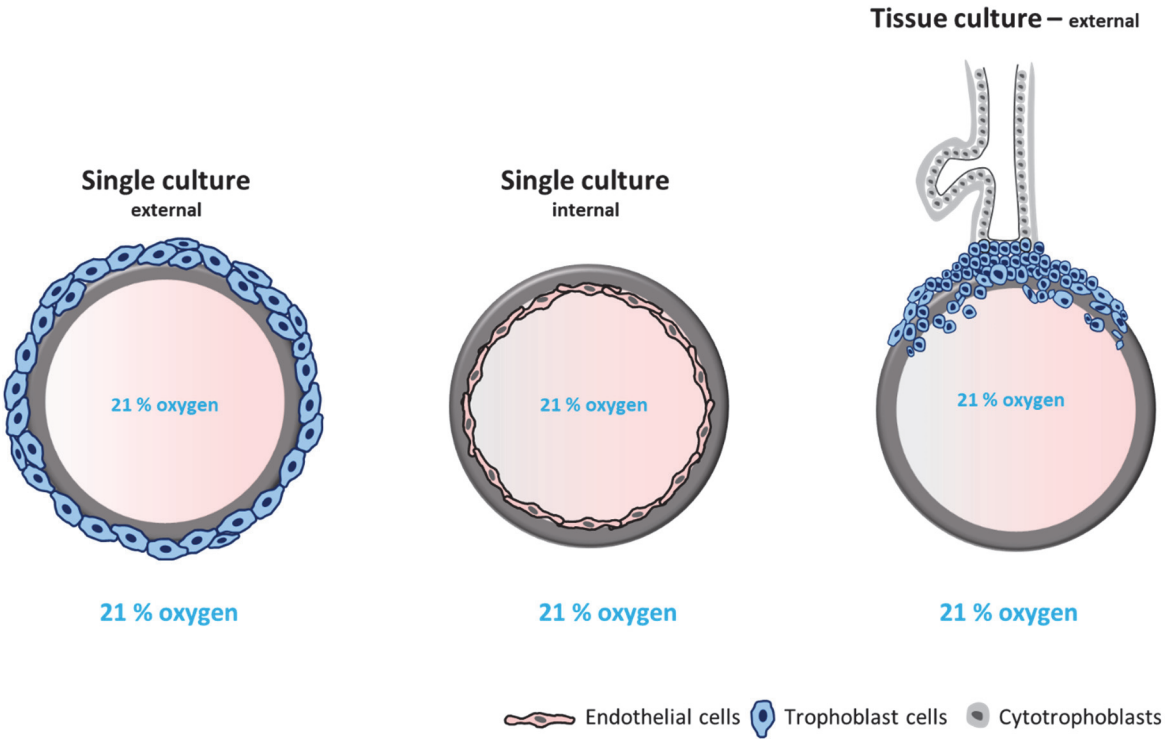

Figure 5: Schematic representation of single cultured trophoblast cells on the external side and single cultured endothelial cells on the internal side of a PCL/PLA tube. The illustration also shows the scheme of a first-trimester placental villi cultured on the outer surface of a homogeneous PCL/PLA tube.

3.5.4 Co-cultivation of ACH-3P and HIVECs on tubular PCL/PLA scaffolds

For co-cultivation of cells, the internal seeding was done as a first step, the external seeding was done directly afterwards. The internal cellularization with HIVECs was performed as described in 3.5.2.

The external seeding procedure for co-cultivation differs from single culture cellularization. Per tube 1.5 x T75 flaks of ACH-3P cells (7.5×10^5 cells/ml) were seeded on the external side of the PCL/PLA scaffold. Therefore, the cells were suspended in 200 µl low-glucose Dulbecco's modified Eagle medium (Nutrient Mixture F-12) supplemented with 10% FBS (Thermo Fisher Scientific), 1% L-glutamine (Thermo Fisher Scientific) and 1% PS (Thermo Fisher Scientific). The ACH-3P cell suspension was brushed on the outer surface of the tube until the whole suspension was depleted. The formation was covered with a sterile lid and incubated for 1 h under standard culture conditions in a 95% humidified atmosphere at 37 °C, 5% CO_2 and 21% O_2. Subsequent, the whole bioreactor was filled with medium, that the cellularized tube was completely covered. Non-attached cells of the inner scaffold surface were removed after 24 h by changing the medium by rinsing the tube with fresh medium. The co-cellularized PCL/PLA tube was incubated under standard conditions for 12 days. For respective experiments the co cultivated scaffold with ACH-3P cells and HIVECs were also cultivated at reduced oxygen conditions (2.5% O_2). A schematic representation of a co-cultivated PCL/PLA hollow fiber under different oxygen conditions is shown in Figure 6.

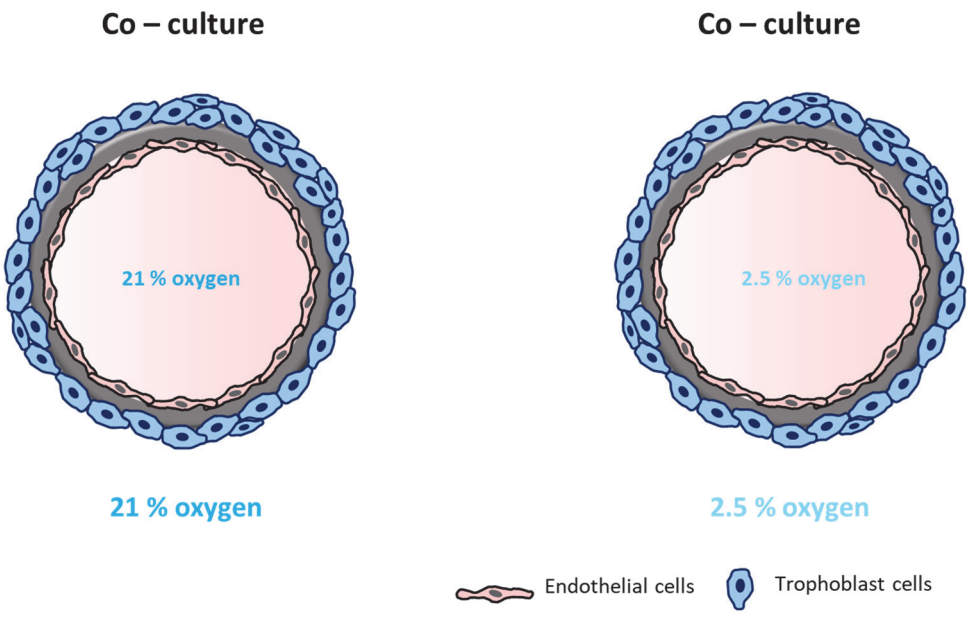

Figure 6: Schematic representation of the co-culture of trophoblast cells on the external side and endothelial cells on the internal side of a homogeneous PCL/PLA tube under different oxygen concentrations.

3.6 Histologogical processing by establishing embedding methods for thermo-sensitive material

PCL/PLA scaffolds provide a variety of possibilities for cell and tissue culture projects due to porosity and surface modifications. However, the histological processing of thermosensitive electrospun PCL/PLA scaffolds fails, as PCL is characterized by its low-melting temperature (Tm = 60 C). The high melting point of PLA (Tm = 180 °C) in combination with PCL does not increase the feasibility of the material. Thus, the melting point of the material is far below temperatures achieved in conventional paraffin embedding and histological processing. The histological processing and automated dewatering, and the standard paraffin embedding of PCL/PLA scaffolds led to the dissolution of the thermo-sensitive material.

For this reason, we established an alternative thermo-sensitive embedding method.

3.6.1 Cryo-fixation and cryo-sectioning of un-/cellularized PCL/PLA scaffolds

Un-/cellularized PCL/PLA scaffolds with ACH-3P cells were fixed in 3.7% paraformaldehyde (PFA; Diapath S.P.A., Martinengo BG, Italy) for 15 min and then were washed in 1 × PBS. Cryosections were produced by embedding the membranes in Tissue-Tek® O.C.T. Compound at -20 °C (Sakura®, Alphen aan den Rijn, The Netherlands) that were then sectioned on a cryotome (Microm HM 560; Histocom, Zug, Schwitzerland) to slices of 7 µm and mounted on SuperFrost Plus™ slides (Thermo Fisher Scientific). Sections were air-dried for 24 h and stored at -20 °C until they were stained. Hematoxylin and eosin (HE) staining was performed on the cellularized scaffolds (58).

3.6.2 Automatized dehydration and standard paraffin embedding of un-/cellularized PCL/PLA scaffolds

Un-/cellularized PCL/PLA scaffolds with ACH-3P cells were fixed in 3.7% PFA for 15 min and washed in 1 × PBS. Automatized dehydration and tissue processing for paraffin embedding of fixed PCL/PLA scaffolds was performed with a Tissue-Tek® VIP® 5 Vacuum Infiltration Processor (Sakura®, Alphen aan den Rijn, The Netherlands) according to conditions listed in Table 1. Standard paraffin embedding of the scaffolds was performed with standard paraffin wax (melting point at a minimum 56 °C; Vogel GmbH & Co. KG, Fernwald, Germany) with the Dispenser Unit of the paraffin embedding center TES Valida® (MEDITE Cancer Diagnostics, Orlando, USA). The paraffin in the paraffin tank was heated to 61 °C to avoid rapid cooling of the standard paraffin while embedding (58).

Table 1: Protocol for tissue dehydration and standard paraffin embedding used by Tissue-Tek® VIP® 5 vacuum infiltration processing. Reproduction from Fuchs *et al.* 2018 (58) with permission of publisher "SPRINGER-VERLAG" by license number 4676480552184.

	Time (min)	Temperature (C°)
Paraformaldehyde (3.7%)	0	40
60% Ethanol	60	40
80% Ethanol	60	40
96% Ethanol	60	40
100% Ethanol	60	40
100% Ethanol	60	40
100% Ethanol	60	40
Tissue Clear	60	40
Tissue Clear	60	40
Tissue Clear	60	40
Paraffin(56 °C)	60	56
Paraffin(56 °C)	60	56
Paraffin(56 °C)	60	56
Embedding		61

3.6.3 Gelatin embedding (5%, 10%, and 25%) followed by automatized dehydration and standard paraffin embedding of un-/cellularized PCL/PLA scaffolds

Un-/cellularized PCL/PLA scaffolds were fixed in 3.7% PFA for 15 min and washed with 1 × PBS. Samples were incubated in 5% gelatin (bovine skin; Sigma-Aldrich, St. Louis, MO, USA) for 30 min at 37 °C followed by an incubation step in 5%, 10% or 25% gelatin solution for 30 min at 37 °C. Afterwards, the samples were incubated for 15 min at 4 °C to harden the gelatin-scaffold block. The construct was transferred to a larger well, prewarmed gelatin solution (5%, 10% or 25%) was added, and the samples were cooled for 15 min at 4 °C. The blocks were transferred into a 3.7% PFA solution (RT, 24 h) and washed in 1 × PBS at

RT. Finally, the PFA-fixed and gelatin-stabilized PCL/PLA scaffolds were embedded in standard paraffin with a Tissue-Tek® VIP® 5 Vacuum Infiltration Processor (Sakura®, Alphen aan den Rijn, The Netherlands) and TES Valida (MEDITE Cancer Diagnostics, Orlando, USA) using the parameters listed in Table 1.

Formalin-fixed-paraffin-embedded (FFPE) blocks were cut into 7 µm sections using an automated rotary microtome (HM355 with STS & Cool-Cut, Thermo Fisher Scientific, Waltham, Massachusetts, USA), and the sections were then transferred to SuperFrost Plus™ slides and dried overnight at 45 °C. HE staining was performed on cellularized scaffolds (58).

3.6.4 Low-melting-point paraffin embedding of un-/cellularized PCL/PLA scaffolds

Un-/cellularized PCL/PLA scaffolds were fixed in 3.7% PFA for 15 min and washed with 1 × PBS. Dehydration and low-melting-point paraffin (melting point 50 °C; Carl Roth, Karlsruhe, Germany) embedding of fixed PCL/PLA scaffolds was performed with a KOS Microwave Multifunctional Tissue Processor (Milestone, Sorisole, Italy). Embedding conditions are listed in Table 2. Embedded scaffolds were cut to sections of 7 µm and transferred to SuperFrost Plus™ slides and dried overnight at 45 °C. HE staining was performed on cellularized scaffolds (58).

Table 2: Protocol for tissue dehydration and low-melting-point paraffin embedding used by KOS microwave multifunctional tissue processing. Reproduction from Fuchs *et al.* 2018 (58) with permission of publisher "SPRINGER-VERLAG" by license number 4676480552184.

	Time (min)	Temperature (C°)
100% Ethanol	13	45
Isopropanol	13	45
Low-melting-point paraffin (50 °C)	23	50
Embedding		

3.6.5 Low-melting-point paraffin embedding of first trimester placental villi cultured on PCL/PLA scaffolds

First-trimester placental villi cultured on PCL/PLA scaffolds were fixed in 3.7% PFA for 24 h and washed with 1 × PBS. Dehydration and low-melting-point paraffin embedding of fixed samples was performed with a KOS Microwave Multifunctional Tissue Processor. Embedding conditions are listed in Table 2. Embedded scaffolds were cut to sections of 5 µm and transferred to SuperFrost Plus™ slides and dried overnight at 45 °C. HE staining was performed on first trimester placental villi cultured scaffolds.

3.6.6 Acrylic resin embedding of un-/cellularized PCL/PLA scaffolds

Un-/cellularized and PCL/PLA scaffolds were fixed in 3.7% PFA for 15 min and washed with 1 × PBS. Specimens were dehydrated with an ethanol series of 50%, 70% to 96% for 15 min each. The scaffold was then treated with 96% ethanol and acrylic resin (LR white; 1:1; Sigma-Aldrich, St. Louis, MO, USA) for 1 h, followed by two incubations with LR white resin for 1 h. The scaffolds were manually embedded in LR white resin in airtight gelatin-capsules (Pohl-Boskamp GmbH & Co. KG, Hohenlockstedt, Germany). For polymerization, the closed capsules were incubated for 3 d at 45 °C. LR white resin blocks were cut into 3 µm sections using a Leica EM UC7 ultramicrotome (Leica Biosystems, Wetzlar, Germany) and mounted on SuperFrost Plus™ slides for 3 h at 47 °C. Cellularized scaffolds were analysed with toluidine blue staining (Agar Scientific, Essex, UK) (58).

3.7 First-trimester placental tissue preparation

Serial FFPE sections (5 µm) were transferred to SuperFrost Plus™ slides and baked for 3 h at 60 °C. Before applying antigen retrieval and immunofluorescence staining, FFPE sections were deparaffinised using Histolab Clear® (Histolab®, Askim, Sweden) solution four times for 5 min each and rehydrated through a graded series of 100%, 96%, 70% and 50% ethanol, followed by three washing steps in distilled water for 3 min each.

3.8 Antigen retrieval testing for placenta specific immunological analyses

To investigate whether pepsin offers an alternative as a thermo-sensitive antigen retrieval method, 17 placenta-relevant antibodies were tested on first trimester placenta tissue (gestational age: 9 weeks) after multiple antigen retrieval treatments.

For standardization of the immunofluorescence staining for each antibody four different Antigen Retrieval slide treatments were performed: (a) no pretreatment, (b) pretreatment with pepsin (Sigma-Aldrich) for 30 min at 37°C (58), and heat induced pretreatment while slides were immersed in (c) in citrate buffer with ph6 or (d) antigen retrieval solution buffer with ph9 (Leica Biosystems, Nussloch, Germany).

An enzymatic antigen retrieval with pepsin was performed by incubating the deparaffinised first trimester placental villi FFPE sections with 2 mg/ml pepsin in 0.1M HCl (Sigma-Aldrich) for 30 min at 37 °C. The treatment was performed in a humidified chamber. The digestions were stopped by washing the slides with distilled water for 2 min.

Heat-induced antigen retrieval (c and d) was performed in a decloaking chamber (Biocare Medical™). The deparaffinised placental villi FFPE sections were completely immersed in

antigen retrieval solution or citrate buffer and steamed for 7 min at 120 °C. Treated slides were cooled at RT for 20 min, washed and stored in distilled water until use.

3.9 Immunofluorescence

Immunofluorescence of external cellularized PCL/PLA tubes with ACH-3P for cell size analysis was performed using a goat-anti-rabbit antibody conjugated with Alexa Flour 633 (A21070; Thermo Fisher Scientific, Waltham, Massachusetts, USA) for detection of CK7 (rabbit antibody) and to visualize ACH-3P cells.

Sections with external seeded ACH-3P were washed with 1 × PBS and incubated with UV Block (Thermo Fisher Scientific, Waltham, Massachusetts, USA) for 10 min. The primary antibody, polyclonal rabbit CK7, was diluted 1:200 in antibody diluent and incubated for 30 min. Subsequently, slides were washed with 1 × PBS and incubated with the secondary antibody, Alexa Fluor 633 goat anti-rabbit (1:200; Thermo Fisher Scientific, Waltham, Massachusetts, USA) for 30 min. Finally, the slides were washed, and the nuclei were stained with DAPI (1:2000; Thermo Fisher Scientific, Waltham, Massachusetts, USA) for 5 min. Rabbit immunoglobulin fraction (5 µg/ml, diluted in antibody diluent, Agilent Technologies) served as a negative control. Sections were mounted with ProLong™ Gold Antifade Reagent (Thermo Fisher Scientific, Waltham, Massachusetts, USA).

Depending on the primary antibody species, immunofluorescence staining on first trimester placenta sections was performed using a goat–anti-rabbit (A21070; Thermo Fisher Scientific, Waltham, Massachusetts, USA) or a goat-anti-mouse (A21050; Thermo Fisher Scientific) antibody conjugated with Alexa Flour 633 (Cy5 – channel) for detection of the primary antibody.

First-trimester placenta sections (5 µm) were washed with 1 × PBS and followed by background blocking with UV Block (Thermo Fisher Scientific) for 10 min. Primary antibody, was diluted depending on the antigen retrieval pretreatment and as recommended in the antibody datasheet, in antibody diluent and incubated for 30 min (used dilutions see Table 3). For antibody stock concentrations see Appendix Table 7. Subsequently, slides were washed with 1 × PBS and incubated with the secondary antibody, Alexa Fluor 633 goat–anti-rabbit or goat–anti-mouse (1:200; Thermo Fisher Scientific) for 30 min at RT. Finally, the slides were washed, and nuclei were stained with DAPI (1:2000; Thermo Fisher Scientific) for 5 min. Sections were mounted with ProLong™ Gold Antifade Reagent (Thermo Fisher Scientific). Rabbit and mouse immunoglobulin fraction diluted in antibody diluent (Agilent Dako) served as a negative control.

Table 3: Comparison of pretreatments for the detection of various antigens in formalin-fixed, paraffin-embedded first trimester placenta tissue.

				Pretreatmentm†			
Antibody	**Animal source**	**Antibody source***	**Code/clone**	**no AR**	**Pepsin**	**Steamer ph6**	**Steamer ph9**
ALPPL2	rabbit	Thermo Fisher Scientific[a]	PA5-22336	1:200	1:100	1:200	1:200
β-Actin	mouse	abcam[b]	AC-15 /ab6276	1:400	1:200	1:400	1:400
CD 163	rabbit	DB Biotech[c]	K20-T	1:100	1:50	1:100	1:100
CD31	rabbit	abcam[b]	Ab28364	1:50	1:25	1:50	1:50
CD34 II	mouse	Agilent Dako[d]	M7165/QBEnd 10	1:50	1:25	1:50	1:50
Cytokeratin 7	rabbit	OriGene Technologies[e]	AP06204PU-N	1:200	1:200	1:200	1:200
Cytokeratin 7	mouse	Thermo Fisher Scientific[a]	OV-TL 12/30	1:400	1:200	1:400	1:400
Desmin	mouse	Agilent Dako[d]	M0760/D33	1:100	1:50	1:100	1:100
E-Cadherin	rabbit	Cell Signalling Technology[f]	24E10	1:400	1:200	1:400	1:400
HLA-G	mouse	Santa Cruz[g]	4H84	1:100	1:50	1:100	1:100
Ki-67	mouse	Agilent Dako[d]	M7187	1:50	1:25	1:50	1:50
Leptin	mouse	Santa Cruz[g]	sc-48408	1:50	1:25	1:50	1:50
Smooth Muscle Actin	mouse	Agilent Dako[d]	1A4 /M0851	1:50	1:25	1:50	1:50
ß-HCG	rabbit	Thermo Fisher Scientific[a]	Ab-2 /RB-059-A	1:100	1:50	1:100	1:100
Vimentin	mouse	Agilent Dako[d]	V9/M0725	1:200	1:100	1:200	1:200
vWF	rabbit	Agilent Dako[d]	F3520	1:3000	1:1000	1: 3000	1: 3000
ZO-1	rabbit	abcam[b]	ab96587	1:100	1:50	1:100	1:100

* Superscript letters refer to sources and manufacturers section, which can be found in the Appendix 7.1.

Antibodies that showed positive staining on first trimester placenta sections after pepsin digestion were tested on PCL/PLA scaffolds seeded with ACH-3P cells or tissue. Immunofluorescence staining was performed after pepsin digestion as described above using goat–anti-rabbit or a goat-anti-mouse antibody conjugated with Alexa Flour 633 (Cy5 – channel) for detection of the primary antibody.

3.10 Sample preparation and enzymatic antigen retrieval testing of PCL/PLA scaffolds cellularized with ACH-3P for immunological analyses

Low-melting-point paraffin sections (7 µm or 5 µm) mounted on SuperFrost Plus™ slides were dewaxed using Histolab Clear® (Histolab®, Askim, Sweden) solution four times for 5 min each and then rehydrated in a graded series of 100%, 96%, 70% to 50% ethanol, followed by three washing steps in distilled water for 3 min each. An enzymatic antigen retrieval with pepsin was performed by incubating cellularized membrane sections with 2 mg/ml pepsin (Sigma-Aldrich, St. Louis, MO, USA) in 0.1 M HCl (Sigma-Aldrich,) for 30 min at 37 °C. Enzymatic antigen retrieval with proteinase K was performed by incubating cellularized membrane sections with 20 µg/ml proteinase K (Roche, Basel, Switzerland) in TE buffer (pH 8.0) (70, 71). Both treatments were performed in a humidified chamber. The digestions were stopped by washing the slides with distilled water for 2 min. For application

of the *in situ* detection padlock probe method samples were dehydrated using an ethanol series of 70%, 85%, and 99.5% for 1 min each and stored at −80 °C until use (58).

3.11 Immunohistochemistry

Immunostaining was performed using an UltraVision Detection System HRP Polymer Kit (Thermo Fisher Scientific, Waltham, Massachusetts, USA) according to the manufacturer's protocol. In brief, endogenous peroxidase was blocked using a hydrogen peroxidase block for 10 min. After three washing steps with 1 × TBS, background blocking was performed using the Ultra Vision Protein Block for 5 min. Polyclonal rabbit Cytokeratin 7 (CK7) - antibody (AP06204PU-N; OriGene Technologies) for external ACH-3P cellularized PCL/PLA membranes was diluted 1:200 to a final concentration of 5 µg/ml in antibody Diluent (Agilent Technologies, Santa Clara, CA, USA) while mouse HLA-G - antibody (4H84; Santa Cruz, Dallas, TX, USA) for tissue cultured PCL/PLA scaffolds was diluted 1:50. For antibody stock concentrations see Appendix Table 7. Antibodies were incubated on slides for 30 min at RT. Slides were then washed three times, and detection was achieved by incubation with an anti-rabbit UltraVision HRP-labeled polymer for 15 min and 3-amino-9-ethylcarbacole (AEC; Thermo Fisher Scientific, Waltham, Massachusetts, USA) for 10 min. Nuclei were stained with hematoxylin, and slides were aqueous mounted with Kaiser's glycerol gelatin (Merk Millipore, Darmstadt, Germany). Rabbit IgG (X0936; 1:1500; Agilent Dako, Santa Clara, CA, USA) and mouse IgG1 (X0931; 1:200; Agilent Dako) served as negative controls (58).

Immunohistochemical double staining was performed on co-cultivated PCL/PLA slides using the Polink polymer detection system DS-MR-Hu A1 Kit (anti-mouse/DAB polymers; anti-rabbit/Vector Blue Substrate; GBI Labs, USA, WA) according to the manufacturer's instructions. Primary antibodies were diluted in antibody diluent (Dako) as listed in Table 4: For antibody stock concentrations see Appendix Table 7. Binding of primary mouse antibodies was visualized with the chromogen of Polink kit, termed "DAB" (brown) while primary rabbit antibodies were detected with "Vector Blue Substrate" (blue). For this protocol, a hematoxylin counterstain is not recommended.

Table 4: Antibodies used for IHC double staining. Antibodies shaded equally were used on one slide.

Antibody	Animal source	Antibody source*	Code/clone	Dilution
Cytokeratin 7	mouse	Thermo Fisher Scientific[a]	OV-TL 12/30	1:500
vWF	rabbit	Agilent Dako[d]	F3520	1:1000
Ki-67	mouse	Agilent Dako[d]	M7187	1:50
Cleaved Caspase 3	rabbit	Cell Signalling Technology[f]	#9664	1:200

3.12 *In situ* padlock probe technology and immunofluorescence

Oligonucleotides for beta actin were used as previously published (72, 73). The ACTB padlock probe was ordered to be 5'-phosphorylated (Integrated DNA Technologies, Coralville, IA, USA). The LNA primer was purchased from Exiqon (Exiqon, Vedbaek, Denmark) and the detection probe from Biomers (Biomers, Ulm, Germany). The LNA-primer-, padlock probe- and detection probe-sequences are listed in Table 3.

Antigen retrieval of the cellularized membranes was performed by pepsin digestion as previously described. All *in situ* reactions were performed in secure-seals hybridization chambers (Sigma-Aldrich, St. Louis, MO, USA) with a volume of 50 µl according to the method described by El-Heliebi *et al.* (2017) (73). In addition to single staining, padlock probes for targeting the housekeeping gene ACTB were combined with immunofluorescence staining for CK7. Therefore, immunofluorescence for CK7 was performed immediately after the *in situ* padlock probe ligation step as described elsewhere (74). To continue the *in situ* padlock probe method, the rolling circle amplification, as well as detection probe hybridization step, was applied after IF staining. Reverse transcription master mix without TranscriptMe reverse transcriptase (DNA-Gdansk, Poland) served as a negative control.

Table 5: Oligonucleotide sequences for *in situ* padlock probe technology. Reproduction from Fuchs *et al.* 2018 (58) with permission of publisher "SPRINGER-VERLAG" by license number 4676480552184.

Primer	**Sequence (5´ - 3´)**
ACTB*	C+GG+GC+GG+CG+GATCGGCAAAG
Padlock probe	Sequence (5´ - 3´)
plp_ACTB*	AGCCTCGCCTTTGCCTTCCTTTTACGA**CCTCAATGCACATGTTTGGCTCC**TCTTCGCCCCGCGAGCACAG
Detection probe	**Sequence (5´ - 3´)**
D1_ATTO 550	ATTO 448- **CCTCAATGCACATGTTTGGCTCC**

Padlock probe was 5'-phosphorylated. The fluorophore of the detection oligonucleotide was 5' conjugated
+: the following base is LNA modified; underlined: target complement sequence, bold: the complementary detection probe sequence

3.13 Image acquisition and evaluation of embedding methods

In order to identify which of the selected embedding method provides optimal morphological and structural results we used the visibility of fiber structure and discrimination of coarse- and fine-meshed structures as parameters to assess the qualitative outcome of the processed scaffolds.

Therefore, analysis was performed by scanning the cellularized scaffolds to take 20× and 40× microscope images. Brightfield and fluorescence images were acquired using the Zeiss

Observer Z1 inverted microscope (Carl Zeiss, Oberkochen, Germany) equipped with a 120 W HXP Mercury short-arc lamp. For brightfield images the Axiocam 506 camera (Carl Zeiss, Oberkochen, Germany) was used. Fluorescence images of CK7of low-melting-point paraffin and cryoembedded samples for cell size analysis were taken with the Axiocam 702 mono (Carl Zeiss, Oberkochen, Germany) equipped with an excitation and emission filter-set for visualization of DAPI, FITC, Cy3, and Cy5. The 40× objective ((LD Achroplan 40×/0.60 corr., D=0-2mm); Carl Zeiss, Oberkochen, Germany), the 20× objective ((LD Plan-Neofluar 20×/0.40 corr., D=0-1.5mm); Carl Zeiss,), and the ZEN 2 blue software (Version 2.0.0.04.8.2.0; Carl Zeiss) was used for capturing both the brightfield and fluorescence images. For enhanced visualization, brightness and contrast of each image was adjusted. Overlay images of fluorescence and brightfield channels were generated by using the open-source GNU Image Manipulation Program (GIMP) version 2.8.22 (open source software, http://www.gimp.org) (58).

Images of immunofluorescence stained ACH-3P cells and tissue with placenta specific antibodies were captured using the Zeiss Observer Z1 inverted microscope (Carl Zeiss, Oberkochen, Germany) equipped with the Colibri 7 LED illumination system (Carl Zeiss). Fluorescence images were taken using the 20× objective and the Axiocam 702 mono (Carl Zeiss) equipped with an excitation and emission filter set for visualization of DAPI, FITC, Cy3, and Cy5. ZEN 3 blue software (Version 3.0.79.0000; Carl Zeiss) was used for capturing fluorescence images. *In situ* detection stained sections were also captured with the parameters mentioned above.

For enhanced visualization, brightness and contrast of each image was adjusted.

3.13.1 Quantitative analysis of antibody staining after different antigen retrieval pretreatments

We performed an automatized analysis of the mean fluorescence intensity of the Cy5 channel and a qualitative evaluation to discriminate between cell types and structures within the first trimester placental villi and to assess the outcome of the four different antigen retrieval pretreatment methods.

Analysis was performed by scanning the same morphological spot over all serial slides consisting of 36 tiles of 20 × microscope images, corresponding to a total area of 6.4 mm². Brightfield and fluorescence images were acquired using the Zeiss Observer Z1 inverted microscope (Carl Zeiss, Oberkochen, Germany) equipped with the Colibri 7 LED illumination system (Carl Zeiss). For brightfield images, the Axiocam 506 camera (Carl

Zeiss) was used, and fluorescence images were taken with the Axiocam 702 mono (Carl Zeiss) equipped with an excitation and emission filter set for visualization of DAPI, FITC, Cy3, and Cy5. The 20 × objective (LD Plan-Neofluar 20×/0.40 corr., D = 0–1.5 mm; Carl Zeiss), and the ZEN 3 blue software (Version 3.0.79.0000; Carl Zeiss) was used for capturing both the brightfield and fluorescence images.

For fluorescence imaging the exposure time of the Cy5 channel was set to the most intense staining per series (shortest exposure time = most intense staining) via the function “Auto-Exposure”. For standardization exposure time was kept the same across the series of the four different antigen retrieval treatments per antibody. The exposure time of the FITC and CY3 channel was kept the same across all images to detect background fluorescence.

We used the open-source cell image analysis software CellProfiler (version 3.1.8, (75)) to evaluate the mean signal intensity of the Cy5 channel over the entire region of the 36 tiles of 20 × images. Specific positive antibody staining exclusively appears in the range of wavelengths specific for the dye used to label the secondary antibody (76). Therefore, signals detected in multiple channels (unspecific staining) were counted as false positive findings. To exclude these false positive signals from the analysis due to autofluorescence background the CY3 channel was subtracted from the CY5 channel. Additionally, existing background noise was eliminated by using a threshold to improve the signal/background ratio.

Therefore, the Cell Profiler pipeline was designed to exclude false positive staining before determining the mean intensity of the Cy5 channel. In brief, Cy3 images were subtracted from Cy5 images with the “ImageMath” module using the operation tool “Substract”. A two-class thresholding with a lower bound of 0.007 and an upper bound of 1 was applied with the threshold strategy “Global” and the thresholding method “Otsu” using the module “Threshold”. The parameter “Threshold correction factor” was set to 1 while the “Threshold smoothing scale” was set to 3. “Measure Image Intensity” was used to calculate the mean intensity of the processed CY5 channel per image and exported into an Excel-Sheet with the “ExportToSpreadsheet” tool.

Representative pictures are shown in this doctoral thesis. For enhanced visualization, brightness and contrast of the example images were adjusted.

3.13.2 Morphological analysis

In addition to the automated quantitative image analysis an evaluation of the immunofluorescence stained cell populations within the first trimester placenta sections was conducted. A subjective histological classification of various cell types occurring in first trimester placentas was performed regarding the specific staining reaction and the presence of nonspecific background for each antibody. Individual cell types including cytotrophoblasts (CT), syncytiotrophoblasts (SCT), endothelial cells (EC), extravillous trophoblasts (EVT), fibroblasts (F), smooth muscle cells (SMC), Hofbauer cells (HBC) and proliferating cells (pC) were evaluated. Additionally, a classification category for unspecific staining was introduced, marked in red to classify irregular and insufficient antibody staining all over the tissue. Green colouring was used to mark specific staining pattern. An intensity grading system was applied, using " - " for negative staining, " ○ " to display a positive staining reaction and " ● " indicating the cell type that appears the brightest within an antigen retrieval group all over the tissue (if there are intensity differences between cell types). " ⊙ " marks cell types that show a brighter signal in some parts of the tissue compared to other positive stained cell types within an antigen retrieval treatment group. Results of the qualitative evaluation are shown in Table 6.

3.13.3 Quantitative cell size analysis

In order to verify the low-melting-point embedding method selected by qualitative analysis as the method of choice, a quantitative analysis was performed.

Therefore, the open-source cell image analysis software CellProfiler (version 3.1.5, (77)) was used to evaluate the cell size of ACH-3P cells attached on the PCL/PLA scaffolds after the low-melting-point paraffin embedding and cryofixation. The pipeline was designed for quantification of the cell size by staining the intermediate filaments by CK7. Briefly, DAPI images were processed with the "Identify Primary Objects" module to identify the number of cell nuclei. The modules "Identify Secondary Object" and "Measure Image Area Occupied" were used for the measurement of CK7, displaying the cell area. Unspecific signals, which were simultaneously detectable in at least two fluorescence channels, were filtered by the "MaskObject" module. Overlay images of the evaluated cell area and nuclei outlines (Figure 16 c, d) were created using the modules "Overlay Objects" on Cy5 channel images combined with the module "Overlay Outlines" of DAPI objects. We have taken images in the Cy5 channel and used their pixel values to calculate the cell size (pixel/area ratio = 0.054289 µm² for images of low-melting-point embedded sections (40 x) and pixel/area ratio = 0.085849 µm² for images of cryofixation embedded sections (20 x)) in relation to the number of nuclei (Figure 16). More than 3200 cells were analysed per embedding method.

3.14 Statistical analyses

Statistical analysis for automatized mean intensity analysis was performed using the GraphPad Prism software, version 6.01 (GraphPad Prism, Inc., La Jolla, USA). To identify outliers a ROUT test was performed with a Q value of 1%. (78) Cleaned data were used for further analysis. To test if the data follow a Gaussian distribution a Kolmogorov-Smirnov test was performed. For multiple comparison of all four groups an one-way ANOVA was applied to compare the mean fluorescence intensities of the Cy5 channel. Tukey's test was applied as a correction of multiple comparison. Results were considered statistically significant when $p < 0.05$ (*$p < 0.05$, **$p < 0.01$, ***$p < 0.001$, and ****$p < 0.0001$). Representative pictures are shown in the publication.

Statistical analysis for automatized cell size analysis was also performed using the GraphPad Prism software, version 6.01 (GraphPad Prism, Inc., La Jolla, USA) for parametric comparison of two groups. An unpaired t-test was applied to compare the mean cell size of attached cells on the processed samples. Results were considered statistically significant when $p < 0.05$ (*$p < 0.05$, **$p < 0.01$, ***$p < 0.001$, and ****$p < 0.0001$). Representative pictures are shown in the publication.

4 Results

Please note that parts of the "Results" section are based on the publication of Fuchs *et al.* 2018 (58).

4.1 PCL/PLA characterization

4.1.1 Two-layer scaffold

SEM images allow distinct identification of the inner and the outer layer of two-layer PCL/PLA scaffolds as shown in Figure 7 c. All fibers crossing a diagonal line were measured at three spots left and right of the crossing (Figure 7 b). Electrospun fibers of the densely packed inner layer (PCL/PLA 100/50 mg/ml) showed a mean diameter of 1.05 µm (Figure 7 a, d) whereas the fiber diameter increased to 2.45 µm (Figure 7 b, d) for the high porous outer layer (PCL 200 mg/ml) (n=1600). Additionally, the wall cross-sections of both layers showed no delamination (c).

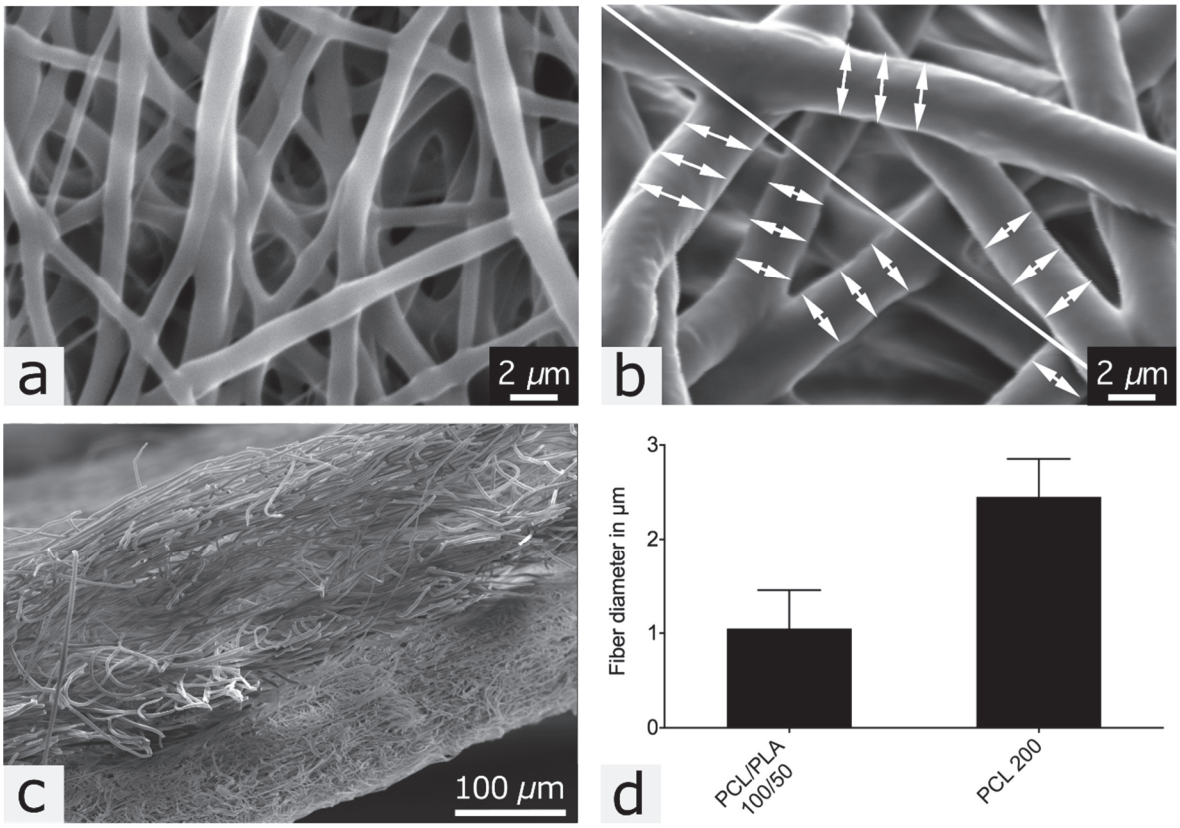

Figure 7: SEM images of the inner PCL/PLA layer **(a)** and outer PCL layer **(b)**. All fibers crossing a diagonal line were measured on three spots left and right of the crossing **(b)**. Wall cross sections showed no delamination of both layers **(c)**. Fibers of the densely packed inner layer showed a mean diameter of 1.05 µm, whereas fibers of the highly porous outer layer had diameter of 2.45 µm (n = 1600) **(d)** .

Reproduction modified from Fuchs *et al.* 2018 (58) with permission of publisher “SPRINGER-VERLAG” by license number 4676480552184.

4.1.2 Mono-layer scaffold

SEM images show cross section and the top-view of the mono-layered PCL/PLA scaffold (PCL200/PLA100) as shown in Figure 8 a and b. Fiber thicknesses correspond to the size of the fibers of the outer layer of the two-layered PCL/PLA membrane. The diameter of the high porous fibers result in a size of 2.45 µm (Figure 8 b). Furthermore, the wall cross-section showed no delamination.

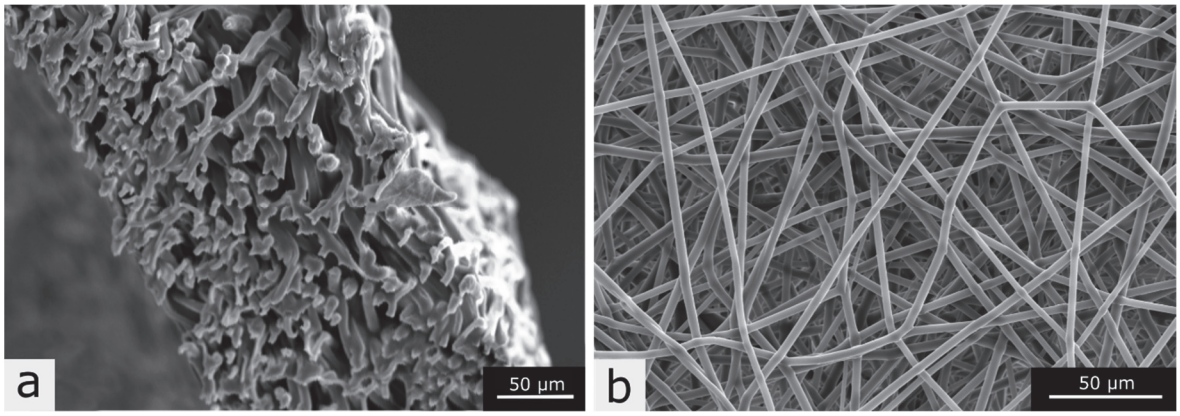

Figure 8: SEM images of the mono-layered PCL/PLA PCL/PLA scaffold (PCL200/PLA100). **(a)** showing an axial- and **(b)** showing the top-view of the scaffold.

4.2 Histologogical processing by establishing an embedding method for thermo-sensitive materials

4.2.1 Cryo-fixation and -sectioning of un-/cellularized PCL/PLA scaffolds

Cryofixation and sectioning of uncellularized PCL/PLA scaffolds was possible and created sections with spots of shrunken and diminished fibers throughout the specimen. No differences in fiber structures were seen between cryosections of uncellularized and cellularized PCL/PLA scaffolds (Figure 9 a; Figure 10 a, b). In summary, cryofixation and sectioning of un-/cellularized PCL/PLA scaffolds produced sections with moderate deformations (58).

4.2.2 Acrylic resin embedding and sectioning of un-/cellularized PCL/PLA scaffolds

Acrylic resin processed un-/cellularized membranes displayed fiber structures that were unchanged in size and diameter (Figure 9 d; Figure 10 c, d). Coarse- and fine-meshed structures can be clearly distinguished. However, sectioning of the scaffolds is limited to a thickness of 3 µm (58).

4.2.3 Automatized dehydration and standard paraffin embedding of un-/cellularized PCL/PLA scaffolds

Automatized dehydration and paraffin embedding of fixed un-/cellularized PCL/PLA membranes at temperatures up to 61 °C resulted in a dissolved PCL/PLA mesh. An increase in time for PCL/PLA scaffold fixation from 1 to 24 h strengthened the material, but did not influence the thermostability of PCL/PLA. Summarizing, automatized dehydration and standard paraffin embedding led to melted PCL/PLA scaffolds (58).

4.2.4 Standard paraffin embedding following gelatin stabilization (10% and 25%) of cellularized PCL/PLA scaffolds

A gelatin stabilization of uncellularized PCL/PLA membranes at concentrations of 10% and 25% gelatin prior to embedding in standard paraffin (up to 61 °C) improved the stability of PCL/PLA scaffolds to a certain level, while gelatin concentrations of 5% did not increase thermostability and led to a dissolved PCL/PLA network. Membrane sections treated with a gelatin concentrations of 10% and 25% in combination with the standard paraffin embedding showed partially shrunken and melted fibers, but a generally improved appearance in comparison to the other unprocessed and uncellularized PCL/PLA scaffolds (Figure 9 b, c). However, microtome sectioning of cellularized PCL/PLA membranes stabilized with 10% or 25% gelatin did not produce any usable paraffin sections. Stabilization of cellularized PCL/PLA membranes with a gelatin concentration of 5% led to the dissolution of the PCL/PLA fibers. Stabilisation of the membrane with concentrations of 10% and 25% gelatine resulted in the detatchment of the gelatine core from the surrounding paraffin block. Briefly, the combination of gelatin (10% and 25%) stabilization and standard paraffin embedding increased thermostability of uncellularized but not of cellularized PCL/PLA scaffolds (58).

4.2.5 Low-melting-point paraffin embedding of un-/cellularized PCL/PLA scaffolds

Embedding of un-/cellularized PCL/PLA scaffolds with low-melting-point paraffin (max. 50 °C) by microwave tissue processing produced comparable sections of PCL/PLA scaffolds. Scaffold and fibers appeared stable and solid as fiber diameter and pore size remained unchanged (Figure 9 e). In addition, cellularized membranes revealed characteristic cell morphology (Figure 10 e, f). The shape and size of the cells appeared similar to cells cultivated in conventional cell culture. Therefore, this technique was used as the method of choice for further procedures (58).

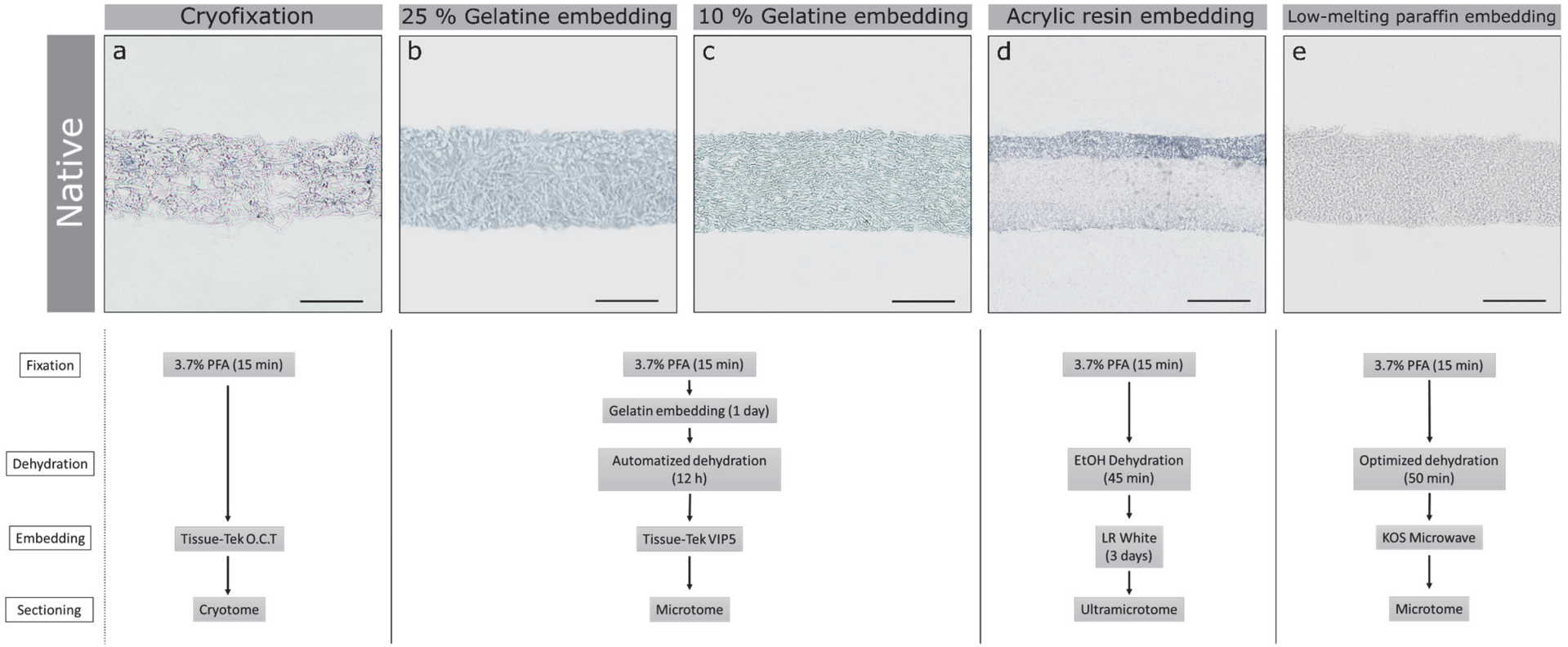

Figure 9: Comparison of different fixation and embedding methods of uncellularized PCL/PLA scaffolds. Bright field images of unstained sections. **(a)** Embedding and cryosectioning in OCT compound. **(b)** Stabilization with 10% gelatin, fixation in 3.7% PFA and standard paraffin embedding. **(c)** Stabilization with 25% gelatin, fixation in 3.7% PFA and standard paraffin embedding. **(**d**)** Fixation in 3.7% PFA and embedding in acrylic resin. **(e)** Fixation in 3.7% PFA and embedding in low-melting-point paraffin maintained optimal structure of uncellularized PCL/PLA membranes out of all variants of fixation and embedding. *PCL/PLA* polycaprolactone/polylactide, *OCT* optimal cutting temperature compound, *PFA* paraformaldehyde. Scale bars represent 100 µm.

Reproduction and modified from Fuchs *et al.* 2018 (58) with permission of publisher “SPRINGER-VERLAG” by license number 4676480552184.

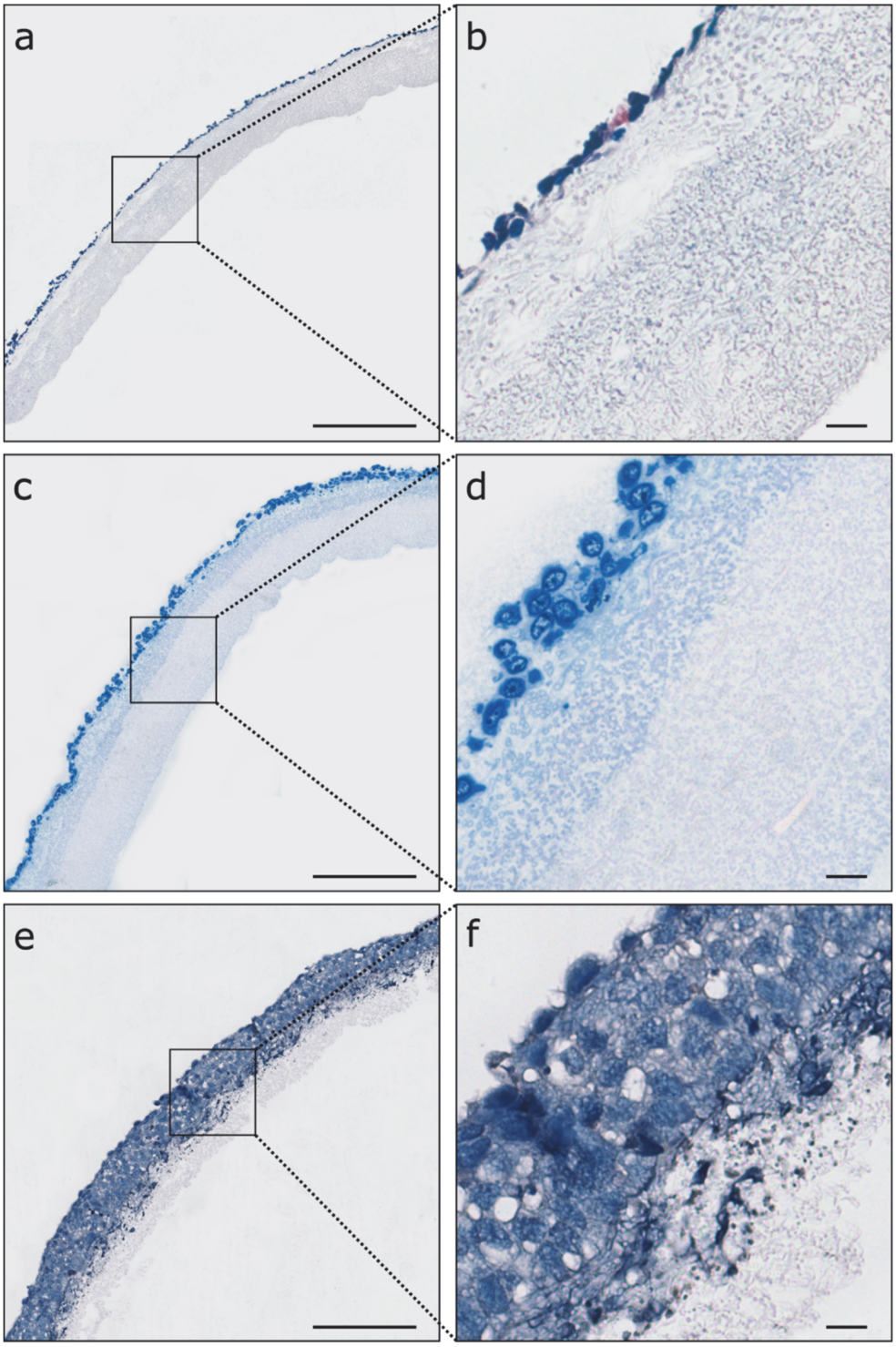

Figure 10: Comparison of different fixation and embedding methods of cellularized PCL/PLA membranes. Rows represent the respective embedding methods. Sections were stained and imaged with bright field imaging. **(a, b)** Embedding and cryosectioning in OCT compound; HE staining. **(c, d)** Fixation in 3.7% PFA, embedding in acrylic resin; toluidine blue staining. **(e, f)** Fixation in 3.7% PFA, embedding in low-melting-point paraffin (max. 50 °C); HE staining. *PCL/PLA* polycaprolactone/polylactide, *OCT* optimal cutting temperature compound, *PFA* paraformaldehyde, *HE* hematoxylin and eosin. Scale bars in **a, c, e** represent 200 µm, and those in **b, d, f** represent 20 µm.

4.3 Histological characterization of first trimester placenta with relevant Antibodies after Pepsin Digestion

17 antibodies that are known to play a role in placental development were tested on their binding specificity on first trimester placenta serial sections after four different antigen retrieval pretreatments (79, 80). Table 3 summarizes the full names and clone numbers of the used antibodies as well as the animal source, the company and the concentrations used according to the antigen retrieval pretreatment.

In order to get a better overview, we split the antibody fluorescence images with their according automatized intensity analysis into two Figures. Images listed in Figure 11 show a specific antibody binding after pepsin digestion. Fluorescence images presented in Figure 12 show no staining after the enzymatic pepsin digestion. The graphs in the last column in Figure 11 and Figure 12 show the mean fluorescence intensities of the antibody signals per mm^2.

In addition to the automated quantitative image analysis an evaluation of the immunofluorescence stained cell populations within the first trimester placenta sections was conducted. Results of the qualitative analyses is shown in Table 6.

While the enzymatic digestion seems to improve the staining of selected antibodies, it appears that in some cases the epitopes are completely degraded so that antibody binding is no longer possible.

4.3.1 Alkaline phosphatase, placenta like 2 (ALPPL2)

ALPPL2 antibody showed the most intense staining after a heat induced antigen retrieval with ph9 (81). ALPPL2 antibody showed a positive staining result after all four pretreatments. Hardly visible by eye, the antibody staining after pepsin digestion showed a positive signal. This was also confirmed by the automatized quantitative fluorescence analysis (Figure 11 a1-a6). The qualitative evaluation showed that the treatment with ph6 and ph9 resulted in a more intense staining of the CTs compared to the SCTs. No pretreatment (noAR) resulted in an equally intensive staining of CT as well as SCT. After treatment with pepsin only a weak staining was observed, occurring exclusively in the SCT.

4.3.2 β-human chorionic gonadotropin (β-hCG)

The automatized analysis as well as the qualitative analysis revealed that β-hCG antibody yielded optimal results when enzymatic antigen retrieval with pepsin was applied (Figure 11 b1-b6). β-hCG antibody showed a positive staining result after all four pretreatments.

Regarding the qualitative analysis, after antigen retrieval with Pepsin, ph6 and ph9 a specific staining is visible exclusively in the SCT. Without a pretreatment (noAR) an extremely weak staining can be observed in the SCT as well as in the CT. Pepsin digestion improves staining of β-hCG on first trimester placental villi and showed a significant increase of the staining after automatized image analysis.

4.3.3 CD34II

The staining of the transmembrane phosphoglycoprotein CD34II showed a positive staining result after all four pretreatments. The most intense staining occurred after a heat induced antigen retrieval with ph6, which could be determined by quantitative analysis (Figure 11 c1-c6). Qualitative analysis revealed a specific staining of endothelial cells after each pretreatment.

4.3.4 Cytokeratin 7 (CK7)

CK7 staining with the rabbit anti-CK7 antibody showed a definite staining after an antigen retrieval with pepsin, ph6 and ph9. Optimal results were obtained after a pretreatment with ph9, according to the quantitative analysis. Without a pretreatment no staining was observed. (Figure 11 d1-d6) The qualitative analysis indicated that after a pretreatment with pepsin only the CT showed a fluorescence staining, whereas after the treatment with ph6 or ph9 both the CT as well as the CT were stained. However, the qualitative analysis over large image sections did not provide a clear result regarding the staining intensity between CT and SCT after a pretreatment with ph6 and ph9. While in some image sections the CT appears more intensively stained than the SCT, this cannot be observed in other image areas.

In contrast to the anti-CK7 staining with the rabbit antibody, antibody staining of CK7 with the mouse antibody revealed a staining after all pretreatments, including no pretreatment (noAR). While staining intensity after no pretreatment was very weak, the staining after ph6 and ph9 showed similar staining intensities emphasized by quantitative analysis (Figure 11 e1-e6). The qualitative analysis showed that CT and SCT are stained after all antigen retrieval methods, although different intensities were obtained depending on the treatment. While the CT showed a brighter staining than the SCT after pepsin digestion, the staining after ph6 treatment reveals no difference in intensity between the trophoblast types. After the treatment with ph9 a more intense staining of the CT can be observed in many areas, but not in all. Therfore, a defined conclusion concerning the staining intensity is not feasible.

For qualitative analysis, the example images given do not always provide a comprehensive basis.

4.3.5 E-Cadherin

The staining of the transmembrane protein E-cadherin showed a positive staining result after the pretreatment with pepsin, ph6 and ph9. Without a pretreatment no staining was observed. Optimal results were obtained after the pretreatment with ph9, evidenced by the quantitative analysis (Figure 11 f1-f6). The qualitative analysis indicated that after the pretreatments that showed a positive staining results only the CT showed a fluorescence staining.

4.3.6 Von Willebrand factor (vWF)

The automatized analysis as well as the qualitative analysis revealed that the natobody for vWF yielded optimal results when enzymatic antigen retrieval with pepsin was applied (Figure 11 g1-g6). The endothelial marker vWF showed positive staining result after the pretreatments with pepsin, ph6 and ph9. No staining was observed without a pretreatment (noAR). The qualitative evaluation indicated that the treatment with pepsin, ph6 and ph9 resulted specific staining of endothelial cell.

4.3.7 Zona Occludens Protein 1 (ZO-1)

The ZO-1 antibody against the Tight junction protein-1 showed positive staining results after all kinds of pretreatments except without pretreatment (noAR). Optimal fluorescence staining was obtained after the pretreatment with ph9 (Figure 11 h1-h6). The qualitative analysis revealed that the ZO-1 antibody yielded specific staining of endothelial cells after pepsin digestion, whereas a pretreatment with ph6 led to a specific florescence signal of endothelial cells and unspecific staining of CT and SCT. After a pretreatment with ph9 several cell types showed a specific fluorescence signal, such as EC, CT, SCT and fibroblasts. However, ECs showed the brightest signal over all specifically stained cell types.

4.3.8 β-Actin

β-Actin antibody showed positive staining results after no pretreatment and pretreatment performed with ph6 and ph9. Staining of the samples pretreated with ph9 revealed the most intense signals, emphasized by the quantitative analysis (Figure 12 a1-a6). The qualitative evaluation showed that the treatment with pepsin and ph6 resulted in a more intense fluorescence signal of the fibroblasts in the entire tissue area in contrast to the other specifically stained cell types such as CTs, SCTs, ECs, EVTs, SMCs and HBCs. Treatment with ph9 showed no differences in the staining intensity between cell types.

4.3.9 CD31

The endothelial cell marker anti-CD31 revealed specific staining after the pretreatments with ph6 and ph9. According to the quantitative analysis the fluorescence signal showed

the brightest signal after the treatment with ph6 (Figure 12 b1-b6). The qualitative evaluation displayed a specific staining of endothelial cells after both kinds of treatments.

4.3.10 Desmin

The muscle specific Desmin antibody revealed optimal staining results after the pretreatment with ph9. Specific staining was also observed after pretreatment with ph6 (Figure 12 c1-c6). Untreated samples showed a moderately positive signal. The qualitative analysis indicates a specific staining of fibroblasts after all kinds of treatments, with the exception of pepsin digestion.

4.3.11 Human leukocyte antigen-G (HLA-G)

The HLA-G antibody specific for staining of extravillous trophoblasts displayed fluorescence signals after the pretreatments with ph6 and ph9. As the quantitative analysis shows, optimal results are achieved after the pretreatment with ph9 (Figure 12 d1-d6). The qualitative evaluation revealed that only EVTs are stained by the pretreatments mentioned.

4.3.12 Ki-67

The proliferation marker Ki-67 showed positive fluorescence signals after the pretreatments with ph6 and ph9. The brightest signals were obtained after treatment with ph9 (Figure 12 e1-e6). The qualitative analysis reveals a specific staining of proliferating nuclei after the pretreatment with ph6 or ph9.

4.3.13 Leptin

Leptin antibody showed positive staining results after the treatments with ph6 and ph9, with optimal results after treatment with ph6. This is evidenced by qualitative analysis (Figure 12 f1-f6). The qualitative analysis showed a specific staining of CT as well as SCT after both treatments. However, the staining revealed poor cellular integrity, no clear differentiation between the cells was possible. After treatment with ph6, a weak background staining of fibroblast can be observed.

4.3.14 Smooth muscle Actin (SMA)

Anti-smooth muscle actin displayed specific staining after no pretreatment (noAR), and the treatments with ph6 and ph9. Most intense staining results were achieved after the treatment with ph9 (Figure 12 g1-g6). Qualitative analysis revealed a very weak staining after no pretreatment of fibroblasts, whereas strong and specific staining of fibroblasts was achieved after pretreatment with ph6 and ph9.

4.3.15 Vimentin

The antibody against the structural protein vimentin displayed specific staining after the pretreatments with ph6 and ph9 and without pretreatment (noAR). Brightest signals were observed after the treatment with ph9, emphasized by the quantitative analysis (Figure 12 h1-h6). Qualitative analysis obtained specific staining of fibroblasts after all kinds of treatments, with the exception of pepsin digestion. However, staining of untreated samples is hardly visible.

4.3.16 CD163

The macrophage marker CD163 displays varying results after the different kinds of pretreatments. Quantitative analysis shows specific staining after pepsin digestion, pretreatment with ph6 and the pretreatment with ph9. However, qualitative analysis indicates that the high values for the specific staining after pepsin digestion are due to an unspecific staining (Figure 12 i1-i6). After the treatments with ph6 and ph9, however, specific staining of the Hofbauer cells was observed. Optimal results were obtained after the pretreatment with ph6.

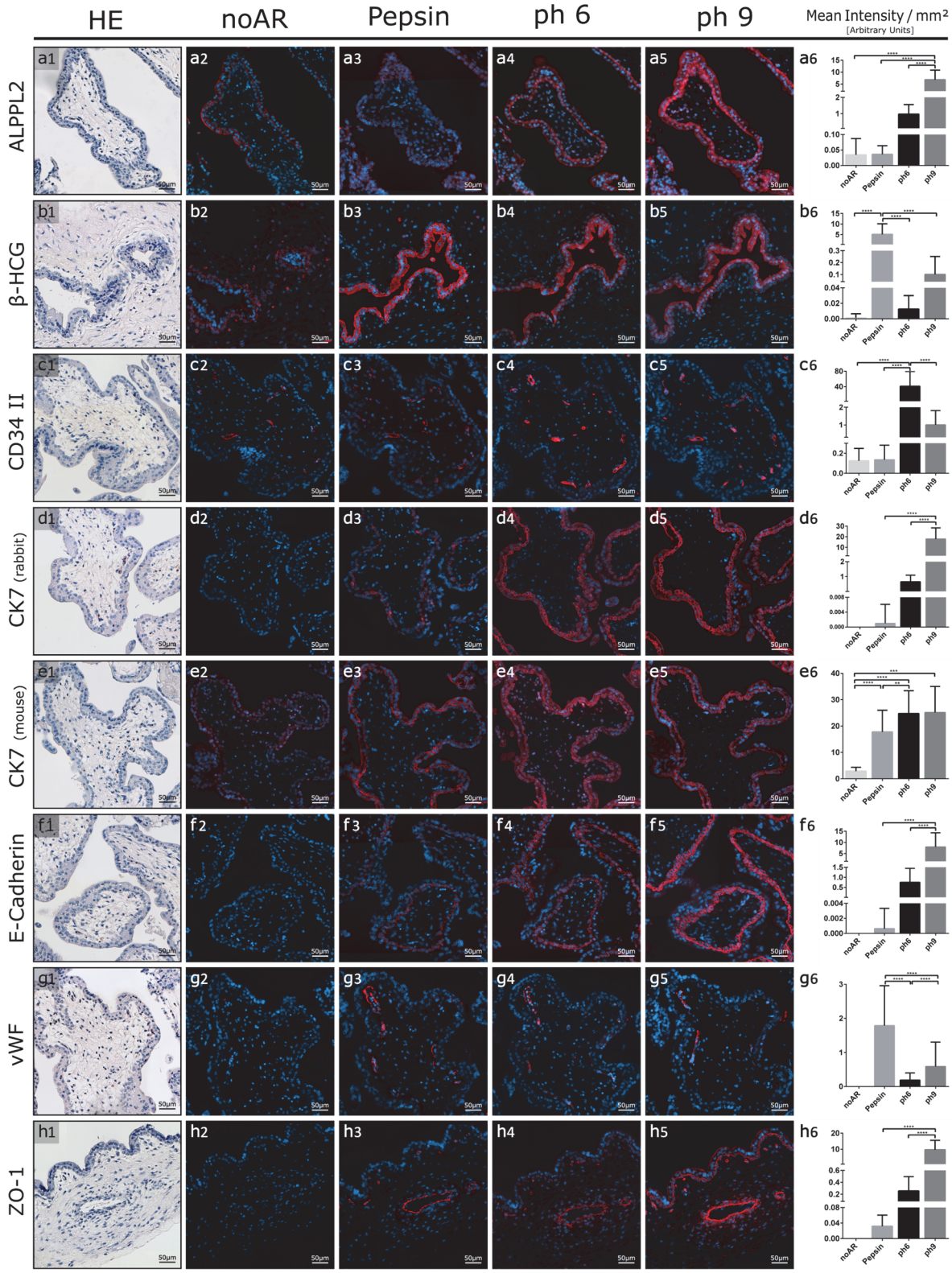

Figure 11: Tested antibodies show specific binding on first trimester placental tissue after enzymatic digestion with pepsin. HE staining (column 1) reveals a morphological overview of the tissue. Fluorescence stained serial sections with four different antigen retrieval pretreatments (noAR, Pepsin, ph6, ph9) are shown in columns. Graphs in column 6 show the automatized analysis of the mean fluorescence intensity per mm² of the antibody used.

Abbreviations: **noAR**; no Antigen retrieval, **Pepsin**; pepsin digestion, **ph6**: steam heat with citrate buffer, **ph9**; steam heat with ph9.

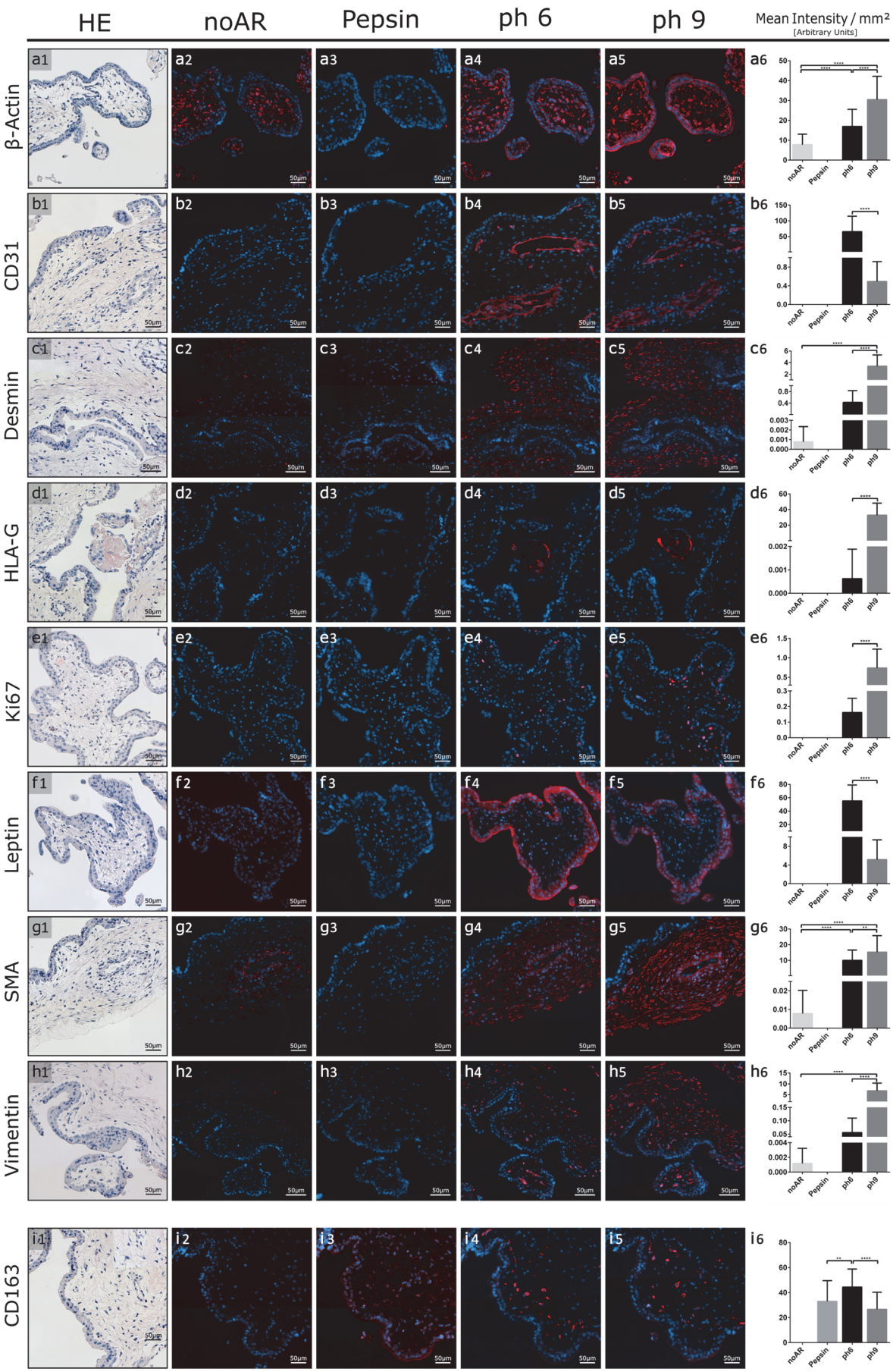

Figure 12: Tested antibodies show no binding on first trimester placental tissue after enzymatic digestion with pepsin. Abbreviations: **noAR**; no Antigen retrieval, **Pepsin**; pepsin digestion, **ph6**: steam heat with citrate buffer, **ph9**; steam heat with ph9.

Table 6: Qualitative evaluation of the antibody reaction pattern of different cell types occurring in first trimester placenta samples. Staining specificity was assessed according to the four different AR pretreatments.

	noAR								Pepsin								ph6								ph9							
	CT	SCT	EC	EVT	Fib	SMC	HBC	pC	CT	SCT	EC	EVT	Fib	SMC	HBC	pC	CT	SCT	EC	EVT	Fib	SMC	HBC	pC	CT	SCT	EC	EVT	Fib	SMC	HBC	pC
ALPPL2	○	○	-	-	-	-	-	-	-	○	-	-	-	-	-	-	●	○	-	-	-	-	-	-	●	○	-	-	-	-	-	-
β-Actin	○	○	○	○	●	○	○	-	-	-	-	-	-	-	-	-	○	○	○	○	●	○	○	-	○	○	○	○	○	○	○	-
β-HCG	●	○	-	-	-	-	-	-	-	○	-	-	-	-	-	-	-	○	-	-	-	-	-	-	-	○	-	-	-	-	-	-
CD 163	-	-	-	-	-	-	-	-	○	○	○	○	○	○	○	○	-	-	-	-	-	-	○	-	-	-	-	-	-	-	○	-
CD31	-	-	-	-	-	-	-	-	-	-	-	-	-	-	-	-	-	-	○	-	-	-	-	-	-	-	○	-	-	-	-	-
CD34 II	-	-	○	-	-	-	-	-	-	-	○	-	-	-	-	-	-	-	○	-	-	-	-	-	-	-	○	-	-	-	-	-
Cytokeratin 7 (rabbit)	-	-	-	-	-	-	-	-	○	-	-	-	-	-	-	-	⊙	○	-	-	-	-	-	-	⊙	○	-	-	-	-	-	-
Cytokeratin 7(mouse)	○	○	-	-	-	-	-	-	●	○	-	-	-	-	-	-	○	○	-	-	-	-	-	-	⊙	○	-	-	-	-	-	-
Desmin	-	-	-	-	○	-	-	-	-	-	-	-	-	-	-	-	-	-	-	-	○	-	-	-	-	-	-	-	○	-	-	-
E-Cadherin	-	-	-	-	-	-	-		○	-	-	-	-	-	-		○	-	-	-	-	-	-	-	○	-	-	-	-	-	-	-
HLA-G	-	-	-	-	-	-	-	-	-	-	-	-	-	-	-	-	-	-	-	○	-	-	-	-	-	-	-	○	-	-	-	-
Ki-67	-	-	-	-	-	-	-	-	-	-	-	-	-	-	-	-	-	-	-	-	-	-	-	○	-	-	-	-	-	-	-	○
Leptin	-	-	-	-	-	-	-	-	-	-	-	-	-	-	-	-	-	○	-	-	○	-	-	-	-	○	-	-	-	-	-	-
Smooth Muscle Actin	-	-	-	-	○	-	-	-	-	-	-	-	-	-	-	-	-	-	-	-	○	○	-	-	-	-	-	-	○	○	-	-
Vimentin	-	-	-	-	○	-	-	-	-	-	-	-	-	-	-	-	-	-	-	-	○	-	-	-	-	-	-	-	○	-	-	-
vWF	-	-	-	-	-	-	-	-	-	-	○	-	-	-	-	-	-	-	○	-	-	-	-	-	-	-	○	-	-	-	-	-
ZO-1	-	-	-	-	-	-	-	-	-	-	○	-	-	-	-	-	-	-	○	-	○	-	-	-	○	○	●	-	-	-	-	-

Abbreviations: **CT**; Cytotrophoblast, **SCT**; Syncytiotrophoblast, **EC**; endothelial cells, **EVT**; extravillous Trophoblasts, **Fib;** Fibroblasts, **SMC**; smooth muscle cells, **HBC**; Hofbauer cells, **pC**; proliferating Cell, **-;**no staining, **red**; unspecific staining, **green**; specific staining

○ marks cell types that show positive staining within an AG treatment group

⊙ marks cell types that show a more intense staining compared to other positive stained cell types in some parts of the tissue within an AR treatment group.

● marks the cell type that show the most intense staining compared to other positive stained cell types within an AR treatment group.

4.4 Comparison of proteinase K and pepsin digestion as enzymatic antigen retrieval methods for low-melting-point paraffin embedded cellularized PCL/PLA scaffolds for immunohistochemical staining of CK7

Trophoblast cellularized membranes fixed in 3.7% PFA, embedded in low-melting-point paraffin, and pretreated with proteinase K for antigen retrieval revealed irregular an insufficient staining of CK7 with poor cellular integrity (Figure 13 a, b). In contrast, the most intense and specific immunohistochemically staining of CK7 was observed using an enzymatic pretreatment with pepsin (Figure 13 c, d). Pepsin digestion appeared to be the most effective antigen retrieval method to treat cellularized, temperature-sensitive PCL/PLA membranes. Hence, this technique proved to be the method of choice for further experiments requiring antigen retrieval. Rabbit immunoglobulins served as a negative control.

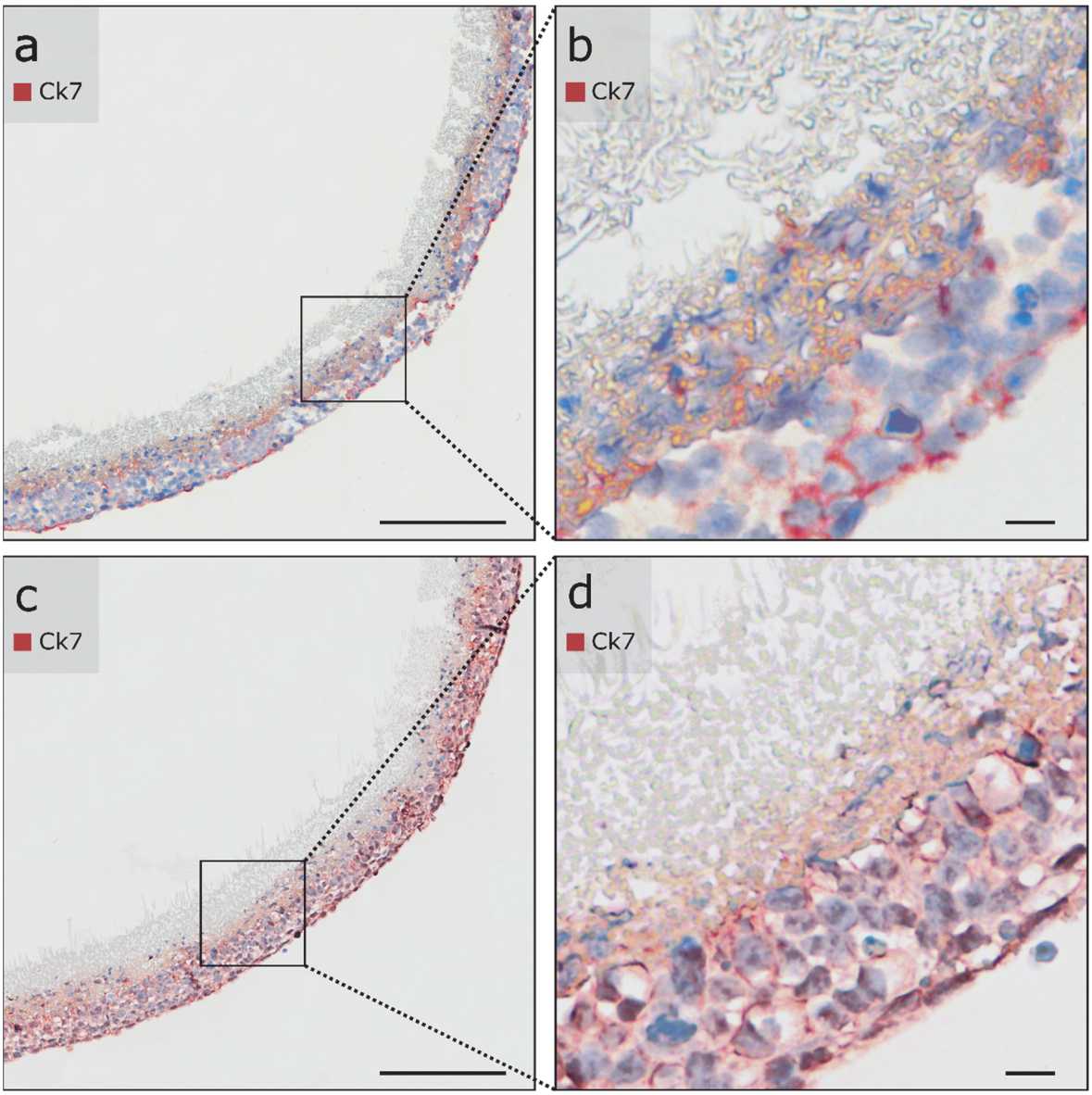

Figure 13: Enzymatic antigen retrieval of PCL/PLA membranes cellularized with trophoblast cells. Columns represent different enzymatic antigen retrievals. Membranes were fixed in 3.7% PFA and embedded in low-melting-point paraffin (max. 50 C). Sections were immunostained with anti-CK7. Nuclei were counterstained with hematoxylin. Sections were imaged with bright field. **(a, b)** Antigen retrieval with proteinase K digestion for 30 min reveals unspecific staining of CK7 with poor cellular integrity. **(c, d)** Antigen retrieval with pepsin digestion for 30 min provides specific immunohistochemically staining of CK7 and optimal morphology of cellularized PCL/PLA membranes. *CK7* Cytokeratin 7, *PCL/PLA* polycaprolactone/polylactide, *PFA* paraformaldehyde. Scale bars in **a, c** represent 200 µm and in **b, d** 20 µm.

Reproduction from Fuchs *et al.*2018 (58) with permission of publisher “SPRINGER-VERLAG” by license number 4676480552184.

4.5 Immunofluorescence staining of trophoblast cells in low-melting-point paraffin embedded PCL/PLA scaffolds

DAPI staining confirmed successful cellularization of PCL/PLA membranes with ACH-3P cells (Figure 14 a, b). ACH-3P cells migrated to the centre of the PCL/PLA membrane (Figure 14 c, d). The cells stopped migrating at the coarse-meshed/fine-meshed interface, as the cell size is too large for invading the fine-meshed fiber network of the two-layered scaffold. In addition, immunofluorescence of CK7 showed distinct staining of ACH-3P cells (Figure 14 e, f).

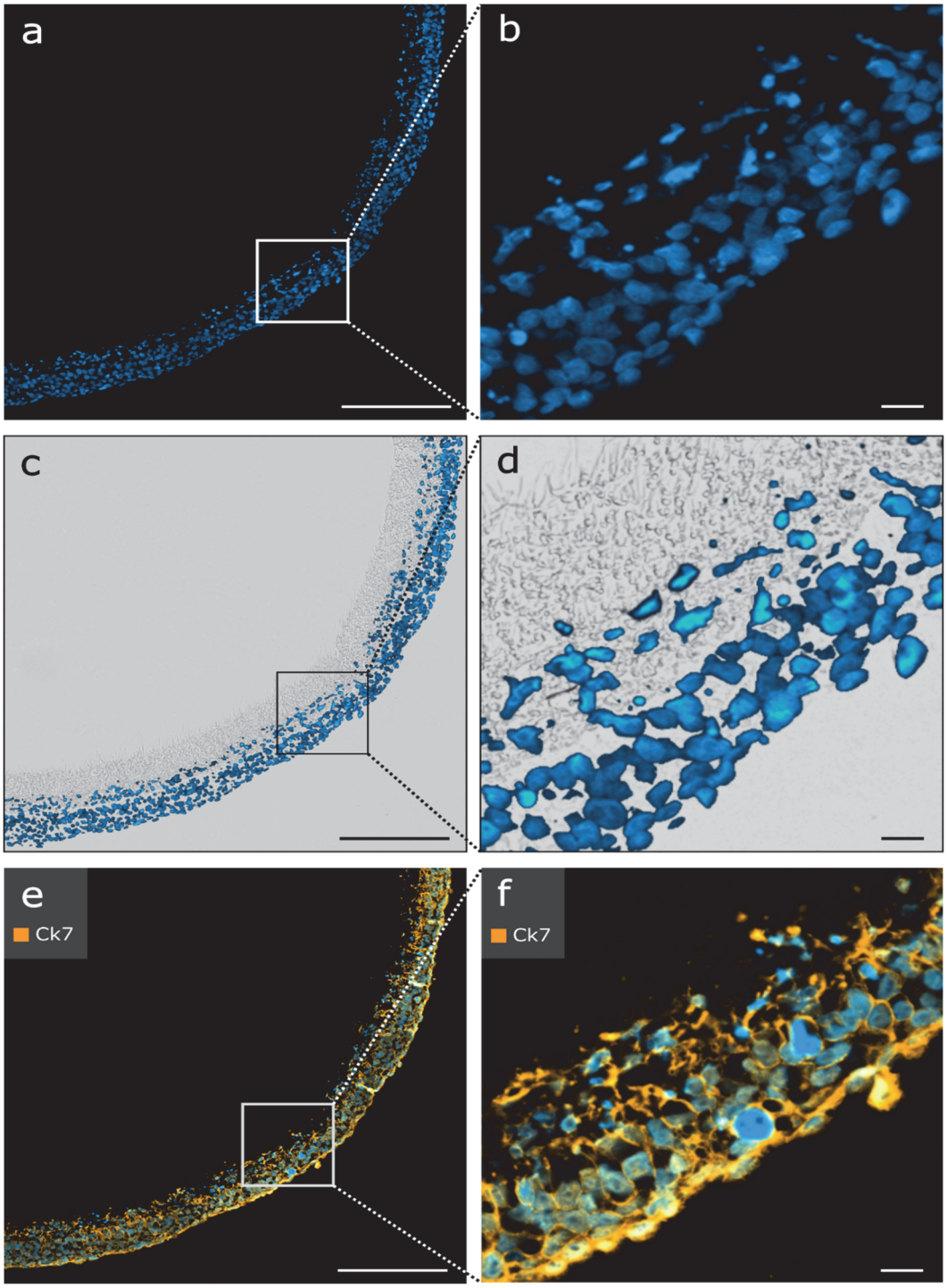

Figure 14: Immunofluorescent staining of cellularized PCL/PLA membranes cellularized with trophoblast cells. Sections were fixed in 3.7% PFA, embedded in low-melting-point paraffin (max. 50 C), and antigen retrieval was performed with pepsin for 30 min. Nuclei were counterstained with DAPI (blue). **(a, b)** DAPI staining reveals successful cellularization of the PCL/PLA membrane. **(c, d)** Overlay image with fluorescence and bright field microscopy. Trophoblast cell migration into the PCL/PLA membrane is visualized with DAPI staining. **(e, f)** Sections are immunostained with anti-CK7. CK7 is used with Alexa Fluor 633 secondary antibody. Immunofluorescence demonstrates positive expression of CK7 in trophoblast cells. *CK7* cytokeratin 7, *PCL/PLA* polycaprolactone/polylactide, *PFA* paraformaldehyde. Scale bars in **a, c, e** represent 200 µm, and those in **b, d, f** represent 20 µm.

Reproduction from Fuchs *et al.*2018 (58) with permission of publisher “SPRINGER-VERLAG” by license number 4676480552184.

4.6 *In situ* padlock probe detection in combination with immunostaining for CK7 on low-melting-point paraffin-embedded cellularized PCL/PLA scaffolds

After pepsin digestion, the cellularized PCL/PLA scaffolds were processed for *in situ* padlock probe technology and immunofluorescence staining of CK7. Single treatment with *in situ* padlock probe technology for ACTB mRNA transcripts displayed clear ACTB signals appearing as red fluorescence dots (Figure 15 a–c). The combination of *in situ* padlock probe technology and immunofluorescence offers ideal conditions for effective spatial discrimination between mRNA transcripts and proteins. The cells showed expression of CK7 (orange fluorescence signals) and exhibited clear ACTB signals (red fluorescence signals) present at the border of the cell nucleus (Figure 15 d–f). Negative controls showed no staining for CK7 and no expression of ACTB (data not shown). Thus, *in situ* padlock probes can be successfully combined with immunostaining on cellularized thermosensitive PCL/PLA membranes.

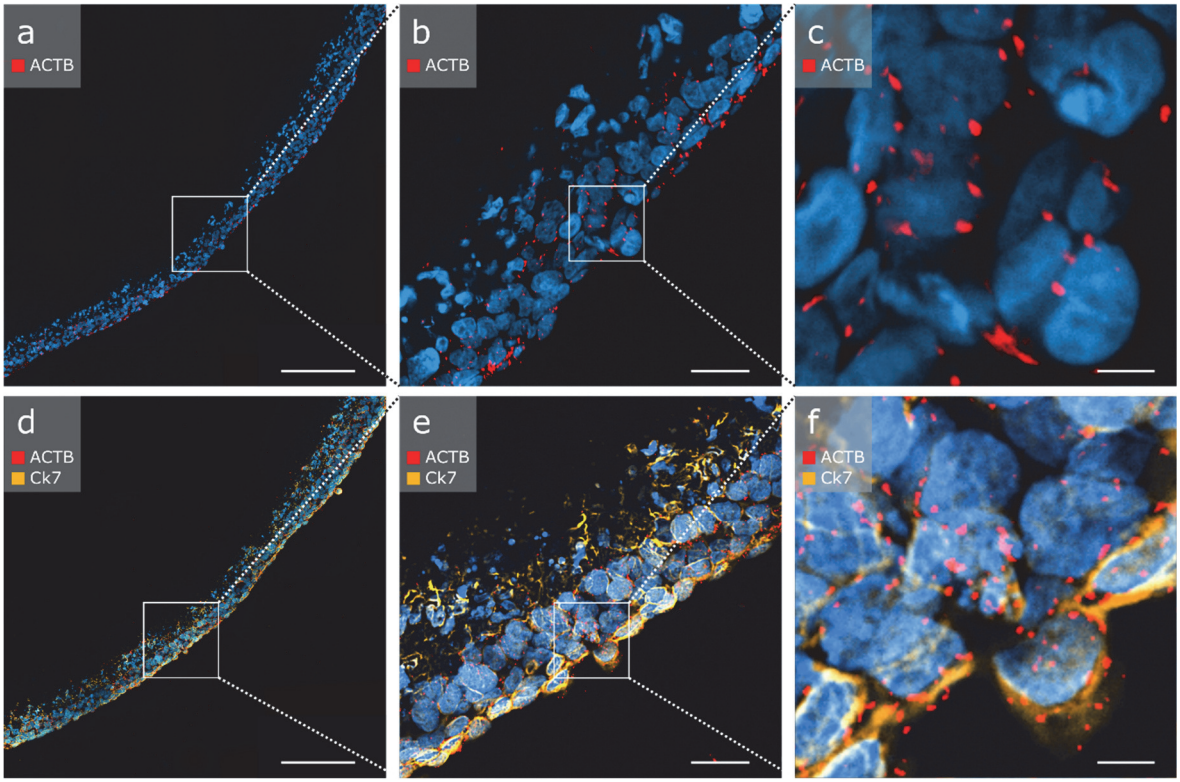

Figure 15: In situ padlock probe method applied on cellularized PCL/PLA membranes. Nuclei were counterstained with DAPI (blue). **(a–c)** In situ detection of ACTB mRNA transcripts using padlock probes. Single dots represent ACTB transcripts**. (d–f)** In situ detection of ACTB (red) mRNA transcripts using padlock probes combined with immunofluorescent staining of CK7 (orange). Scale bars in **a, d** represent 200 µm, those in **b, e** represent 50 µm, and those in **c, f** represent 10 µm. *ACTB* beta actin, *CK7* cytokeratin 7, *PCL/PLA* polycaprolactone/polylactide, *DAPI* 4′,6-diamidino-2-phenylindole

Reproduction from Fuchs *et al.* 2018 (58) with permission of SPRINGER-VERLAG by license number 4676480552184.

4.7 Analysis of cell morphology after cryofixation and low-melting-point paraffin embedding

An automatized cell analysis was cunducted to validate the influence of the selected embedding methods on the cell specific morphology. Analysis of the cell size revealed that low-melting-point paraffin embedding preserved cell morphology much better than cryofixation. Thus, after cryofixation the average cell size was reduced by 14% compared to the cell size after low-melting-point paraffin embedding, 160 ± 8 µm2 and 186 ± 6 µm2 (p = 0.0351), respectively (Figure 16).

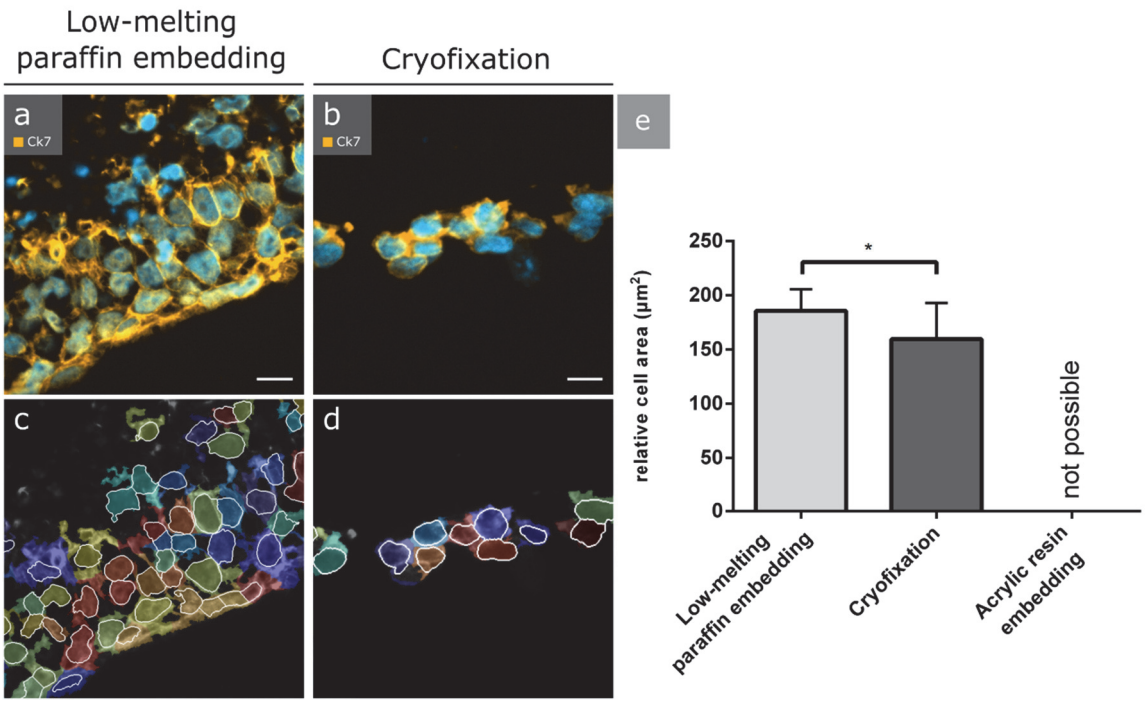

Figure 16: Automatized analysis of cells attached on PCL/PLA scaffolds after low-melting-point paraffin embedding and cryofixation. Overlay images of the immunofluorescent channels DAPI (nuclei, blue) and Cy5 (intermediate filaments, orange) of **(a)** low-melting-point paraffin-embedded and **(b)** cryofixed samples are shown. **(c, d)** Output images of the quantification of cell nuclei and cell area by the CellProfiler software are displayed. The coloured areas show the cellular regions. Cell nuclei are indicated by white frames. **(e)** The relative cell area of each embedding method shows the difference between the embedding methods. (*p < 0.05). **Ck7:** Cytokeratin 7; Scale bars in **a** and **b** represents 20 µm.

4.8 Placenta specific antibody characterization in the 3D cell culture model of the human placenta

To establish the 3D cell culture placental model, we proceeded as follows:

After testing the different antibodies on first trimester placenta sections (Figure 11, Figure 12), a single cell culture with external seeded ACH-3P cells was first prepared on PCL/PLA tubes (Figure 17).

In a second step, a tissue culture with first trimester explants was performed, cultivated on the outside of the PCL/PLA membrane. Staining with different placenta specific antibodies after pepsin digestion was also tested in this context. (Figure 19).

In these approaches, the major interest was to observe migrating trophoblast cells.

The next step was to establish a co-culture system in the trophoblast cell line ACH-3P was cultivated on the outside and endothelial (HIVEC) cells were cultured on the internal side of a mono-layer PCL/PLA tube.

4.8.1 Single Culture (Cell line)

After antibodies were tested on pepsin-digested first trimester placentas (Figure 11 and Figure 12), antibody characterization was done on two-layer scaffolds cellularized with ACH-3P cells on the outer surface used in the 3D cell culture model of the human placenta.

As the cell line ACH-3P was generated by fusion of first trimester trophoblasts and the choriocarcinoma cell line AC1-1, it is characterized by the expression of the specific EVT markers as described in chapter 1.4.

Thus, seven antibodies whose associated proteins are very likely to be expressed by the ACH-3P cell line were tested for their binding specificity after the pretreatment with pepsin. The antibodies tested include: β-hCG, CK7 (rabbit), CK7 (mouse), E-cadherin, ZO-1, HLA-G and Ki-67. Table 3 summarizes the full names and clone numbers of the used antibodies as well as the animal source, the company and the concentrations used according to the antigen retrieval pretreatment. Table 7 summarises the stock concentrations of the antibodies used.

Figure 17 shows antibody binding after pepsin digestion on ACH-3P attached on the external surface of PCL/PLA hollow fibers. Staining of HLA-G (Figure 17 k, l) and KI-67(Figure 17 m, n) after pepsin digestion showed no staining. Positive staining results were obtained after staining with β-hCG, CK7 (rabbit), CK7 (mouse), E-cadherin and ZO-1.

While β-hCG (Figure 17 a, b) and ZO-1 (Figure 17 i, j) displayed a moderate staining, high signal intensities were detected after antibody staining with CK7 (rabbit) (Figure 17 c, d), CK7 (mouse) (Figure 17 e, f) and E-cadherin (Figure 17 g, h). The CK7 mouse antibody displayed a more consistent staining and revealed better morphological cell integrity compared to the CK7 rabbit antibody.

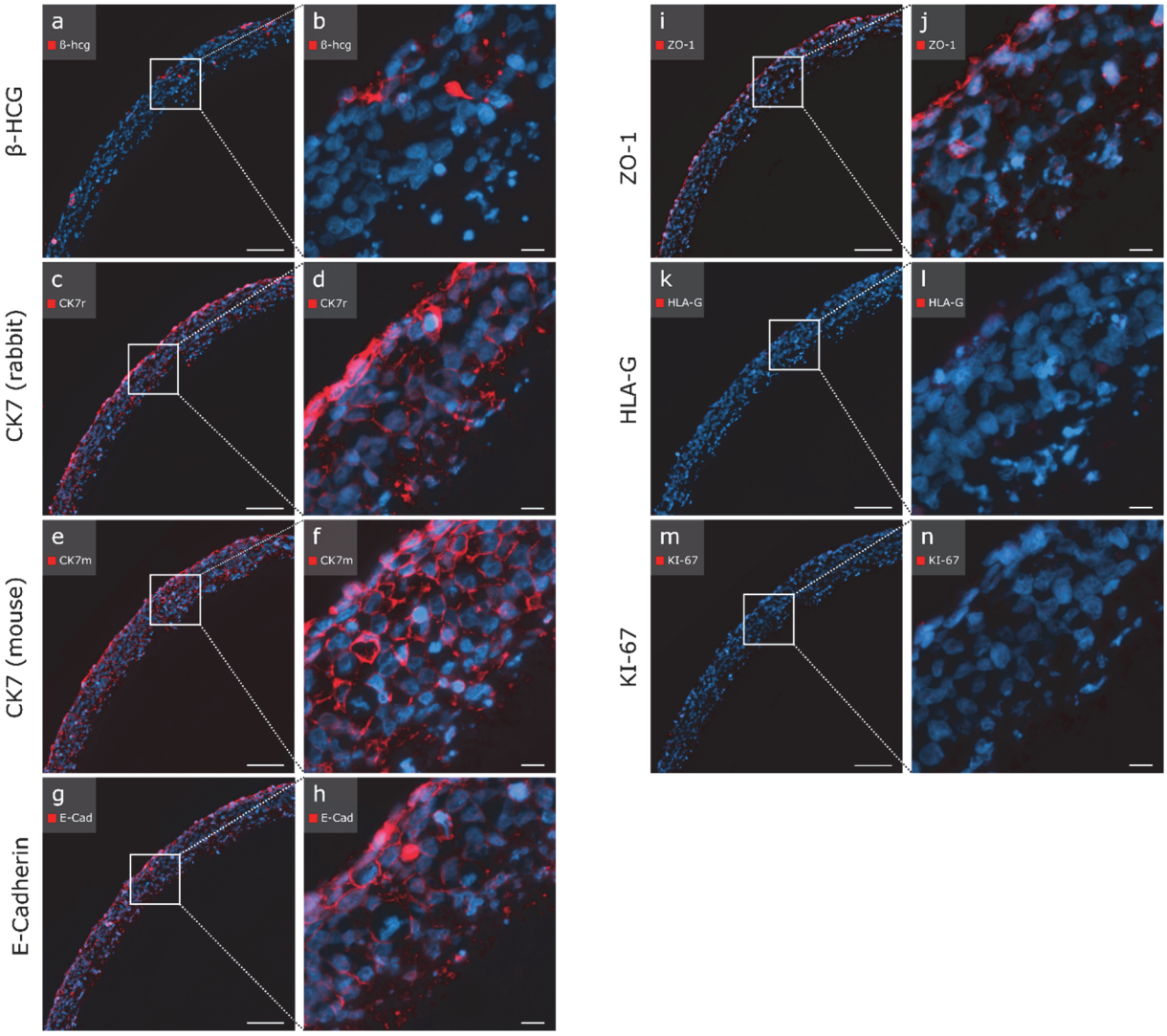

Figure 17: Testing of antibody on two-layer PCL/PLA scaffolds cellularized with ACH-3P on the external surface enzymatically pretreated with pepsin. Testing of antibodies after pepsin digestion, on PCL/PLA scaffolds cellularized with ACH-3P on the outer surface. All antibodies tested showed a positive signal, in exception for HLA-G **(k, l)** and K1-67 **(m, n)**. Scale bars in **a**, **c**, **e**, **g**, **l**, **k**, **m**, represent 100 µm, and those in **b**, **d**, **f**, **h**, **j**, **l**, **n** represent 20 µm.

4.8.2 Tissue Culture under normoxic conditions (Tissue)

A further step towards establishing a 3D cell culture model of the human placenta was the cultivation of first trimester placenta villi on the external side of mono-layered PCL/PLA tubes (Figure 18 a).

Hence, tissue culture was performed as described in chapter 3.5.3. Figure 18 shows a PCL/PLA membrane cultured with first trimester placenta villi on the external side for seven days under normoxic conditions (21% O_2). Some of the villi adhered to the membrane, as can be seen in Figure 18 c.

The PCL/PLA parts with adhered villi were used for further investigations to observe the migration pattern of the EVTs.

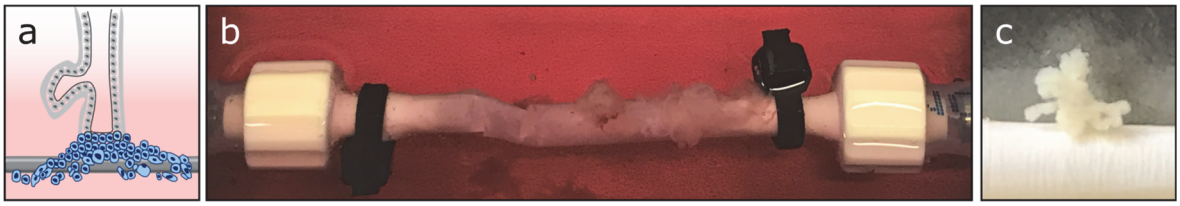

Figure 18: First trimester villi cultured on a mono-layered PCL/PLA tube for 7 days with an oxygen concentration of 21%. **(a)** Scheme of first trimester explant cultivated on the PCL/PLA tube. **(b)** Image of a PCL/PLA tube fixed in a metal housing with the first trimester villi cultured on its external surface. **(c)** First trimester villi adhering to the PCL/PLA tube.

In a first step, the migration of EVTs from the first trimester villi towards the membrane was investigated by HE staining (Figure 19 a, b). In order to distinguish the cells that migrated into the membrane, an immunohistochemical staining using the HLA-G antibody (typical marker for extravillous trophoblast cells) was performed on a serial section to verify the migrated cell type.

Staining with HLA-G antibody after pepsin digestion as antigen retrieval showed positive staining results (Figure 19 c). Thus, it was possible to characterize the cells that migrated into the PCL/PLA membrane as EVTs.

In addition, immunofluorescence staining with placenta specific antibodies which showed positive staining results after pepsin digestion in Figure 11, was conducted on tissue sections of adhered first trimester villi on mono-layered PCL/PLA tubes (Figure 19).

Antibodies used include: CD34II, ALPPL2, CK7 rabbit, CK7 mouse, E-cadherin, HLA-G, β-hCG, vWF and ZO-1. Table 3 summarises the full names and clone numbers of the antibodies as well as the animal source, company and concentrations used according to the antigen retrieval pretreatment. Table 7 summarises the stock concentrations of the antibodies used.

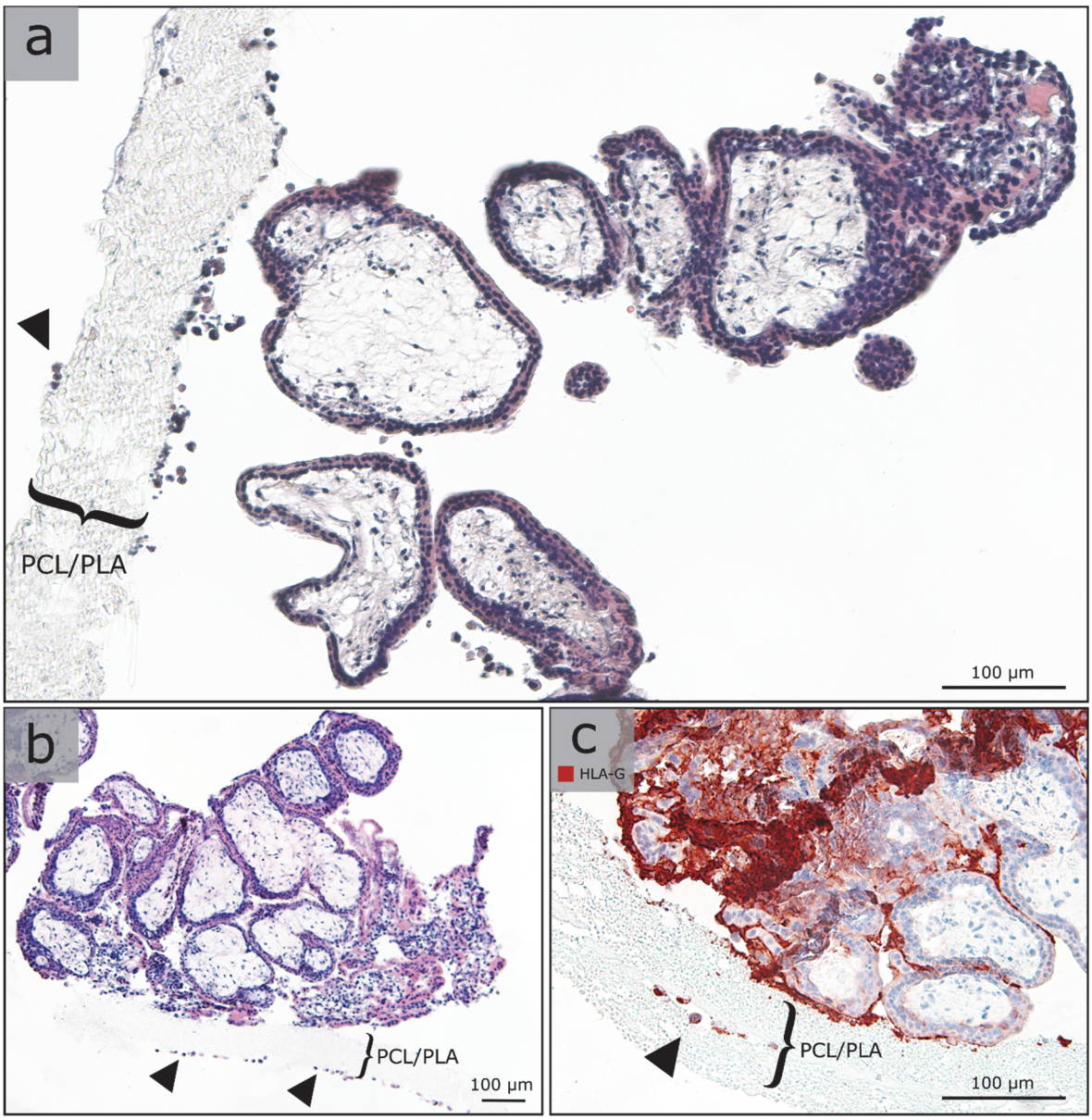

Figure 19: First trimester villi cultivated for 7 days on the outer durface of the monolayered PCL/PLA scaffold under normoxic (21% O_2) conditions. Light fiber-like structures marked with curly brackets indicate mono-layer PCL/PLA membranes, black arrowheads highlight migrated EVTs. **(a, b)** HE staining shows that single trophoblasts migrated through the PCL/PLA membrane. **(c)** HLA-G staining (typical marker for extravillous trophoblast cells (EVTs)) displays that migrated cells can be characterized as EVTs.

All antibodies used in Figure 20 showed positive staining results after pepsin digestion on sections of external adhered first trimester placental villi on PCL/PLA. The CD34II antibody showed specific staining of endothelial cells, marking blood vessels occurring in villous stroma of the first trimester villi (Figure 20 a, b).

A positive signal of alkaline phosphatase placental like 2 (ALLPL2) antibody was observed after the treatment with pepsin occurring exclusively in the SCT and migrated EVTs (Figure 20 c, d).

Both the rabbit and the mouse CK7 antibody showed a positive staining after pepsin digestion on membrane-adhered first trimester placental villi. The staining with CK7 mouse antibody (Figure 20 g, h) led to brighter and more distinct staining than the CK7 rabbit antibody (Figure 20 e, f). In relation to CK7 mouse antibody, CK7 rabbit antibody displayed poor cellular integrity. However, both antibodies revealed positive signals on migrating EVTs within the PCL/PLA membrane.

In addition, a positive result was achieved after the staining of the transmembrane protein E-cadherin. After the pretreatment with pepsin the CT cells as well as the migrating EVTs displayed a positive fluorescence signal (Figure 20 i, j).

The specific EVT marker HLA-G revealed a positive staining of existing EVTs in membrane-adhered first trimester villi, as well as a positive signal of migrated EVTs within the PCL/PLA membrane (Figure 20 k, l). Migrated cells can be characterized as EVTs.

As expected, SCT was stained positive for β-hCG after pepsin digestion. Additionally, the migrated EVTs within the membrane showed a positive signal for β-hCG (Figure 20 m, n).

The endothelial marker vWF displayed a positive staining result on first trimester placenta villi after the pretreatment with pepsin. The vWF antibody exhibited a specific staining of endothelial cells marking the blood vessels within the villous stroma of first trimester villi. EVTs that have been migrated through the PCL/PLA appeared negative for vWF (Figure 20 o, p).

After enzymatic pretreatment with pepsin, the ZO-1 displayed positive staining results of first trimester placenta villi. ZO-1 antibody yielded specific fluorescence signals of several cell types, such as EC, CT, SCT and fibroblasts. Even migrated EVTs appeared positive for ZO-1 (Figure 20 q, r).

In summary, the cultivation of first-trimester explants on the outside of a mono-layered PCL/PLA hollow fiber under normoxic conditions (21% O2) revealed that individual trophoblast cells migrate through the PCL/PLA membrane. Positive staining for HLA-G indicates that migrated cells can be characterized as EVTs.

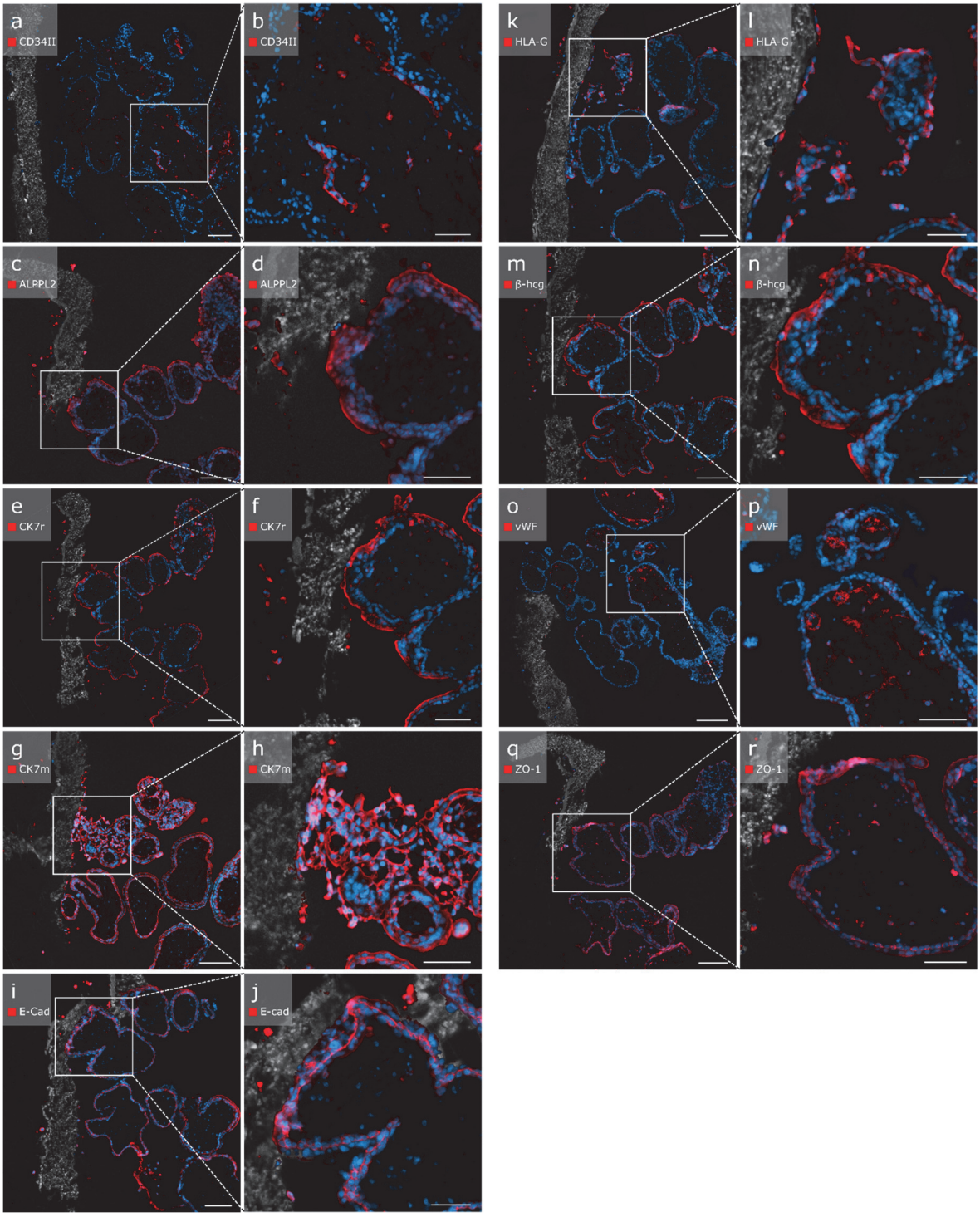

Figure 20: Immunofluorescence staining with placenta specific antibodies on first trimester placental villi adhered to mono-layered PCL/PLA scaffolds. White boxes indicate the zoom-in area of the right image. All antibodies used displayed a positive fluorescent signal. Scale bars in a, c, e, g, l, k, m, o, q represent 100 µm, and those in b, d, f, h, j, l, n, p, r represent 50 µm.

4.8.3 Co-cultivation of ACH-3P and HIVECs on mono-layer PCL/PLA holoow fibers under hypoxic conditions (2.5% O_2)

As Figure 21 shows, hypoxic conditions (2.5% O_2) lead to the proliferation of ACH-3P trophoblast cells. The images a and b of Figure 21 provide an HE-stained overview of the mono-layered PCL/PLA membrane co-cultured with ACH-3P cells on the outer surface and HIVECs on the internal surface. Figure 21 c and d show a double staining with CK7 antibody, representative for trophoblast cells and vWF antibody, representative for endothelial cells, marking the different cell types as expected. Additionally, Ki-67 revealed proliferating cells only in the trophoblast population as shown in Figure 21 e, f. Cleaved Caspase 3 antibody (CASP3) displayed that hardly any cells entered apoptosis. No migrating cells could be detected.

In general, it can be concluded that the co-cultivation of ACH-3P and HIVECs under hypoxia conditions lead to the proliferation of trophoblast cells.

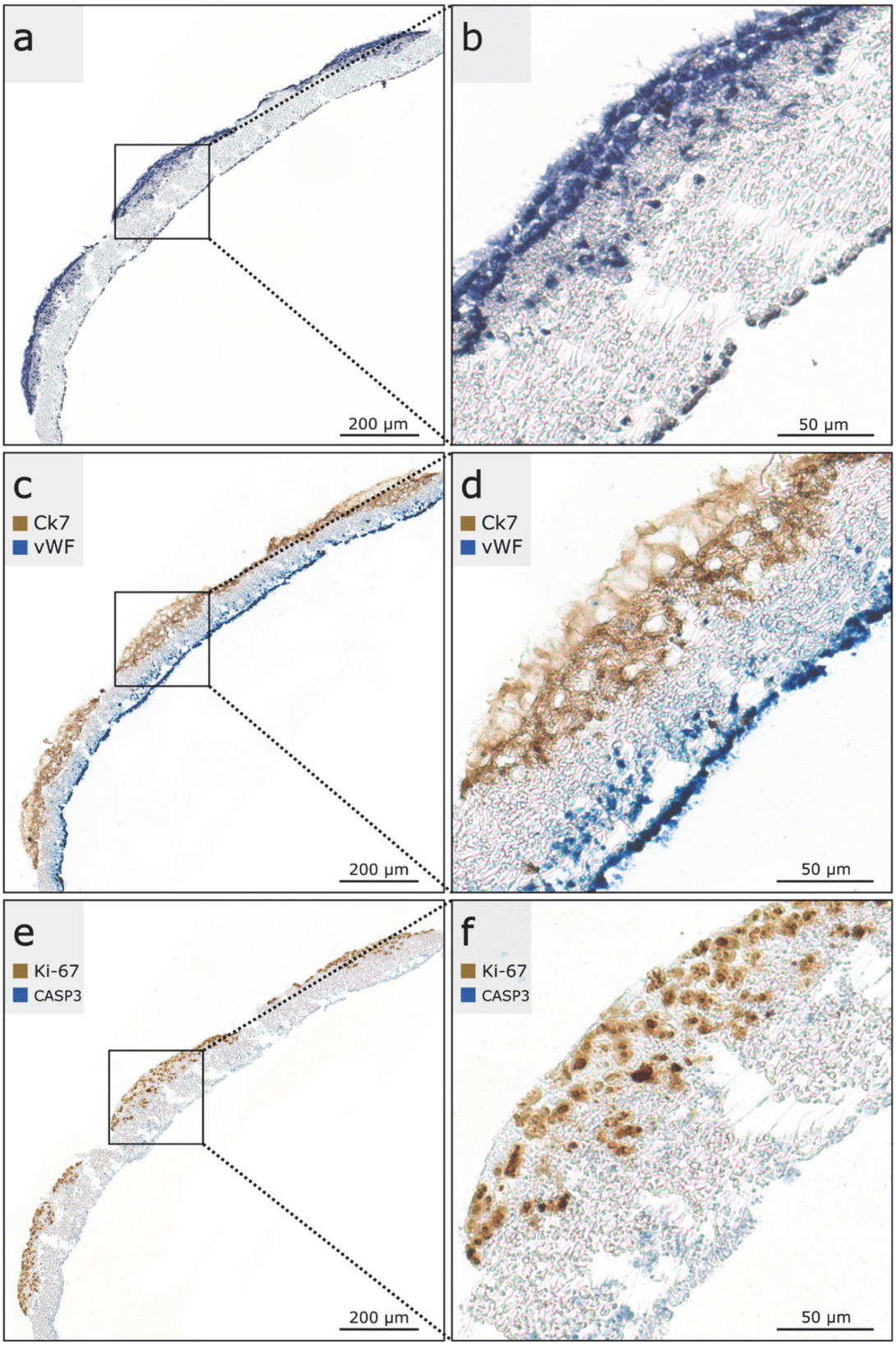

Figure 21: ACH-3P cells on the external surface of PCL/PLA co-cultivated for 7 days with primary endothelial cells (HIVEC = human vena iliaca endothelial cells) in the inner compartment of the PCL/PLA hollow fiber under hypoxic (2.5% O^2) conditions. **(a)** and **(b)** show a HE staining of both cell types. **(c)** and **(d)** display characterization of the two cell types with the CK7 (typical marker for trophoblast cells) and vWF (typical marker for endothelial cells) markers. **(e, f)** Ki-67 showed proliferating cells only in the trophoblast population and Casp3 antibody staining did not reveal any apoptotic cells. Basically, it can be seen that trophoblast cells expand under hypoxic conditions. No nuclear counterstain was applied.

4.8.4 Co-Culture (Tissue 21%)

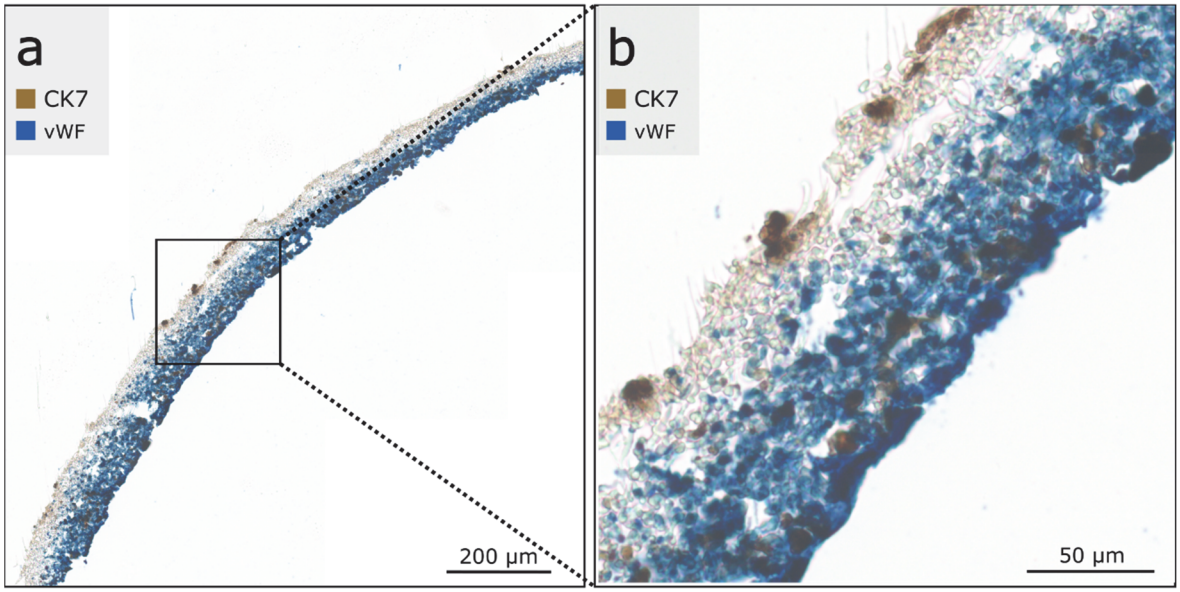

Figure 22: Immunohistochemical double staining of a co-cultured PCL/PLA hollow fiber cellularized with ACH-3P (external surface) and HIVEC (internal surface) for cytokeratin 7 (Ck7, brown, serves as marker for trophoblasts) and von Willebrand factor (vWF, blue, serves as marker for endothelial cells). Brown coloured trophoblast cells are found between the endothelial cells. No nuclear counterstain was applied.

A co-cultivation of ACH-3P trophoblast cells on the external surface and primary endothelial cells (HIVEC) on the internal side of a mono-layered PCL/PLA scaffold was conducted under normoxic (21% O_2) conditions for seven days. Figure 22 a and b show the characterization of the two cell by staining of CK7 and vWF.

EVT cells invade the PCL/PLA fiber meshwork towards primary endothelial cells on the inner surface. Brown coloured trophoblasts are found between the endothelial cells (blue).

In general, it can be concluded that trophoblast cells cultivated on the external surface begin to migrate towards endothelial cells on the internal side of the PCL/PLA hollow fiber under normoxic conditions.

5 Discussion

Please note that parts of the "Discussion" section are based on the publication of Fuchs *et al.* 2018 (58).

The present study focused on the establishment of basic requirements and methods for a matrix-based 3D placenta cell culture system to investigate the interaction of maternal arterial and vein endothelial cells with trophoblasts. Here, human iliac venous endothelial cells and the trophoblast cell line ACH-3P were used. The main focus was on the directed migration of trophoblast cells towards endothelial cells under normoxic (21% O_2) or hypoxic (2.5% O_2) conditions including the associated histological characterization of the cells. Although artificial organ systems pose limitations compared to *in vivo* studies, *in vitro* model systems are still essential for investigations of trophoblast invasion. Trophoblast cells invade maternal endothelial structures *in vivo* for which reason endothelial cells from the iliac vein were used as a model throughout this study. An alternative to the conventional histological processing methods had to be found for thermosensitive samples due to the application of a matrix-based system that is comprised of biodegradable and heat-sensitive materials. Since there were hardly any heat-reduced alternatives to the standard histological protocols described in the literature, a suitable method for histological embedding of thermosensitive materials had to be established additionally within this project.

5.1 Heat induced effects on thermosensitive PCL/PLC membranes while histological processing

The histological treatment and analysis of thermosensitive materials like PCL/PLA, as used in this study, require the adaptation of already existing protocols. Besides cryo-embedding most histological embedding methods include processing steps at temperatures above 61 °C. Since the melting temperature of PCL/PLA is 51°C, it was necessary to keep the processing temperature below this level, in order to identify the scaffold structure and cell-membrane interactions after the embedding procedure.

Specific antibody staining is essential for the histological analysis of the samples for which epitope demasking by antigen retrieval is required in most cases. In the absence of this process, the majority of antibody staining techniques such as immunohistochemistry or immunofluorescence do not yield any results on the tissue. Generally, antigen retrieval is performed at temperatures of about 120°C. Since there is hardly any literature offering

solutions to avoid heat exposure in histological embedding methods or antigen retrieval methods, information on handling procedures that involve thermos-sensitive materials are completely missing.

Hence, several histological techniques for heat-sensitive materials like electrospun PCL/PLA scaffolds were compared in this study, including cryofixation, gelatine embedding with subsequent automated dehydration and standard paraffin embedding, as well as an acrylic resin embedding technique and the established method of low-melting-point paraffin.

In this regard, cryofixation seems to be the method of choice for these applications. However, compared to paraffin-embedded sections, frozen tissue sections are usually thicker, resulting in lower microscopic resolution making it difficult to capture tissue morphology in detail. However, it is assumed that cryofixation preserves antigens and antigenicity more efficiently (82).

Following the publication of Hruschka *et al.* (83) we tested embedding the PCL/PLA scaffold in different gelatine concentrations before embedding them in standard paraffin to increase the heat stability of the material. The simple application of the gelatine embedding technique makes it attractive for a wide range of cell-material interactions studies. Sectioning the gelatine/paraffin blocks, however, caused a major problem, as the unequal density of the materials led to the separation of the gelatine core from the paraffin block.

Similar observations were also obtained by other research groups such as Brown *et al.* and James *et al.* They assume that, cellularized scaffolds exhibit an enormous spatial discontinuity during the phases of cell proliferation compared to mature natural tissues. It is possible that this discontinuity within the cell-material interaction is the reason for the difficulties during preparation (84, 85).

Generally, histological embedding in acrylic resin is carried out at temperatures of 60 °C or higher. Since the method is also used for immunolabeling, embedding at room temperature is possible (86, 87). Basically, acrylic resin embedding is used for the investigation of tissue ultrastructure resulting in the fact that it is hardly possible to produce sections with a thickness greater than 3 µm, presenting a difficulty for conventional light microscopy. With exception of the toluidine blue staining, the high density of the resin prevents standard histological staining such as HE staining or immunohistochemistry, as hardly any dye has the ability to penetrate the resin (88). In addition, the method has an extensive processing time of up to several days. Consequently, the method is not suitable for a quick immunohistological characterization of cells.

In order to obtain histological images with fibers unchanged in diameter and structure, and preserved scaffold formation, the embedding of uncellularized and cellularized PCL/PLA scaffolds in low-melting-point paraffin at a temperature of 50 °C turned out to be the most efficient method. Compared to all alternative methods, this variant of fixation and embedding seemed to be the best available technique as it preserved an intact structure of the unprocessed and cellularized PCL/PLA scaffolds.

5.2 Influence of antigen retrieval on antibody binding on villi of first trimester placenta

Tissue samples are generally fixed prior to histological processing using fixatives. There are several reasons for tissue fixation, including the preservation of the biological material as close as possible to its natural state (89). During the fixation with formaldehyde, methylene bridges cross-link reactive sites within and between different proteins (85, 90). As a consequence, the tertiary and quaternary structures of proteins are modified while primary and secondary structures are preserved (90). Temperature and duration of fixation, however, significantly reduces immunoreactivity for many antigens (91, 92). In order to perform immunohistochemical or immunofluorescence staining on formaldehyde fixed samples, usually antigen retrieval is required (90).

Antigen retrieval reveals epitopes and other cellular targets providing access to antibodies and oligonucleotides (93). Besides heat-induced antigen retrieval methods, enzymatic digestion with proteolytic enzymes such as proteinase K or pepsin offers a useful alternative to prevent heat-induced modifications of the thermosensitive PCL/PLA scaffold (70). The working mechanism of antigen retrieval by enzymes is not yet fully understood. Nevertheless, it is assumed that the bonds existing between the proteins and the fixative are cleaved in an unspecific way (94–96). This cleavage activity is determined by the duration and temperature of the enzymatic digestion (91).

Using heat to invert modifications caused by formalin on the protein structure has revolutionized IHC and expanded the number of antibodies that can be used in formalin fixed tissue samples. However, heat treatment is not applicable for all kind of samples, especially if these reveal thermosensitive properties. In some cases, heat exposure may also reduce or eliminate the detection of certain antibodies rather than improve it (97–99).

Consequently, in most of these studies histological analysis is completely missing due to the material characteristics.

Since the establishment of the matrix-based 3D placenta cell culture system includes thermosensitive and biodegradable PCL/PLA membranes, a heatless antigen retrieval method was required for low-melt-point-paraffin embedded samples for further immunohistochemical or immunofluorescence analysis.

Therefore, we examined 17 placenta-specific antibodies for their binding properties on formalin-fixed and low-melting-point paraffin embedded first trimester placenta sections after four different antigen retrieval methods. To evaluate which type of antigen retrieval is most appropriate for the applied antibody and whether enzymatic digestion with pepsin represents a valid alternative to heat-induced antigen retrieval, a comprehensive screening was conducted. The immunofluorescence staining results were analysed in a quantitative and qualitative way.

While all examined antigens could be detected after pretreatment with steam heat with either ph6 or ph9, not a single antibody showed positive staining after pretreatment with pepsin only. However, eight antibodies showed positive binding properties after pepsin digestion, making the enzymatic method a heat-free antigen retrieval alternative for these antibodies (Figure 11). Two of these eight antibodies, specifically β-hCG and vWF, even showed improved binding properties after pepsin digestion in contrast to the steam heat pretreatment.

Not all antibodies were found to give verifiable results after enzymatic digestion. In some cases, enzymatic antigen retrieval led to complete or incomplete epitope degradation. As shown in Figure 12, eight antibodies were completely lacking in staining reaction as their epitopes have probably been completely degraded. This result closely parallels the findings of Battifora *et al.* (91) and Daneshtalab *et al.* (100) which argue, that overdigestion damages the morphology and immunoreactivity of the tissue and may cause a reduction in the number of antigenic sites available for immunohistochemical staining.

Interestingly, CD163, showed an unspecific staining pattern throughout the tissue after pepsin digestion. We assume that this result is due to incomplete degradation of the cross-links, as non-specific primary antibody reactions may also occur according to the presence of unreacted hydroxymethyl groups after formaldehyde fixation. Additionally, depending on the type of epitope and antibody, non-specific interactions may appear between the primary antibody and other antigens in the tissue (100). Battifora *et al.* also states that there are antigens that are resistant to digestive enzymes (91). Therefore, it is generally assumed that the point at which tissue gets over digested is variable and depends not only on the duration of fixation, but also on the antigen and the type of tissue examined (100).

Further, no antigen retrieval was necessary in eight cases to obtain a positive staining signal. However, all of these antibodies showed a more intense immunofluorescence staining signal after the pretreatment with steam heat or enzymatic digestion.

In conclusion, when applying enzymatic digestion with pepsin as an alternative to heat induced antigen retrieval methods, the result of immunohistochemical staining is related to the duration of the fixation and digestion step and has to be determined for each antigen individually.

For antibodies that did not show a positive result using enzymatic digest in this study, the duration of pepsin digestion to receive positive staining results can be determined by further investigations. It is likely that shortening the digestion time would yield positive results for some antibodies.

5.3 Automatized-quantitative and qualitative analysis of antibody staining

In recent decades, researchers have recognized the importance of the field of quantitative image analysis in histology. With the introduction of digital scanners for whole slides, entire histological specimens can now easily be digitized and automatically analysed. The increased amount of image data opened this extensive evaluation opportunity to a wide range of scientific research areas (101).

Today, automated quantitative analysis is a tool in clinical routine and is increasingly demanded in scientific research. However, the application in new areas is often challenging, since analytical procedures have to be designed individually for each specific research questions always.

The major advantage of an automated computational analysis is a more objective and thus less biased interpretation of data. The benefits of computer-based evaluation are plentiful, although the methods are not entirely problem-free. The main problem with automated analysis is the possibility of misinterpretation of data before and after evaluation, especially by unqualified professionals (102, 103).

In this study, a quantitative analysis of the signal intensity of the antibodies was crucial and is nowadays indispensable in research. Nevertheless, the qualitative aspect of the appropriate histologic antibody binding to its respective target remains essential for an overall assessment of the antibody specificity. As the qualitative analysis in this study

demonstrates, the application of different antigen retrieval methods often stains different cell types, which can be observed regarding β-HCG and the two investigated CK7 antibodies. This aspect has to be considered in quantitative analyses, to avoid misinterpretation.

To give an example, the CK7 rabbit antibody was found to bind to all trophoblast populations and uterine glands without any reactivity to mesenchymal stroma as described in the literature after heat induced pretreatments with ph6 or ph9 (79, 104). However, the CK7 rabbit antibody showed differences in its staining pattern intensity depending on the antigen retrieval pretreatment. After the pretreatment with ph6 (Figure 11, c) a more intense staining of the CT was observed compared to the SCT. After the treatment with ph9, the CK7 rabbit antibody showed hardly any difference in the staining intensities between CTs and the SCT cells. However, the antibody showed an exclusive staining of CT cells after enzymatic digestion with pepsin. If no antigen retrieval method was applied, the CK7 rabbit antibody did not show any staining signal at all.

Being ignorant of these peculiarities may lead to misinterpreting a high fluorescence signal as equal to a very intense staining of the cell type expected to be stained. However, high levels of fluorescence in quantitative analysis can occur as a result of accumulating signals due to the fact that additional cell types were stained by the AG method used. Consequently, the total fluorescence level of the image increases, but not the fluorescence intensity of a single cell type. These differences in cell type staining have to be considered before interpreting quantitative analysis data.

Hence, our analysis shows that an enzymatic digestion with pepsin can often serve as an alternative to heat-affected antigen retrieval methods, but it is not suitable for every antibody. In addition, for histological preparations a quantitative analysis must be accompanied by a qualitative analysis and vice versa in order to give a comprehensive statement on the data.

To evaluate whether cryofixation or low-melting-point paraffin embedding is the preferred method for thermosensitive embedding for ACH-3P cellularized PCL/PLA samples, both variants were stained with human CK7 and the relative cell size was determined quantitatively. The comparison of the cell size showed that low-melting-point paraffin embedding conserved cell morphology more effectively than cryofixation. The average cell size after cryofixation was reduced significantly by 14% compared to the cell size after low-melting-point paraffin embedding. Hence, low-melting-point paraffin embedding in combination with pepsin antigen retrieval appeared to be the most beneficial technique for the visualization of cell morphology and fiber-structure of cellularized PCL/PLA scaffolds

when compared to all variants related to the methods of fixation, embedding and thermosensitive antigen retrieval methods. This approach allows histological analysis of the attached cells and evaluation of cell-scaffold interactions.

In addition, we were interested in whether our novel histological procedure is a feasible method for low-melting-point paraffin embedded and enzymatically treated samples when applied to highly specific methods. Therefore, the *in situ* padlock probe method (73, 105), a mRNA-based staining technique was applied on our samples by targeting the mRNA transcripts for the housekeeping ACTB, which yielded positive results (Figure 15). Further, the combination of this method with immunofluorescence for CK7 resulted in positive signals from both techniques.

Repeatable results were obtained with all tested methods, including immunohistochemistry, immunofluorescence and *in situ* padlock probe techniques. Low-melting-point paraffin embedding combined with enzymatic antigen recovery offers a cost-effective and convenient method that perfectly suits histological processes involving heat sensitive material with complex physical characteristics.

In summary, we were able to develop a convenient heat-reduced method to histologically characterize the migration of cells in thermo-sensitive materials. This method allowed the morphological assessment of cells cultured on complex materials and, for the first time, to analyse these quantitatively. It also offers an adequate alternative to standard preparations for histological investigations in a variety of sensitive samples.

5.4 3D cell culture system of the placenta – Invasion of EVTs

In recent years, the invasion of trophoblasts into the myometrium and the associated plug building of spiral arteries and remodelling of veins and lymphatic vessels has been extensively studied (12, 17, 106, 107). Extravillous trophoblasts invade the decidual interstitium to the upper third of the myometrium during the first trimester of pregnancy. This results in anchoring the placenta in the uterus. The process is responsible for a histiotrophic nutrition of the fetus when uterine glands are opened into the intervillous space and for establishing a haemotrophic nutrition at the beginning of the second trimester (12).

Although it has been shown that certain cytokines produced by trophoblast cells and paracrine factors secreted by the endothelial cells influence the invasion process of the trophoblasts (108–111), the exact mechanism of invading of EVTs still remain unclear.

Moser *et al.* speculates that none of the pathways of extravillous trophoblast invasion, neither interstitial, endovascular nor endoglandular is specifically directed. This suggests that EVTs are just highly invasive cells and simply attach to and invade any structure within their vicinity. The coherent evidence stems from *in vivo* scenarios, as embryos can attach to and invade into the tissue of the fallopian tubes, ovaries and peritoneum. In addition, there are *in vitro* studies supporting this hypothesis, since *in vitro* cultured EVTs, in addition to decidual tissue, also attach to and invade various offered matrices such as collagen I, laminin and matrigel (12).

This assumption is consistent with the results of the present work, considering that both, the trophoblast cell line ACH-3P and EVTs of first trimester villi, adhere and invade into the PCL/PLA material as shown in Figure 17 - 20.

5.5 The influence of oxygen on extravillous trophoblasts

The effect of oxygen on migration of EVT cells needs to be taken into account. Due to the lack of connection to the maternal blood system, embryo development in the first trimester of pregnancy takes place in an oxygen-deficient environment (23). It is speculated that the naturally occurring oxygen gradient is one of the main reasons that trophoblast cells start migrating towards endothelial cells (13).

Our findings show that trophoblast cells (ACH-3P as well as primary EVTs) that were single cultured or co-cultured with primary endothelial cells in the matrix-based 3D cell culture system, begin to increase the proliferation under hypoxic conditions (2.5% O_2). However, they do not start to invade the PCL/PLA material as shown in Figure 21. These findings are in line with previous *in vitro* results from other research groups. Kilbur *et al.*, for instance, observed that HTR-8/SVneo cells, a human first trimester CT cell line, show both increased proliferation and reduced invasion through Matrigel when cultured in 2% oxygen conditions (112).

At oxygen concentrations of 21% and under single culture conditions, many ACH-3P cells could be found within the PCL/PLA membrane of the 3D cell culture model of the placenta (Figure 17). The trophoblast cell line showed hardly any proliferation compared to reduced O_2 conditions but started to migrate. Same observations were made for primary EVTs from first trimester placenta villi, which also started migrating into the membrane at normoxic (21% O_2) conditions (Figure 19, Figure 20). Co-culture experiments displayed that many ACH-3P cells could be found within the primary endothelial cells on the internal side of the

matrix based 3D - placenta cell culture system at oxygen concentrations of 21% as shown in Figure 22.

According to these results, we conclude that trophoblast cells begin to migrate under normoxic (21% O_2) conditions and switch their properties from a proliferative to an invasive phenotype.

These findings are in agreement with the in vitro data by Genbacev *et al.* (113) who showed that in vitro hypoxia shifted the balance between the proliferative and the invasive phenotype of extravillous trophoblasts towards the proliferative one (114). This effect is potentially due to a shift in the expression pattern, which changes trophoblast cells that are sufficiently supplied with oxygen (115). James *et al.* points out that there are two opposing opinions about the effect of hypoxia (2.5 % O_2) on trophoblast differentiation in the first trimester of human pregnancy. On the one hand, hypoxia promotes a proliferative trophoblast phenotype to create a high number of trophoblasts to invade maternal decidua. On the other hand, conflicting results showed that hypoxia promotes an invasive trophoblast phenotype, which may be important to achieve sufficient depth and extent of trophoblast invasion (13).

Huppertz *et al.* comprehensively argues that trophoblastic cell columns develop at the tips of the anchoring villi, precisely at the border between the actual placenta and the decidua basalis, and thus develop within the oxygen gradient. The proximal parts of the cell columns are exposed to the lowest oxygen levels within the whole columnar structures and is known as the site of proliferation. These proliferating trophoblasts passively push their daughter cells towards maternal tissue at the end of the distal parts of the cell columns. Due to the higher oxygen level in this area, the proliferation of the daughter cells stops and shifts to a high invasive potential. Consequently, they migrate towards the myometrium and potentially reach spiral arteries, veins and lymphatic vessels (10, 23, 116).

Whether trophoblasts migrate towards endothelial cells or whether they start to migrate in an undirected manner under normoxic conditions cannot be concluded from our results. According to the hypothesis of Moser *et al.* (12), which assumes that EVTs are highly invasive cells that invade in an undirected manner into various materials, there would be no correlation between endothelial cells and the migration pattern of trophoblasts. This hypothesis is supported by our results as ACH-3P and EVTs of first trimester placenta villi also migrate into the PCL/PLA membrane under single culture conditions.

Co-culture experiments in this work were initially conducted using the ACH-3P cell line as trophoblast substitute on the external side of the 3D – placenta cell culture system and primary endothelial cells on the inner surface. It is controversial to what extent fusion cell

lines such as ACH-3P can serve as substitutes for primary extravillous trophoblasts and whether these cell lines reflect the behaviour and characteristics of an *in vivo* situation. However, cell lines provide a fundamental basis for ongoing studies.

Concluding, we were able to establish a new matrix-based 3D placenta cell culture system in which we could demonstrate the migration pattern of trophoblast cells under different oxygen concentrations. The migration of trophoblast cells could not only be demonstrated under single culture conditions using the cell line ACH-3P and first trimester placenta villi, but also under co-culture conditions trophoblast migration towards primary endothelial cells was shown.

Without a doubt, these assumptions have to be verified by further experiments. Since the receipt of first trimester placenta villi was discontinued during the project, unfortunately it was no longer possible to conduct co-culture experiments with primary trophoblasts in the 3D - placenta cell culture system.

For future prospects of this project it would be interesting to investigate the interaction between primary trophoblasts of first trimester placental villi and primary endothelial cells via the matrix-based 3D placenta cell culture system. The migration behaviour of trophoblasts at different oxygen concentrations needs to be further investigated, alongside various factors and parameters released into the medium by endothelial cells. These may be discovered as triggers for the proliferation or migration behaviour of trophoblast cells. It is likely that further results obtained in this system may contribute to a better understanding of the invasion process of trophoblasts into maternal arteries, veins and lymphatic vessels and may help clarifying certain pregnancy disorders in the future.

6 Bibliography

1. Burton GJ, Fowden AL. The placenta: a multifaceted, transient organ. Philos Trans R Soc Lond B, Biol Sci 2015; 370(1663):20140066. doi: 10.1098/rstb.2014.0066.

2. Garnica AD, Chan WY. The role of the placenta in fetal nutrition and growth. J Am Coll Nutr 1996; 15(3):206–22. doi: 10.1080/07315724.1996.10718591.

3. Gude NM, Roberts CT, Kalionis B, King RG. Growth and function of the normal human placenta. Thromb Res 2004; 114(5-6):397–407. doi: 10.1016/j.thromres.2004.06.038.

4. Hisanaga H, Iioka H, Moriyama I, Nabuchi K, Morimoto K, Ichijo M. The mechanism of human placental urea transport: a study using placental brush border (microvillous) membrane vesicles. Asia Oceania J Obstet Gynaecol 1991; 17(1):67–72.

5. Meschia G. Fetal oxygenation and maternal ventilation. Clin Chest Med 2011; 32(1):15–9. doi: 10.1016/j.ccm.2010.11.007.

6. Rama S, Rao AJ. Regulation of growth and function of the human placenta. Mol Cell Biochem 2003; 253(1-2):263–8. doi: 10.1023/a:1026076219126.

7. Syme MR, Paxton JW, Keelan JA. Drug transfer and metabolism by the human placenta. Clin Pharmacokinet 2004; 43(8):487–514. doi: 10.2165/00003088-200443080-00001.

8. Benirschke K. The human placenta. J. D. Boyd and W. J. Hamilton. Heffer, Cambridge, 365 pp. 1970. Teratology 1973; 8(1):77–8. doi: 10.1002/tera.1420080118.

9. Pijnenborg R, Vercruysse L, Carter AM. Deep trophoblast invasion and spiral artery remodelling in the placental bed of the lowland gorilla. Placenta 2011; 32(8):586–91. doi: 10.1016/j.placenta.2011.05.007.

10. Huppertz B, Weiss G, Moser G. Trophoblast invasion and oxygenation of the placenta: measurements versus presumptions. Journal of Reproductive Immunology 2014; 101-102:74–9. doi: 10.1016/j.jri.2013.04.003.

11. Boyd JD, Hamilton WJ. The human placenta. Cambridge: Heffer; 1970.

12. Moser G, Weiss G, Sundl M, Gauster M, Siwetz M, Lang-Olip I et al. Extravillous trophoblasts invade more than uterine arteries: evidence for the invasion of uterine veins. Histochem Cell Biol 2017; 147(3):353–66. doi: 10.1007/s00418-016-1509-5.

13. James JL, Stone PR, Chamley LW. The regulation of trophoblast differentiation by oxygen in the first trimester of pregnancy. Hum Reprod Update 2006; 12(2):137–44. doi: 10.1093/humupd/dmi043.

14. al-Lamki RS, Skepper JN, Burton GJ. Are human placental bed giant cells merely aggregates of small mononuclear trophoblast cells? An ultrastructural and immunocytochemical study. Human Reproduction 1999; 14(2):496–504. doi: 10.1093/humrep/14.2.496.

15. Bischof P, Irminger-Finger I. The human cytotrophoblastic cell, a mononuclear chameleon. Int J Biochem Cell Biol 2005; 37(1):1–16. doi: 10.1016/j.biocel.2004.05.014.

16. Moser G, Windsperger K, Pollheimer J, Sousa Lopes SC de, Huppertz B. Human trophoblast invasion: new and unexpected routes and functions. Histochem Cell Biol 2018; 150(4):361–70. doi: 10.1007/s00418-018-1699-0.

17. Windsperger K, Dekan S, Pils S, Golletz C, Kunihs V, Fiala C et al. Extravillous trophoblast invasion of venous as well as lymphatic vessels is altered in idiopathic, recurrent, spontaneous abortions. Hum Reprod 2017; 32(6):1208–17. doi: 10.1093/humrep/dex058.

18. Moser G, Huppertz B. Implantation and extravillous trophoblast invasion: From rare archival specimens to modern biobanking. Placenta 2017; 56:19–26. doi: 10.1016/j.placenta.2017.02.007.

19. Moser G, Gauster M, Orendi K, Glasner A, Theuerkauf R, Huppertz B. Endoglandular trophoblast, an alternative route of trophoblast invasion? Analysis with novel confrontation co-culture models. Hum Reprod 2010; 25(5):1127–36. doi: 10.1093/humrep/deq035.

20. Burton GJ, Jauniaux E, Charnock-Jones DS. Human Early Placental Development: Potential Roles of the Endometrial Glands. Placenta 2007; 28:S64-9. doi: 10.1016/j.placenta.2007.01.007.

21. Rodesch F, Simon P, Donner C, Jauniaux E. Oxygen measurements in endometrial and trophoblastic tissues during early pregnancy. Obstet Gynecol 1992; 80(2):283–5.

22. Jauniaux E, Watson AL, Hempstock J, Bao YP, Skepper JN, Burton GJ. Onset of maternal arterial blood flow and placental oxidative stress. A possible factor in human early pregnancy failure. Am J Pathol 2000; 157(6):2111–22. doi: 10.1016/S0002-9440(10)64849-3.

23. Huppertz B. Oxygenation of the placenta and its role in pre-eclampsia. Pregnancy Hypertens 2014; 4(3):244–5. doi: 10.1016/j.preghy.2014.04.016.

24. Burton GJ, Jauniaux E. Placental oxidative stress: from miscarriage to preeclampsia. J Soc Gynecol Investig 2004; 11(6):342–52. doi: 10.1016/j.jsgi.2004.03.003.

25. Jauniaux E, Hempstock J, Greenwold N, Burton GJ. Trophoblastic Oxidative Stress in Relation to Temporal and Regional Differences in Maternal Placental Blood Flow in Normal and Abnormal Early Pregnancies. Am J Pathol 2003; 162(1):115–25.

26. Kaufmann P, Black S, Huppertz B. Endovascular trophoblast invasion: implications for the pathogenesis of intrauterine growth retardation and preeclampsia. Biol Reprod 2003; 69(1):1–7. doi: 10.1095/biolreprod.102.014977.

27. Huppertz B. Maternal-fetal interactions, predictive markers for preeclampsia, and programming. Journal of Reproductive Immunology 2015; 108:26–32. doi: 10.1016/j.jri.2014.11.003.

28. Ghulmiyyah L, Sibai B. Maternal mortality from preeclampsia/eclampsia. Semin Perinatol 2012; 36(1):56–9. doi: 10.1053/j.semperi.2011.09.011.

29. Gathiram P, Moodley J. Pre-eclampsia: its pathogenesis and pathophysiolgy. Cardiovasc J Afr 2016; 27(2):71–8. doi: 10.5830/CVJA-2016-009.

30. Uzan J, Carbonnel M, Piconne O, Asmar R, Ayoubi J-M. Pre-eclampsia: pathophysiology, diagnosis, and management. Vasc Health Risk Manag 2011; 7:467–74. doi: 10.2147/VHRM.S20181.

31. Figueras F, Gratacós E. Update on the diagnosis and classification of fetal growth restriction and proposal of a stage-based management protocol. Fetal Diagn Ther 2014; 36(2):86–98. doi: 10.1159/000357592.

32. Lyall F, Bulmer JN, Duffie E, Cousins F, Theriault A, Robson SC. Human Trophoblast Invasion and Spiral Artery Transformation : The Role of PECAM-1 in Normal Pregnancy, Preeclampsia, and Fetal Growth Restriction. Am J Pathol 2001; 158(5):1713–21.

33. Frøen JF, Gardosi JO, Thurmann A, Francis A, Stray-Pedersen B. Restricted fetal growth in sudden intrauterine unexplained death. Acta Obstet Gynecol Scand 2004; 83(9):801–7. doi: 10.1111/j.0001-6349.2004.00602.x.

34. Roberts JM, Redman CW. Pre-eclampsia: more than pregnancy-induced hypertension. Lancet 1993; 341(8858):1447–51.

35. Sullivan MHF. Endocrine cell lines from the placenta. Mol Cell Endocrinol 2004; 228(1-2):103–19. doi: 10.1016/j.mce.2003.03.001.

36. Jia R-Z, Ding G-C, Gu C-M, Huang T, Rui C, Wang Y-X et al. CDX2 enhances HTR-8/SVneo trophoblast cell invasion by altering the expression of matrix metalloproteinases. Cell Physiol Biochem 2014; 34(3):628–36. doi: 10.1159/000363028.

37. Park H-R, Kamau PW, Loch-Caruso R. Involvement of reactive oxygen species in brominated diphenyl ether-47-induced inflammatory cytokine release from human extravillous trophoblasts in vitro. Toxicol Appl Pharmacol 2014; 274(2):283–92. doi: 10.1016/j.taap.2013.11.015.

38. Hiden U, Wadsack C, Prutsch N, Gauster M, Weiss U, Frank H-G et al. The first trimester human trophoblast cell line ACH-3P: a novel tool to study autocrine/paracrine regulatory loops of human trophoblast subpopulations--TNF-alpha stimulates MMP15 expression. BMC Dev Biol 2007; 7:137. doi: 10.1186/1471-213X-7-137.

39. Fröhlich JD, Huppertz B, Abuja PM, König J, Desoye G. Oxygen modulates the response of first-trimester trophoblasts to hyperglycemia. Am J Pathol 2012; 180(1):153–64. doi: 10.1016/j.ajpath.2011.09.012.

40. Chaiwangyen W, Ospina-Prieto S, Morales-Prieto DM, Pereira de Sousa FL, Pastuschek J, Fitzgerald JS et al. Oncostatin M and leukaemia inhibitory factor trigger signal transducer and activator of transcription 3 and extracellular signal-regulated kinase 1/2 pathways but result in heterogeneous cellular responses in trophoblast cells. Reprod Fertil Dev 2016; 28(5):608–17. doi: 10.1071/RD14121.

41. Bilban M, Tauber S, Haslinger P, Pollheimer J, Saleh L, Pehamberger H et al. Trophoblast invasion: assessment of cellular models using gene expression signatures. Placenta 2010; 31(11):989–96. doi: 10.1016/j.placenta.2010.08.011.

42. Koledova Z. 3D Cell Culture: An Introduction. Methods Mol Biol 2017; 1612:1–11. doi: 10.1007/978-1-4939-7021-6_1.

43. Edmondson R, Broglie JJ, Adcock AF, Yang L. Three-dimensional cell culture systems and their applications in drug discovery and cell-based biosensors. Assay Drug Dev Technol 2014; 12(4):207–18. doi: 10.1089/adt.2014.573.

44. Amelian A, Wasilewska K, Megias D, Winnicka K. Application of standard cell cultures and 3D in vitro tissue models as an effective tool in drug design and development. Pharmacol Rep 2017; 69(5):861–70. doi: 10.1016/j.pharep.2017.03.014.

45. Kapałczyńska M, Kolenda T, Przybyła W, Zajączkowska M, Teresiak A, Filas V et al. 2D and 3D cell cultures - a comparison of different types of cancer cell cultures. Arch Med Sci 2018; 14(4):910–9. doi: 10.5114/aoms.2016.63743.

46. Shamir ER, Ewald AJ. Three-dimensional organotypic culture: experimental models of mammalian biology and disease. Nat Rev Mol Cell Biol 2014; 15(10):647–64. doi: 10.1038/nrm3873.

47. Ravi M, Paramesh V, Kaviya SR, Anuradha E, Solomon FDP. 3D cell culture systems: advantages and applications. J Cell Physiol 2015; 230(1):16–26. doi: 10.1002/jcp.24683.

48. Astashkina A, Grainger DW. Critical analysis of 3-D organoid in vitro cell culture models for high-throughput drug candidate toxicity assessments. Advanced Drug Delivery Reviews 2014; 69-70:1–18. doi: 10.1016/j.addr.2014.02.008.

49. Pampaloni F, Reynaud EG, Stelzer EHK. The third dimension bridges the gap between cell culture and live tissue. Nat Rev Mol Cell Biol 2007; 8(10):839–45. doi: 10.1038/nrm2236.

50. Breslin S, O'Driscoll L. Three-dimensional cell culture: the missing link in drug discovery. Drug Discovery Today 2013; 18(5-6):240–9. doi: 10.1016/j.drudis.2012.10.003.

51. Kelm JM, Timmins NE, Brown CJ, Fussenegger M, Nielsen LK. Method for generation of homogeneous multicellular tumor spheroids applicable to a wide variety of cell types. Biotechnol Bioeng 2003; 83(2):173–80. doi: 10.1002/bit.10655.

52. Haycock JW. 3D cell culture: a review of current approaches and techniques. Methods Mol Biol 2011; 695:1–15. doi: 10.1007/978-1-60761-984-0_1.

53. Griffith LG, Swartz MA. Capturing complex 3D tissue physiology in vitro. Nat Rev Mol Cell Biol 2006; 7(3):211–24. doi: 10.1038/nrm1858.

54. Huh D, Hamilton GA, Ingber DE. From Three-Dimensional Cell Culture to Organs-on-Chips. Trends Cell Biol 2011; 21(12):745–54. doi: 10.1016/j.tcb.2011.09.005.

55. James R, Jenkins L, Ellis SE, Burg KJL. Histological Processing of Hydrogel Scaffolds for Tissue-Engineering Applications. Journal of Histotechnology 2004; 27(2):133–9. doi: 10.1179/his.2004.27.2.133.

56. Maltman DJ, Przyborski SA. Developments in three-dimensional cell culture technology aimed at improving the accuracy of in vitro analyses. Biochem Soc Trans 2010; 38(4):1072–5. doi: 10.1042/BST0381072.

57. Bose S, Roy M, Bandyopadhyay A. Recent advances in bone tissue engineering scaffolds. Trends Biotechnol 2012; 30(10):546–54. doi: 10.1016/j.tibtech.2012.07.005.

58. Fuchs J, Mueller M, Daxböck C, Stückler M, Lang I, Leitinger G et al. Histological processing of un-/cellularized thermosensitive electrospun scaffolds. Histochem Cell Biol 2018. Verfügbar unter: https://doi.org/10.1007/s00418-018-1757-7.

59. Pemathilaka RL, Reynolds DE, Hashemi NN. Drug transport across the human placenta: review of placenta-on-a-chip and previous approaches. Interface Focus 2019; 9(5):20190031. doi: 10.1098/rsfs.2019.0031.

60. Antoni D, Burckel H, Josset E, Noel G. Three-dimensional cell culture: a breakthrough in vivo. Int J Mol Sci 2015; 16(3):5517–27. doi: 10.3390/ijms16035517.

61. Mannelli C, Ietta F, Avanzati AM, Skarzynski D, Paulesu L. Biological Tools to Study the Effects of Environmental Contaminants at the Feto-Maternal Interface. Dose Response 2015; 13(4):1559325815611902. doi: 10.1177/1559325815611902.

62. Miller RK, Genbacev O, Turner MA, Aplin JD, Caniggia I, Huppertz B. Human placental explants in culture: approaches and assessments. Placenta 2005; 26(6):439–48. doi: 10.1016/j.placenta.2004.10.002.

63. Yin F, Zhu Y, Zhang M, Yu H, Chen W, Qin J. A 3D human placenta-on-a-chip model to probe nanoparticle exposure at the placental barrier. Toxicol In Vitro 2019; 54:105–13. doi: 10.1016/j.tiv.2018.08.014.

64. Abbas Y, Oefner CM, Polacheck WJ, Gardner L, Farrell L, Sharkey A et al. A microfluidics assay to study invasion of human placental trophoblast cells 2017. doi: 10.17863/CAM.10329.

65. Bhatia SN, Ingber DE. Microfluidic organs-on-chips. Nat Biotechnol 2014; 32(8):760–72. doi: 10.1038/nbt.2989.

66. Kuo C-Y, Eranki A, Placone JK, Rhodes KR, Aranda-Espinoza H, Fernandes R et al. Development of a 3D Printed, Bioengineered Placenta Model to Evaluate the Role of Trophoblast Migration in Preeclampsia. ACS Biomater. Sci. Eng. 2016; 2(10):1817–26. doi: 10.1021/acsbiomaterials.6b00031.

67. Wong MK, Wahed M, Shawky SA, Dvorkin-Gheva A, Raha S. Transcriptomic and functional analyses of 3D placental extravillous trophoblast spheroids. Sci Rep 2019; 9(1):12607. doi: 10.1038/s41598-019-48816-8.

68. Muoth C, Wichser A, Monopoli M, Correia M, Ehrlich N, Loeschner K et al. A 3D co-culture microtissue model of the human placenta for nanotoxicity assessment. Nanoscale 2016; 8(39):17322–32. doi: 10.1039/c6nr06749b.

69. Turco MY, Gardner L, Kay RG, Hamilton RS, Prater M, Hollinshead MS et al. Trophoblast organoids as a model for maternal-fetal interactions during human placentation. Nature 2018; 564(7735):263–7. doi: 10.1038/s41586-018-0753-3.

70. Ramos-Vara JA, Beissenherz ME. Optimization of immunohistochemical methods using two different antigen retrieval methods on formalin-fixed paraffin-embedded tissues: experience with 63 markers. J Vet Diagn Invest 2000; 12(4):307–11. doi: 10.1177/104063870001200402.

71. Ramos-Vara JA. Principles and Methods of Immunohistochemistry. Methods Mol Biol 2017; 1641:115–28. doi: 10.1007/978-1-4939-7172-5_5.

72. Grundberg I, Kiflemariam S, Mignardi M, Imgenberg-Kreuz J, Edlund K, Micke P et al. In situ mutation detection and visualization of intratumor heterogeneity for cancer research and diagnostics. Oncotarget 2013; 4(12):2407–18. doi: 10.18632/oncotarget.1527.

73. El-Heliebi A, Kashofer K, Fuchs J, Jahn SW, Viertler C, Matak A et al. Visualization of tumor heterogeneity by in situ padlock probe technology in colorectal cancer. Histochem Cell Biol 2017; 148(2):105–15. doi: 10.1007/s00418-017-1557-5.

74. El-Heliebi A, Hille C, Laxman N, Svedlund J, Haudum C, Ercan E et al. In Situ Detection and Quantification of AR-V7, AR-FL, PSA, and KRAS Point Mutations in Circulating Tumor Cells. Clin Chem 2018; 64(3):536–46. doi: 10.1373/clinchem.2017.281295.

75. McQuin C, Goodman A, Chernyshev V, Kamentsky L, Cimini BA, Karhohs KW et al. CellProfiler 3.0: Next-generation image processing for biology. PLoS Biol 2018; 16(7):e2005970. doi: 10.1371/journal.pbio.2005970.

76. Weibrecht I, Lundin E, Kiflemariam S, Mignardi M, Grundberg I, Larsson C et al. In situ detection of individual mRNA molecules and protein complexes or post-translational modifications using padlock probes combined with the in situ proximity ligation assay. Nat Protoc 2013; 8(2):355–72. doi: 10.1038/nprot.2013.006.

77. Carpenter AE, Jones TR, Lamprecht MR, Clarke C, Kang IH, Friman O et al. CellProfiler: image analysis software for identifying and quantifying cell phenotypes. Genome Biol 2006; 7(10):R100. doi: 10.1186/gb-2006-7-10-r100.

78. Motulsky HJ, Brown RE. Detecting outliers when fitting data with nonlinear regression - a new method based on robust nonlinear regression and the false discovery rate. BMC Bioinformatics 2006; 7:123. doi: 10.1186/1471-2105-7-123.

79. Blaschitz A, Weiss U, Dohr G, Desoye G. Antibody reaction patterns in first trimester placenta: implications for trophoblast isolation and purity screening. Placenta 2000; 21(7):733–41. doi: 10.1053/plac.2000.0559.

80. Blaschitz A, Hutter H, Dohr G. HLA Class I protein expression in the human placenta. Early Pregnancy 2001; 5(1):67–9.

81. Iles RK, Ind TE, Chard T. Production of placental alkaline phosphatase (PLAP) and PLAP-like material by epithelial germ cell and non-germ cell tumours in vitro. Br J Cancer 1994; 69(2):274–8. doi: 10.1038/bjc.1994.51.

82. Möbius W. Cryopreparation of biological specimens for immunoelectron microscopy. Ann Anat 2009; 191(3):231–47. doi: 10.1016/j.aanat.2008.11.004.

83. Hruschka V, Meinl A, Saeed A, Cheikh Al Ghanami R, Redl H, Shakesheff K et al. Gelatin embedding for the preparation of thermoreversible or delicate scaffolds for histological analysis. Biomed Mater 2013; 8(4):41001. doi: 10.1088/1748-6041/8/4/041001.

84. Brown DA, Chou YF, Beygui RE, Dunn JCY, Wu BM. Gelatin-embedded cell–polymer constructs for histological cryosectioning. J Biomed Mater Res Part B Appl Biomater 2005; 72(1):79–85. doi: 10.1002/jbm.b.30116.

85. Fox CH, Johnson FB, Whiting J, Roller PP. Formaldehyde fixation. J Histochem Cytochem 1985; 33(8):845–53. doi: 10.1177/33.8.3894502.

86. He X, Guo F, Liu B. Oolong tea and LR-White resin: a new method of plant sample preparation for transmission electron microscopy. J Microsc 2018; 270(2):244–51. doi: 10.1111/jmi.12678.

87. McDonald KL. Rapid embedding methods into epoxy and LR White resins for morphological and immunological analysis of cryofixed biological specimens. Microsc Microanal 2014; 20(1):152–63. doi: 10.1017/S1431927613013846.

88. Lowe JS, Anderson PG, Stevens A. Stevens & Lowe's human histology. Fourth edition. Philadelphia, PA: Elsevier/Mosby; 2015.

89. Carson FL, Hladik C. Histotechnology: A self-instructional text. 3rd ed. [Chicago]: American Society for Clinical Pathology Press; 2009.

90. Mason JT, O'Leary TJ. Effects of formaldehyde fixation on protein secondary structure: a calorimetric and infrared spectroscopic investigation. J Histochem Cytochem 1991; 39(2):225–9. doi: 10.1177/39.2.1987266.

91. Battifora H, Kopinski M. The influence of protease digestion and duration of fixation on the immunostaining of keratins. A comparison of formalin and ethanol fixation. J Histochem Cytochem 1986; 34(8):1095–100. doi: 10.1177/34.8.2426335.

92. Leong AS, Gilham PN. The effects of progressive formaldehyde fixation on the preservation of tissue antigens. Pathology 1989; 21(4):266–8.

93. Robinson JM, Vandré DD. Antigen retrieval in cells and tissues: enhancement with sodium dodecyl sulfate. Histochem Cell Biol 2001; 116(2):119–30. doi: 10.1007/s004180100299.

94. McNicol AM, Richmond JA. Optimizing immunohistochemistry: antigen retrieval and signal amplification. Histopathology 1998; 32(2):97–103.

95. Mighell AJ, Hume WJ, Robinson PA. An overview of the complexities and subtleties of immunohistochemistry. Oral Diseases 1998; 4(3):217–23. doi: 10.1111/j.1601-0825.1998.tb00282.x.

96. Syrbu SI, Cohen MB. An enhanced antigen-retrieval protocol for immunohistochemical staining of formalin-fixed, paraffin-embedded tissues. Methods Mol Biol 2011; 717:101–10. doi: 10.1007/978-1-61779-024-9_6.

97. Cuevas EC, Bateman AC, Wilkins BS, Johnson PA, Williams JH, Lee AH et al. Microwave antigen retrieval in immunocytochemistry: a study of 80 antibodies. J Clin Pathol 1994; 47(5):448–52.

98. Ferrier CM, van Geloof WL, Witte HH de, Kramer MD, Ruiter DJ, van Muijen GN. Epitopes of components of the plasminogen activation system are re-exposed in formalin-fixed paraffin sections by different retrieval techniques. J Histochem Cytochem 1998; 46(4):469–76. doi: 10.1177/002215549804600406.

99. Franciosi S, Gasperi R de, Dickstein DL, English DF, Rocher AB, Janssen WGM et al. Pepsin pretreatment allows collagen IV immunostaining of blood vessels in adult mouse brain. J Neurosci Methods 2007; 163(1):76–82. doi: 10.1016/j.jneumeth.2007.02.020.

100. Daneshtalab N, Doré JJE, Smeda JS. Troubleshooting tissue specificity and antibody selection: Procedures in immunohistochemical studies. J Pharmacol Toxicol Methods 2010; 61(2):127–35. doi: 10.1016/j.vascn.2009.12.002.

101. Gurcan MN, Boucheron LE, Can A, Madabhushi A, Rajpoot NM, Yener B. Histopathological image analysis: a review. IEEE Rev Biomed Eng 2009; 2:147–71. doi: 10.1109/RBME.2009.2034865.

102. Nezami E, Butcher JN. Objective Personality Assessment. In: Handbook of Psychological Assessment: Elsevier; 2000. S. 413–35.

103. Gertych A, Ing N, Ma Z, Fuchs TJ, Salman S, Mohanty S et al. Machine learning approaches to analyze histological images of tissues from radical prostatectomies. Comput Med Imaging Graph 2015; 46 Pt 2:197–208. doi: 10.1016/j.compmedimag.2015.08.002.

104. Gauster M, Blaschitz A, Siwetz M, Huppertz B. Keratins in the human trophoblast. Histol Histopathol 2013; 28(7):817–25. doi: 10.14670/HH-28.817.

105. Larsson C, Grundberg I, Söderberg O, Nilsson M. In situ detection and genotyping of individual mRNA molecules. Nat Methods 2010; 7(5):395–7. doi: 10.1038/nmeth.1448.

106. He N, van Iperen L, Jong D de, Szuhai K, Helmerhorst FM, van der Westerlaken LAJ et al. Human Extravillous Trophoblasts Penetrate Decidual Veins and Lymphatics before Remodeling Spiral Arteries during Early Pregnancy. PLoS ONE 2017; 12(1):e0169849. doi: 10.1371/journal.pone.0169849.

107. Craven CM, Morgan T, Ward K. Decidual spiral artery remodelling begins before cellular interaction with cytotrophoblasts. Placenta 1998; 19(4):241–52. doi: 10.1016/s0143-4004(98)90055-8.

108. Lash GE, Naruse K, Innes BA, Robson SC, Searle RF, Bulmer JN. Secretion of angiogenic growth factors by villous cytotrophoblast and extravillous trophoblast in early human pregnancy. Placenta 2010; 31(6):545–8. doi: 10.1016/j.placenta.2010.02.020.

109. Lash GE, Schiessl B, Kirkley M, Innes BA, Cooper A, Searle RF et al. Expression of angiogenic growth factors by uterine natural killer cells during early pregnancy. J Leukoc Biol 2006; 80(3):572–80. doi: 10.1189/jlb.0406250.

110. Weiss G, Huppertz B, Siwetz M, Lang I, Moser G. Arterial endothelial cytokines guide extravillous trophoblast invasion towards spiral arteries; an in-vitro study with the trophoblast cell line ACH-3P and female non-uterine endothelial cells. Placenta 2016; 38:49–56. doi: 10.1016/j.placenta.2015.12.010.

111. Weiss G, Sundl M, Glasner A, Huppertz B, Moser G. The trophoblast plug during early pregnancy: a deeper insight. Histochem Cell Biol 2016; 146(6):749–56. doi: 10.1007/s00418-016-1474-z.

112. Kilburn BA, Wang J, Duniec-Dmuchowski ZM, Leach RE, Romero R, Armant DR et al. Extracellular matrix composition and hypoxia regulate the expression of HLA-G and integrins in a human trophoblast cell line. Biol Reprod 2000; 62(3):739–47. doi: 10.1095/biolreprod62.3.739.

113. Genbacev O, Joslin R, Damsky CH, Polliotti BM, Fisher SJ. Hypoxia alters early gestation human cytotrophoblast differentiation/invasion in vitro and models the placental defects that occur in preeclampsia. J Clin Invest 1996; 97(2):540–50. doi: 10.1172/JCI118447.

114. Kosanke G, Kadyrov M, Korr H, Kaufmann P. Maternal anemia results in increased proliferation in human placental villi. Placenta 1998; 19:339–57. doi: 10.1016/S0143-4004(98)80024-6.

115. Lelic M, Bogdanovic G, Ramic S, Brkicevic E. Influence of maternal anemia during pregnancy on placenta and newborns. Med Arch 2014; 68(3):184–7. doi: 10.5455/medarh.2014.68.184-187.

116. Huppertz B, Gauster M, Orendi K, König J, Moser G. Oxygen as modulator of trophoblast invasion. J Anat 2009; 215(1):14–20. doi: 10.1111/j.1469-7580.2008.01036.x.

7 Appendix

Table 7: Antibodies used for experiments with corresponding stock concentrations according to manufacturer.

Antibody	Animal source	Antibody source*	Code/clone	Concentration (stock solution)
ALPPL2	rabbit	Thermo Fisher Scientific[a]	PA5-22336	1 mg/mL
β-Actin	mouse	abcam[b]	AC-15 /ab6276	2.1 mg/ml
CD 163	rabbit	DB Biotech[c]	K20-T	2 mg/ml
CD31	rabbit	abcam[b]	Ab28364	no information
CD34 II	mouse	Agilent Dako[d]	M7165/QBEnd 10	0.045 mg/ml
Cytokeratin 7	rabbit	OriGene Technologies[e]	AP06204PU-N	1 mg/ml
Cytokeratin 7	mouse	Thermo Fisher Scientific[a]	OV-TL 12/30	0.2 mg/ml
Desmin	mouse	Agilent Dako[d]	M0760/D33	0.111 mg/ml
E-Cadherin	rabbit	Cell Signalling Technology[f]	2,40E+11	no information
HLA-G	mouse	Santa Cruz[g]	4H84	0.2 mg/ml
Ki-67	mouse	Agilent Dako[d]	M7187	no information
Leptin	mouse	Santa Cruz[g]	sc-48408	0.2 mg/ml
Smooth Muscle Actin	mouse	Agilent Dako[d]	1A4 /M0851	0.071 mg/ml
ß-HCG	rabbit	Thermo Fisher Scientific[a]	Ab-2 /RB-059-A	no information
Vimentin	mouse	Agilent Dako[d]	V9/M0725	0.156 mg/ml
vWF	rabbit	Agilent Dako[d]	F3520	7.0 - 13.0 mg/m
ZO-1	rabbit	abcam[b]	ab96587	0.4 mg/mL
cleaved Caspase 3	rabbit	Cell Signalling Technology[f]	#9664	no information
ng Control IgG1	mouse	Agilent Dako[d]	x0931	0.1 mg/ml
ng Control IgG	rabbit	Agilent Dako[d]	x0936	15 mg/ml

* Superscript letters refer to sources and manufacturers section, which can be found in the Appendix 7.1.

7.1 Sources and manufacturers

a. Thermo Fisher Scientific, MA, USA

b. abcam, Cambridge, UK

c. DB Biotech, Kosice, Slovakia, EU

d. Agilent DAKO, Santa Clara, CA, USA

e. OriGene Technologies, Rockville, MD, USA

f. Cell Signalling Technology, Danvers, MA, USA

g. Santa Cruz Biotechnology, Dallas, TX, USA